DYNAMICS AND NONLINEAR, ADAPTIVE CONTROL OF AN AUTONOMOUS UNICYCLE

by

DAVID WILLIAM VOS

Hons. B.Ing (Aero)
University of Stellenbosch, South Africa, (1983)

Submitted in partial fulfillment of the
requirements for the degree of

Master of Science

in

Aeronautics and Astronautics

at the

Massachusetts Institute of Technology

May 1989

Signature of Author _____
Department of Aeronautics and Astronautics
May 12, 1989

Certified by _____
Prof. Andreas von Flotow
Thesis Supervisor, Department of Aeronautics and Astronautics

Accepted by _____
Prof. Harold Y Wachman
Chairman, Department Graduate Comittee

DYNAMICS AND NONLINEAR, ADAPTIVE CONTROL OF AN AUTONOMOUS UNICYCLE

by

DAVID WILLIAM VOS

Submitted to the Department of Aeronautics and Astronautics on May 12, 1989 in partial fulfillment of the requirements for the Degree of Master of Science in Aeronautics and Astronautics

ABSTRACT

This thesis studies the dynamics and active control of a mechanical unicycle with the human rider replaced by a turntable. The unicycle equations of motion are derived, linear in all states except yaw rate which is not considered a perturbation quantity.

Using the specialized linear equations with yaw rate also linearized, the dynamics of the open loop system are studied and shown to decouple into longitudinal and lateral systems for zero turntable angular velocity, and linear controllers are proposed for stabilization. The systems reduce to lower order models by exploitation of the time scale separation of the open loop dynamics. A variation of the LQG control design method is derived and used in both the lateral and longitudinal controller designs. This method allows recovery of LQ regulator inner loop without use of pole zero cancellation strategy, hence potentially offering greater parameter uncertainty robustness.

The lateral controller is continuously gain scheduled and implemented in a bang-bang setting in order to deal with coulomb friction effects between the tire and the ground. An estimation algorithm is defined to continuously determine estimates of the friction and hence adapt the bang-bang control algorithm.

Thesis supervisor: Prof. Andreas von Flotow

Title: Assistant Professor in Aeronautics and Astronautics

ACKNOWLEDGEMENTS

To Andy for the objective criticism and insightful guidance.

To Zingo for being a cool cat.

To life.

LIST OF SYMBOLS

A	state space dynamics matrix
B	state space control distribution matrix
C	state space measurement matrix
C_c	controllability matrix
D	state space feedforward matrix
F	friction in yaw (Newton meters)
F^*	inertia forces
F_a	Newtonian earth fixed reference frame
F_f	unicycle frame fixed reference frame
F_t	turntable shaft fixed reference frame
F_w	wheel axle fixed reference frame
F_{lc}	limit cycle frequency (Hz)
$f_{\dot{\psi}}$	viscous friction coefficient in yaw (Newton meter seconds per radian)
g	acceleration due to gravity (nominally 9.81 m/s^2)
G_{lr}	regulator gain matrix for reduced order plant
g_{lr}	regulator gain matrix for reduced order plant
H	angular momentum vector
H_{kf}	Kalman filter gain matrix
I	identity matrix
Im	torque impulse (Newton meter seconds)
I_1^F	moment of inertia of unicycle frame about axis through centre of mass of frame, in direction f_1 in units kgm^2

I_2^F moment of inertia of unicycle frame about axis through centre of mass of frame, in direction f_2 in units kgm^2

I_3^F moment of inertia of unicycle frame about axis through centre of mass of frame, in direction f_3 in units kgm^2

I_1^T moment of inertia of turntable about axis through centre of mass of turntable, in direction t_1 in units kgm^2

I_2^T moment of inertia of turntable about axis through centre of mass of turntable, in direction t_2 in units kgm^2

I_3^T moment of inertia of turntable about axis through centre of mass of turntable, in direction t_3 in units kgm^2

I_1^W moment of inertia of wheel about axis w_1 through centre of mass, in units kgm^2

I_2^W moment of inertia of wheel about axis w_2 through centre of mass, in units kgm^2

I_3^W moment of inertia of wheel about axis w_3 through centre of mass, in units kgm^2

J optimal quadratic cost

K stiffness matrix

K_t bang-bang controller torque gain

K_ψ heading loop gain

K_Ω velocity loop gain

l_t	position of turntable centre of mass above wheel shaft in meters
LQG	linear quadratic Gaussian controller structure
LQR	linear quadratic regulator
LQG/LTR	linear quadratic Gaussian controller incorporating loop transfer recovery
M	mass matrix
m_f	mass of unicycle frame (kg)
m_t	mass of unicycle turntable (kg)
m_w	mass of wheel (kg)
n_t	turntable gear ratio
n_w	wheel gear ratio
O_o	observability matrix
P	control algebraic Riccati equation solution
Q	state quadratic cost weighting
R	control quadratic cost weighting
r_f	position of frame centre of mass above wheel shaft in meters
r_w	wheel radius (meters)
s	Laplace transform operator
T	sample period (seconds)
T^*	inertia torques
t	time (seconds)
u	input
V	sensor noise covariance
v	right eigenvector
v(t)	sensor noise function

w	left eigenvector
$x(t)$	state vector
$\tilde{x}(t)$	error state vector
$y(t)$	measurement
z	zeros

Subscripts

c	lag compensator/commanded quantity
ct	continuous time
cl	closed loop
dt	discrete time
fs	full state
k	compensator
lc	limit cycle
lr	reduced order
ol	open loop
p	plant
t	discrete time at time 't'

Superscripts

F	unicycle frame
T	turntable/transpose
W	wheel
$\hat{}$	refers to Kalman filter

GREEK SYMBOLS

Γ	discrete time control distribution matrix
Γ_c	constant turntable torque amplitude over one sample interval (Newton meters)
Γ_f	amplitude of pulsewidth modulated turntable torque command (Newton meters)
Γ_t	turntable motor torque (Newton meters)
Γ_w	wheel motor torque (Newton meters)
Δt	time interval (seconds)
Δt_c	constant turntable control torque time interval (s)
Δt_f	friction compensated pulsewidth modulated constant turntable torque time interval (seconds)
Δt_t	equivalent yaw impulse time interval (seconds)
ζ	damping ratio
η	integration dummy variable
$\dot{\eta}$	turntable angular velocity (rad/s)
$\dot{\eta}_o$	turntable reference angular velocity (rad/s)
θ	unicycle frame pitch angle (rad)
$\dot{\theta}$	unicycle frame pitch rate (rad/s)
λ	eigenvalue (rad/s)
$\xi(t)$	process noise
Ξ	process noise covariance matrix
Σ	error state covariance matrix
Φ	discrete time state transition matrix
φ	roll angle (rad)
φ_{max}	maximum phase lag due to lag network

$\dot{\varphi}$ roll rate (rad/s)

ψ heading angle (rad)

ψ_c commanded heading

$\dot{\psi}$ yaw rate (rad/s)

Ω wheel angular velocity (rad/s)

Ω_c commanded wheel angular velocity (rad/s)

Ω_o reference wheel angular velocity (rad/s)

$\omega_{\text{max phase}}$ frequency of maximum phase due to lag network (rad/s)

TABLE OF CONTENTS

1.0 INTRODUCTION

To observe natural phenomena and understand is to experience wonder. To then change the character of such phenomena is tantamount to creation of new natural phenomena according to ones own specifications. Perhaps this desired conquest of nature is the prime motivation for engineering in general and more specifically for trying to control a unicycle automatically?

A large motivating factor in this project is the partial success achieved on a similar project in 1987 at Stanford University, Palo Alto, California [14]. This study addressed a wide range of issues, from design and construction of sensors and electronic hardware as well as the mechanical elements of the unicycle robot, to controller design and implementation. Figure 1 shows the Stanford unicycle robot. The controller design successfully addressed the longitudinal (pitch) control problem in both simulation and testing.

The lateral control problem, however, was only briefly discussed in the linear setting, including (linear) viscous friction, but ignoring the more significant Coulomb friction issue. This design was not implemented on the robot and the extent of the project was thus limited to longitudinal stabilization of the unicycle with laterally stabilizing training wheels fitted.

We have modeled the unicycle robot along the lines of the Stanford example, with a single motor driving the wheel via a gearbox of ratio 12:1 for pitch control and a second motor driving the turntable through gearing of ratio 36:1 for lateral control. The dynamics of the unicycle may be viewed as nonlinear, coupled lateral and longitudinal inverted pendulum motion, the coupling between lateral and longitudinal motion arising through the gyroscopic effects of the turntable and through large yaw rate of the frame.

Roll yaw coupling exists due to gyroscopic effects of both the wheel and turntable. The pitching and rolling motion is intuitively seen to be unstable, with the pitching motion being of smaller time constant than the rolling motion, since pitching occurs about the wheel shaft, which is a shorter moment arm than the rolling moment arm which extends to the contact point between the wheel and the surface. The time constant for the roll instability is dependent on the wheel speed, since the gyroscopic effect is to stabilize the rolling motion, these poles moving toward the origin and outward along the imaginary axis with increasing wheel speed (see figure 4.5.1).

These actuators combined with sensors which measure all angular rates, pitch and roll angles as well as motor speeds, result in the command following heading and forward speed control loops

exhibiting non minimum-phase behaviour, consistent with the motion of a human unicyclist. Physically, in order for the unicyclist to change forward velocity, the wheel speed is slowed in order to generate a pitch error and then in recovery of this error, the new forward (increased) velocity is set. Similar reasoning is valid for the lateral motion- a heading change to the left is achieved by initially incurring a roll error by turning to the right, before recovering on the desired heading.

The lateral and longitudinal linearized dynamics decouple for the turntable reference angular velocity set to zero, since this then essentially elimates gyroscopic effects due to the turntable. The linear control problem is reduced to two decoupled systems by this approximation (clearly, the turntable angular velocity cannot be identically zero for all time if it is to be used for control, but these are second order effects), thus allowing separate design of lateral and longitudinal controllers.

The longitudinal model relies on friction for controllability and this is implicit in the constraint of zero slip between the wheel and the surface. The negative effect of friction between the wheel and the surface is, however, to introduce a discontinuous nonlinearity into yawing motion. The friction in yaw is assumed to exist in the sense of stiction or breakaway

friction and kinematic (dynamic) friction, as well as viscous friction and is modeled as such.

The linearized dynamics yield lateral and longitudinal models of a similar structure which lends itself to a design approach which considers firstly a higher bandwidth inner loop around which the slower outer loop is closed. Each inner loop is a regulation loop since we want only to maintain zero perturbations from the stabilized vertical position and is essentially an LQG structure. The outer loops use properties of the LQG structure to advantage in achieving command following in both heading and forward speed.

The lateral controller is then extended into an adaptive, bang-bang framework for implementation. Pulsewidth modulation is used to ensure that actuator torques are always larger than stiction torques, hence overcoming the restraining friction effects in yaw. An algorithm is defined for continuous estimation of the magnitude of the friction (in yaw) thus enabling the unicycle to operate on terrain where the friction magnitude is unknown.

The lateral controller is then also gain scheduled according to wheel speed in order to account for the time varying effect of varying roll dynamics as a function of wheel speed.

This study demonstrates clearly the limitation of linear

control design on systems containing discontinuous nonlinearities, and the need for careful understanding of the physical dynamics involved in order to achieve, if only in simulation at least, more robust control designs. Also of important value is the demonstrated need for good knowledge of both modern and classical control design techniques in achieving a controller incorporating favorable aspects of both schools.

In implementation, the unicycle robot is to be tested initially on a treadmill, thus allowing easy monitoring and tuning of the controllers which are to be implemented digitally. The longitudinal controller is firstly tuned with the aid of roll stabilizing training wheels, and then the lateral controller. The ultimate goal is complete autonomy with a microprocessor on board and remote control via radio. The unicycle robot construction is complete at time of writing and test results will be available in the near future.

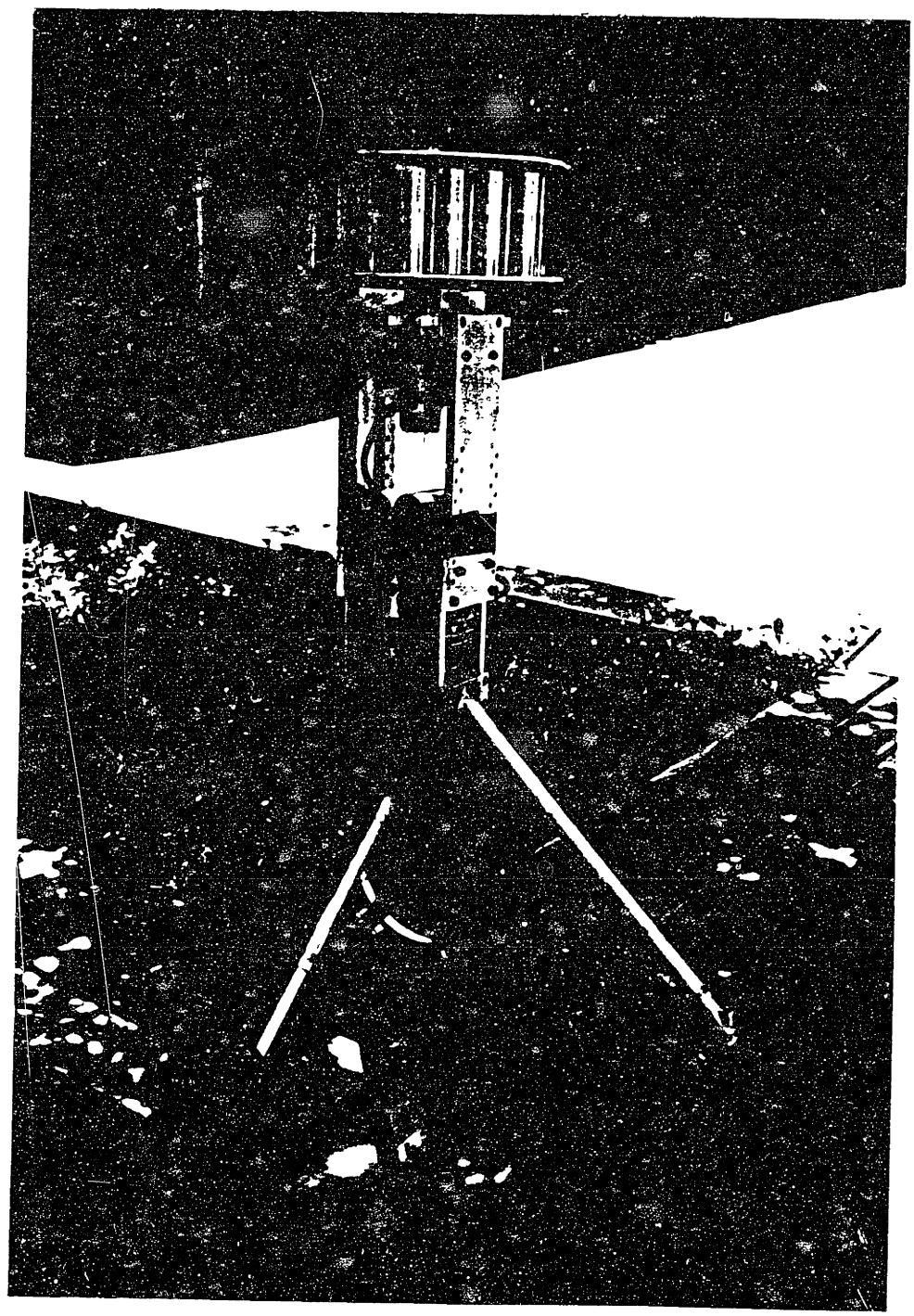

Figure 1. The Stanford unicycle robot [14].

2.0 SENSORS AND ACTUATORS

2.1 The Problem

Successful control of any system is achieved only with the aid of suitable sensors and actuators. The most robust of control structures and benign of plants could easily be transformed into disaster by incorrect choice of sensors and actuators.

The unicycle presents an unusual challenge in that good information as to pitch and roll angles and rates is critical since the system is unstable and recovery from specifically large roll errors is limited. The pitch modes are in the region of 8 rad/s natural frequency or analagously, time to double amplitude for the unstable perturbed response is on the order of 1 tenth of a second. The roll modes are dependant on wheel speed, but are typically on the order of 3 to 4 rad/s. Sensors with time constants greater than 30 or 40 rad/s would suffice.

The resolution requirements are relatively stringent in that the actuators could typically not recover the system from errors greater than ten degrees without saturation or tire slip and by the nature of the system, it is desirable to minimize (stable) limit cycle amplitude due to sensor/actuator resolution.

2.2 Actuators

The unicycle robot has two actuators, selected to emulate the human unicyclist control mechanism. Human unicyclists achieve pitch motion control by pedals connected to the wheel and thus a motor driving the wheel is used for pitch and forward velocity control on the robot. A second motor driving a turntable with axis of rotation aligned with the vertical axis of the frame, is used for lateral control in a reaction wheel sense. This emulates the pivoting about the hips of the human for yaw and roll control of the unicycle.

2.2.1 The Motors

The motors are low armature inertia, dc, high torque units manufactured by INFRANOR inc [9]. These provide high torque to inertia ratios and hence short response times and compact dimensions. The mechanical time constants are 9.24 milliseconds and 19 milliseconds for the turntable and wheel motors respectively.

The model used for the turntable is MO80 with rated voltage 40.3V dc and current 5 amps. The wheel drive motor is model MO301 with rated voltage 24V dc and current 16.5 amps. Both motors have integrally mounted tachometers which are listed to yield measurements to within 0.16 rad/s accuracy.

These motors are controlled via Galil Motion [7] pulsewidth modulated amplifier cards although it is uncertain at this time whether or not the turntable motor will require this since we are implementing a lateral controller which employs pulsewidth modulation.

Gearing of ratio 12:1 is achieved by use of a toothed belt drive on the wheel and the turntable is geared to a ratio of 36:1 via a double set of spur gears each of ratio 6:1.

2.3 Rate Sensors and Inclinometers

The rate sensors are solid state rate gyros produced by Watson Industries inc [15]. These consist of piezoelectric vibrating beam/sensing elements, the sensing element rotated through 90° with respect to the vibrating beam (drive element) as shown in figure 2.3.1. The drive element oscillates at approximately 360 Hz piezoelectrically excited and when an angular rate exists about the sensing axis, coriolis forces cause deflection of the sensing element and this generates the signal. Two such elements are used in a tuning fork arrangement and their signals subtracted in order to reduce common mode vibration effects due to external vibration/acceleration and external acoustic noise.

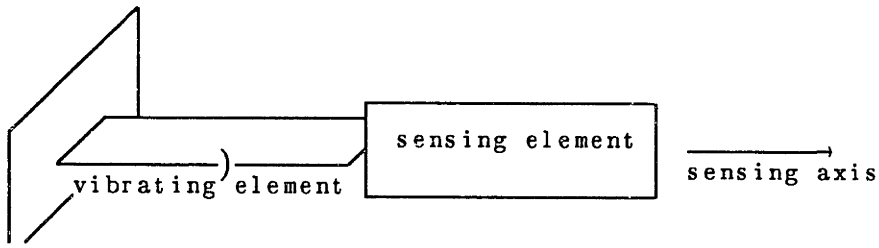

Figure 2.3.1. Schematic of Solid State Rate Sensor

The rate sensors measure full scale rates of 100°/second at 10 Volts and output noise is 15mV rms yielding resolution of approximately 0.15°/second.

Angular displacement information is obtained by use of inclinometers manufactured by the same company and these use combined pendulum and integrated rate signals to measure angular displacement. The resolution here is on the same order as for the rate sensors.

The linearized model is a seven state model, these being wheel angular velocity, pitch angle and rate, roll angle and rate, yaw rate and turntable angular velocity. All of these states are measured using the various sensors described above.

3.0 LONGITUDINAL DYNAMICS AND CONTROLLER DESIGN

3.1 Introduction

The decoupled longitudinal system open loop dynamics are discussed here and a structure as well as simulation results for a stabilizing controller are proposed. The system has non minimum-phase transmission zeros in the outer loop (velocity loop), which poses difficulty for implementation of a typical LQG (Linear Quadratic Gaussian) or LQG/LTR type structure.

Specifically, the LTR (Loop Transfer Recovery) procedure tries to establish high bandwidth filter dynamics and cancel regulator zeros and plant poles in order that the dominant dynamics of the compensated system are only those of the desired regulator. Inherent in this model based method is the problem that the filter retains the non minimum-phase transmission zeros of the plant and as such cannot achieve the necessary pole/zero cancellation for elimination of undesired dynamics, yielding poor designs. Figure 3.1.1 shows the closed loop transfer function relating commanded velocity to system velocity for an LQG/LTR design, which certainly appears undesirable. The LQG/LTR method, however, yields invaluable insights into restructuring the LQG type methodology to the classical approach of inner loop regulator design.

The system has a single actuator in the wheel torque motor and

since this methodology (LQG/LTR) can only deal with 'square' systems i.e. having the same number of inputs and outputs, we are only allowed one sensor and all other states must be estimated from information contained in this single measurement. Logically, since we are controlling velocity in the outer loop, this measurement is selected as the wheel tachometer. This situation is unsatisfactory in the sense that as the plant is of such difficult nature and we have all measurements available, we would like to incorporate this information into the controller to assist in achieving a robust system.

This problem is alleviated by combining the classical concept of closing 'fast' inner loops first, with a reduced order LQG controller structure, thus avoiding the problem of non minimum-phase zeros by seeking an inner plant, which is minimum-phase, about which the LQG reduced order controller is designed.

This is of course only possible if the actuator-plant-sensor structure is such that the faster dynamics can be 'decoupled' (in an inner loop sense), from the slower dynamics and that this then yields a minimum-phase system. Note that for this reduced order system, we have one input and two measurements i.e. a non square system so that the concept of transmission zeros does not apply, but since nonsquare systems do not have any transmission zeros in general [10], this is an easier

system to deal with than the full order one. Also resulting from this fact ('nonsquareness') is the nonexistance of a general solution for the closed loop LQR pole pattern [12].

Of further interest in the longitudinal controller design is the use of classical lag compensation in the outer (velocity) loop to achieve good loop transfer function shape as regards improved command following and disturbance rejection, without significant phase penalty. Since this is done in frequency ranges greater than that of the non minimum-phase zeros (of the square Ω/Γ_w transfer function), which is an unachievable frequency for closed loop system bandwidth, it does not hurt the system phase and significantly does assist in shaping the root locus to yield better damping of the dominant modes of the closed loop system.

3.2 Longitudinal model

The decoupled (from lateral motion) longitudinal system as derived in appendix 1 is repeated below. For state vector $x(t)^T = [\Omega(t) \quad \dot{\theta}(t) \quad \theta(t)]$

$$\mathbf{M}\,\dot{x}(t) + \mathbf{K}\,x(t) + B^1u(t) = 0 \qquad 3.2.1$$

Where

$$\mathbf{M} = \begin{bmatrix} -((m_w + m_f + m_t)r_w^2 + I_2^W) & -(m_w r_f + m_t l_t)r_w & 0 \\ -(m_f r_f + m_t l_t)r_w & -(m_f r_f^2 + m_t l_t^2 + I_2^T + I_2^F) & 0 \\ 0 & 0 & 1 \end{bmatrix}$$

$$K = \begin{bmatrix} 0 & 0 & 0 \\ 0 & 0 & (m_f r_f + m_t l_t)g \\ 0 & -1 & 0 \end{bmatrix}$$

$$B^1 = \begin{bmatrix} n_w \\ -nw \\ 0 \end{bmatrix}$$

Then, rearranging 3.2.1 above

$$\dot{x}(t) = -M^{-1}K\, x(t) - M^{-1}B^1 u(t)$$
$$= A\, x(t) + B\, u(t)$$

The model parameters in appendix 2, yield the following state space model

$$\dot{x}(t) = \begin{bmatrix} 0 & 0 & -194.61 \\ 0 & 0 & 66.051 \\ 0 & 1 & 0 \end{bmatrix} x(t) + \begin{bmatrix} 37.66 \\ -10.76 \\ 0 \end{bmatrix} u(t)$$

3.3 Open Loop Dynamics

The open loop eigenstructure shows the linear longitudinal system constituent of three modes.

Pitch mode pair

$$\lambda = 8.1272 \text{ rad/s} \qquad v = \begin{bmatrix} 0.9462 \\ -0.3211 \\ -0.0395 \end{bmatrix}$$

$$\lambda = -8.1272 \text{ rad/s} \qquad v = \begin{bmatrix} 0.9462 \\ -0.3211 \\ +0.0395 \end{bmatrix}$$

This eigenvalue/eigenvector pair is associated with the pitching motion, which is unstable and of frequency in the region of 1.3Hz. This is representative of the inverted pendulum type dynamics in pitch.

Rolling mode

$$\lambda = 0.0 \text{ rad/s} \qquad v = \begin{bmatrix} 1 \\ 0 \\ 0 \end{bmatrix}$$

The third mode is a pure integrator associated with the rolling

motion of the unicycle wheel.

3.4 Transmission Zeros

The system has one actuator in the wheel torque motor and we measure all states. As discussed in 3.1 the system with the single measurement, $\Omega(t)$, has the following non minimum-phase structure

$$z_1 = -3.2343 \text{ rad/s}$$
$$z_2 = +3.2343 \text{ rad/s}$$

Clearly the non minimum-phase zero is at a frequency roughly half that of the open loop pitch mode and for this reason presents an especially difficult task for the controller in this frequency range and represents a fundamental limit in achievable bandwidth of the closed loop controlled system [6]. This is, however, the physical reality of riding a unicycle in that it is not possible to perform maneuvers in this frequency range.

As discussed in 3.1 above, the reduced order system obtained by considering only the states $\dot{\theta}(t)$ and $\theta(t)$, has no transmission zeros.

3.5 Reduced Order Linear Quadratic Regulator

The inner regulator loop does not do any form of command following, rather regulation to zero of any existing pitch angle and pitch rate deviations from the vertical rest condition.

3.5.1 The Reduced Order Plant

The reduced order state space model for design of the inner loop controller is derived from the full order system by considering only the states $\dot{\theta}(t)$ and $\theta(t)$. For the state vector $x(t)_{lr}^{T} = [\dot{\theta}(t)\ \theta(t)]$ then

$$\dot{x}_{lr}(t) = A_{lr}x_{lr}(t) + B_{lr}u(t)$$

$$= \begin{bmatrix} 0 & 66.051 \\ 1 & 0 \end{bmatrix} x_{lr}(t) + \begin{bmatrix} -10.76 \\ 0 \end{bmatrix} u(t) \qquad 3.5.1.1$$

With measurement

$$y_{lr}(t) = C_{lr}x_{lr}(t)$$

$$= \begin{bmatrix} 1 & 0 \\ 0 & 1 \end{bmatrix} x_{lr}(t) \qquad 3.5.1.2$$

3.5.2 Linear Quadratic Regulator

The linear quadratic regulator yields an optimal least squares regulator by minimizing the cost functional

$$J = \int_0^\infty \{ x^T(t)Qx(t) + u^T(t)Ru(t) \}dt$$

Subject to the constraints of the linear system 3.5.1.1 and 3.5.1.2

Since the more important error we would like to eliminate is pitch angle, we place a heavier penalty on this state in the weighting matrix Q. The expensive control (heavily penalized actuator) LQR solution casts all unstable poles at their respective mirror images about the $j\omega$-axis. By the nature of the modal structure shown in the s-plane plot of figure 3.5.2.1 and following the root square locus [12] or inverse roots characteristic equation [5] reasoning, although not universally applicable to rectangular systems, the cheap control problem (small penalty on the actuator) will tend to move one pole towards the origin. This effectively reduces the bandwidth of the regulator. For this reason the penalty on the actuator is selected fairly large to ensure the closed loop poles are close to the location of the open loop stable pole frequency ($\approx$ 8 rad/s).

The weighting matrices

States: $\mathbf{Q} = \begin{bmatrix} 1 & 0 \\ 0 & 10 \end{bmatrix}$

Control: $R = 100$

Yield the LQR gain

$$g_{lr} = [\ -1.51 \quad -12.29\ ]$$

With closed loop poles

$$\lambda_1 = -8.64 \text{ rad/s} \qquad \lambda_2 = -7.65 \text{ rad/s}$$

Time histories of this system response to an initial pitch angle of ten degrees are shown in figure 3.5.2.2. This inner loop is now incorporated into the full order system in order to design the outer loop compensator.

3.6 Lag Compensator in Outer Loop

The full state model including the closed loop regulator, with the full state vector $X(t)^T = [\Omega(t)\ \dot{\theta}(t)\ \theta(t)]$ and 'A' and 'B' referring to the open loop dynamics and control distribution matrices respectively as in section 3.2 above:

$$\dot{x}(t) = \begin{bmatrix} A(1,1) & A(1,2) & A(1,3) \\ A(2,1) & \multicolumn{2}{c}{\multirow{2}{*}{$\left[\; A_{lr} - B_{lr} g_{lr} \;\right]$}} \\ A(3,1) & & \end{bmatrix} x(t) + B\, u(t)$$

Since the outer loop measures only $\Omega(t)$, we have

$$y(t) = C\, x(t)$$

$$= [1\ 0\ 0]\ x(t)$$

Figure 3.6.1 shows the open loop Bode plot for this system. Recalling from section 3.4 that this loop has two transmission zeros, one being non minimum-phase and at the exact frequency of the minimum-phase zero, it is clear that the net phase contribution of these elements is zero. Thinking in terms of an s-plane root locus, however, negative feedback (positive root locus gain) for the Ω loop closure will drive the integrator into the right half plane due to the presence of the non minimum-phase zero. For this reason we use positive feedback in this loop, the root locus is shown in figure 3.6.2.

This root locus shows that for reasonably damped ($\zeta = 0.72$) oscillatory poles the integrator pole has moved to s=-0.8 rad/s, which is low bandwidth. The Bode magnitude plot of figure 3.6.1.a also shows undesirable characteristics in the

frequency range of 2 rad/s to 9 rad/s. This is due to the two zeros at frequency ≈ 3 rad/s picking the magnitude up and the two poles at ≈ 8 rad/s pulling the magnitude down again. This is easily eliminated by use of a lag network $K_1(s)$ with a zero at 8 rad/s and pole at 3 rad/s.

$$K_1(s) = \frac{3(s + 8)}{8(s + 3)}$$

The maximum phase penalty [3] due to this network is

$$\sin(\varphi_{max}) = \frac{(1 - 3/8)}{(1 + 3/8)} \qquad \text{or } \varphi_{max} = 27^{\circ}$$

at frequency

$$(\omega_{max\ phase})^2 = 3 \times 8 \qquad \text{or } \omega_{max\ phase} = 4.9 \text{ rad/s}$$

The root locus for this lag compensated system is shown in figure 3.6.3 where for damping of the oscillatory mode of ζ = 0.89 the dominant poles are of natural frequency 2.3 rad/s, much improved over the uncompensated system. The lag compensated system Bode magnitude and phase plots of figure 3.6.4 indicate that for phase margin of 60°, the crossover frequency should be set around 1 rad/s. This corresponds to outer loop gain of

$$K_{\Omega} = -0.17 \text{ Nm/rad.s}^{-1}$$

yielding closed loop poles of

$$\lambda_1 = -4.7 \text{ rad/s} \qquad \lambda_2 = -8.07 \text{ rad/s}$$

$$\lambda_{3,4} = -2 \pm j1.04 \text{ rad/s}$$

The Bode magnitude plots for the closed loop transfer function and loop sensitivity (relating output disturbance to plant output) have desirable characteristics as apparent in figures 3.6.6 and 3.6.5 respectively. This is borne out in the time response plots, figures 3.6.7 and 3.6.8, showing response of the system to step command in Ω and recovery from an initial condition pitch angle (θ) of ten degrees, respectively. All units are rad or rad/s and the actuator response units are Newton meters.

3.7 Kalman Filter for LQG Inner Loop

The LQG inner regulator loop is shown in figure 3.7.1. In order to complete this structure we now address the definition of the Kalman Filter.

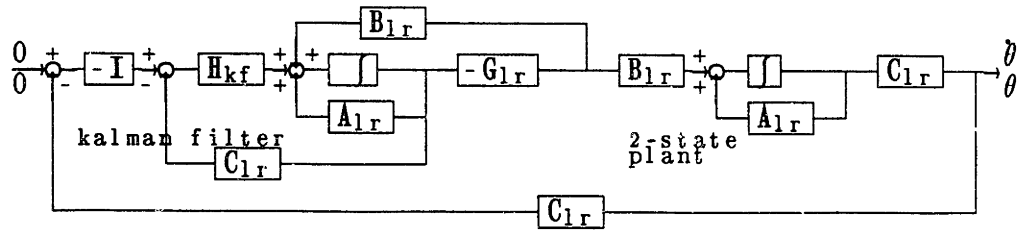

Figure 3.7.1 LQG Inner Loop Regulator Structure

By the non minimum-phase nature of the model, it is not possible to achieve high frequency dynamics in the Kalman filter, in fact the filter dynamics remain in the same frequency range as the regulator dynamics. For this reason, it is not obvious whether or not low pass filtering of the sensor data will suffice in obtaining good plant state information. The Kalman filter structure appears advantageous in that phase penalties are to be incurred either way (low-pass filtering or Kalman filtering), but the Kalman filter uses all sensor data and a model of the plant to improve the individual measurements. However, the design philosophy deviates from the typical Kalman Filter approach of determining the optimal filter to yield best state estimates from noisy sensors and plant processes in a least squares sense. Here, in typical LQG fashion, the sensor noise and process noise intensities are used as parameters for achieving a desired filter structure in terms of bandwidth.

For this system, process noise $\xi(t)$ enters via the torque motor and sensor noise occurs in both sensors (pitch angle and rate) as $v(t)$. The state space model can be written

$$\dot{x}(t) = A\,x(t) + B\,u(t) + B\,\xi(t)$$

and measurement

$$y(t) = C\ x(t) + v(t)$$

Where $\zeta(t)$ and $v(t)$ are assumed to be zero mean Gaussian white noise of constant intensities Ξ and V respectively.

The optimal steady state least squares estimator for this linear time invariant system is of the structure

$$\dot{\hat{x}}(t) = A\ \hat{x}(t) + H_{kf}(y(t) - C\ \hat{x}(t)) + B\ u(t)$$

$$= (A - H_{kf}C)\ \hat{x}(t) + H_{kf}y(t) + B\ u(t)$$

Where the filter gain in the steady state is

$$H_{kf} = \Sigma\ C^{T}V^{-1}$$

With Σ being the steady state error covariance determined as the solution to the Filter Algebraic Riccati equation given by

$$\dot{\Sigma} = 0 = A\ \Sigma + \Sigma\ A^{T} + B\ \Xi\ B^{T} - \Sigma\ C^{T}V^{-1}C\ \Sigma$$

Assuming that the sensor noise is greater on the rate sensor by a factor of 10 than on the angle sensor and the process noise parameter is fiddled to yield as fast as possible dynamics in

the LQG setting, use

Sensor covariance $V = \begin{bmatrix} 20 & 0 \\ 0 & 2 \end{bmatrix}$

Process covariance $\Xi = 1$

This yields filter gain

$$H_{kf} = \begin{bmatrix} 14.3 & 17.3 \\ 1.73 & 2.15 \end{bmatrix}$$

and filter poles at

$\lambda_1 = -9.34$ rad/s $\qquad \lambda_2 = -7.12$ rad/s

and by the nonsquare nature of the filter, there are no transmission zeros.

The filter poles of the LQG inner loop system are in the same region as those of the regulator, however, the performance is not degraded significantly as is seen in comparing the time histories of the LQG inner loop of figure 3.7.2 and those of the LQR loop of figure 3.5.2.2. Figure 3.7.2 shows the states and the estimates of the states, with the estimates tracking the actual states fairly well. Of course due to the filter dynamics being of the same order as the 'plant' the estimates

will always be a little sluggish, but this situation improves when closing the outer loop since one regulator pole moves toward the origin (see section 3.9) and the benefit in having the estimator perform low pass filtering of the sensor signals may prove to outweigh this degradation in performance. If the Kalman filter is not implemented, low pass filtering of each indiviual output ($\dot{\theta}(t)$ and $\theta(t)$) will in all likelihood be necessary.

3.8 Complete Full State System with LQG Inner Loop

All component elements of the longitudinal controller have now been defined and the full state structure can be formed. The block diagram of figure 3.8.1 shows the schematic form of the closed loop system from which the state space model is readily determined as follows. For state vector $x(t)_{fs} = [x_c \; \Omega \; \dot{\theta} \; \theta \; \hat{\dot{\theta}} \; \hat{\theta}]^T = [x_c \; \Omega \; x_{lr} \; \hat{x}_{lr}]^T$. The lag network state is $x_c(t)$.

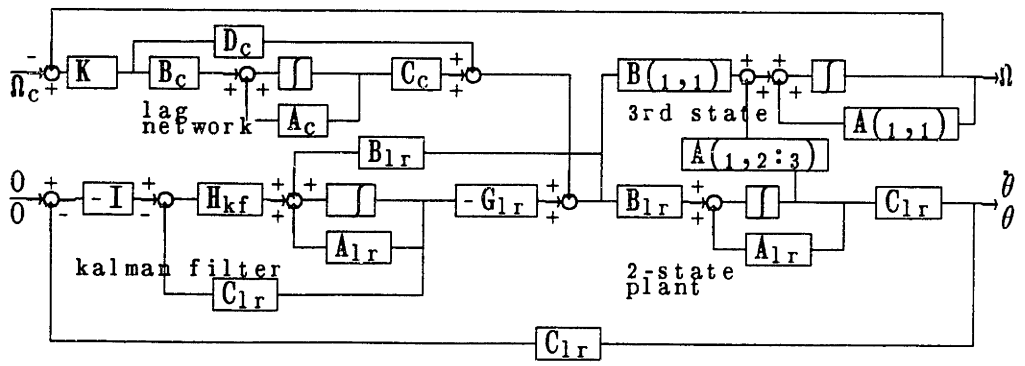

Figure 3.8.1 Complete System Block Diagram

Open Ω loop, inner loop closed:

$$\dot{x}_{fs}(t) = A_{fs}\, x_{fs}(t) + K_{\Omega}\, B_{fs}\Omega_c(t)$$

With

$$A_{fs} = \begin{bmatrix} A_c & 0 & 0 & 0 \\ B(1,1)C_c & A(1,1) & [A(1,2) \;\; A(1,3)] & -B(1,1)g_{lr} \\ B_{lr}C_c & 0 & A_{lr} & -B_{lr}g_{lr} \\ B_{lr}C_c & 0 & H_{kf}C_{lr} & [A_{lr} - B_{lr}g_{lr} - H_{kf}C_{lr}] \end{bmatrix}$$

$$B_{fs} = \begin{bmatrix} B_c \\ B(1,1)D_c \\ B_{lr}D_c \\ B_{lr}D_c \end{bmatrix} \qquad 3.8.1$$

The measurement is only the state Ω

$$\Omega(t) = [0\ 1\ 0\ 0\ 0\ 0]\, x_{fs}(t)$$

The open loop Bode magnitude and phase plots for this complete linear longitudinal system are shown in figure 3.8.2. The addition of the filter in the inner regulation loop has not resulted in any phase loss from the system of figure 3.6.4. The sensitivity and closed loop Bode magnitude plots are shown in figure 3.8.3 and time response simulations to a step wheel velocity (Ω) command are shown in figure 3.8.4, demonstrating

no loss in performance due to inclusion of the filter in the inner loop (compare with figure 3.6.7). See section 4.6.1 for formal explanation as to this result. Essentially we may design the regulator loop as desired and append outer loop dynamics as desired, and inclusion of the filter in the inner loop will not affect these structures as long as the filter is model based.

3.9 Discussion

The reason for the outer loop not seeing any degrading of performance as a result of including the Kalman filter in the inner loop LQG controller, is is that seen from the outer loop, effectively the filter error dynamics are uncontrollable, hence pole zero cancellation occurs i.e. the transfer function relating Ω/Ω_c has some zeros the poles of the filter.This is discussed more fully in section 4.6.1.

The complete longitudinal closed loop system from Ω_c to Ω in figure 3.8.1 has poles and zeros

$$\left.\begin{array}{l}\lambda = -4.73 \\ \lambda = -8.07\end{array}\right\} \text{LQR regulator poles}$$

$$\left.\begin{array}{l}\lambda = -7.12 \\ \lambda = -9.34\end{array}\right\} \text{Kalman filter poles}$$

$\lambda = -2.04 \quad + j1.04$
$\lambda = -2.04 \quad - j1.04$ } Outer loop poles

$z = 3.23$
$z = -3.23$ } Open outer loop transmission zeros

$z = -8.0$ Outer loop lag network zero

$z = -7.12$
$z = -9.34$ } Inner loop filter poles showing up in outer loop transfer function as zeros

Clearly in the outer loop, pole zero cancellation of the filter modes occurs so the response Ω to commanded Ω_c does not see any of these modes, but this is not the case in the inner loop. The inner loop transfer function relating the desired (zero valued) pitch rate and angle to actual (see figure 3.8.1) has a single transmission zero at -8.44 rad/s with poles at -9.34; -8.64; -7.65; -7.12. Clearly here is no cancellation of the filter modes (-9.34 and -7.12) as evidenced in the outer loop. The presence of the filter is clearly apparent in the time history of figure 3.9.2 as compared with figure 3.6.8 in the slightly increased overshoot of specifically $\Omega(t)$. Figure 3.9.2b shows the inner loop Kalman filter states (pitch angle and pitch rate estimates) track the actual states well.

3.10 Low Pass Filter for Tachometer

The remaining issue which has not been specifically addressed here is that of low pass filtering of the outer loop tachometer signal measuring $\Omega(t)$. This depends on the necessity of cleaning up this signal and typically, the low pass filter should be at least one decade above the loop crossover frequency which in this case implies low pass filter bandwidth of at least 10 rad/s. This to ensure that too large a phase penalty is not incurred as a result of such a filter. The reason for not including this in simulation here, is that it is really an implementation issue and all we need to bear in mind are the above mentioned guidelines.

3.11 Compensator State Space Model

Refer to figure 3.8.1 and rewrite the open loop state space model of the compensated system such that it is in the form of figure 3.11.1.

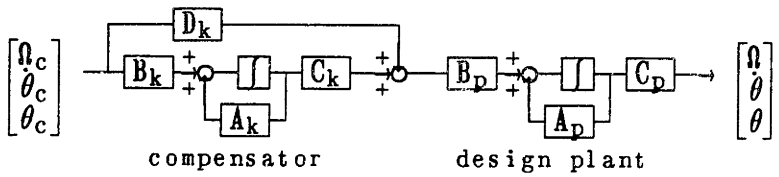

Figure 3.11.1 Cascaded compensator and plant

Define the augmented state for the cascaded system

$x = [x_k \; x_p]^T$, with subscripts k and p referring to the compensator and plant respectively. The state space model for the cascaded system is then for input vector $u(t) = [\Omega_c \; \theta_c \; \dot{\theta}_c]^T$

$$\dot{x}(t) = \begin{bmatrix} A_p & 0 \\ B_p C_p & A_p \end{bmatrix} x(t) + \begin{bmatrix} B_k \\ B_p D_k \end{bmatrix} u(t) \qquad 3.11.1$$

With output

$$y(t) = [\, 0 \quad C_p \,] x(t)$$

Reordering the states of the open loop state space description of equation 3.8.1 for the state vector $x_{fs} = [x_c \; \hat{x}_{lr} \; x_{lr} \; \Omega]^T$ and writing the model with all feedback loops open (with superscript $\hat{}$ referring to the Kalman filter)

$$A = \begin{bmatrix} A_c & 0 & 0 & 0 \\ \hat{B}_{lr} C_c & [\hat{A}_{lr} - \hat{B}_{lr} g_{lr} - H_{kf} \hat{C}_{lr}] & 0 & 0 \\ B(1,1) C_c & -B(1,1) g_{lr} & A(1,1) & A(1,2:3) \\ B_{lr} C_c & -B_{lr} g_{lr} & 0 & A_{lr} \end{bmatrix}$$

$$B = \begin{bmatrix} B_c K & 0 \\ \hat{B}_{lr} D_c K & -H \\ B(1,1) D_c K & 0 \\ B_{lr} D_c K & 0 \end{bmatrix} \qquad 3.11.2$$

$$C = \begin{bmatrix} 0 & 0 & 1 & 0 \\ 0 & 0 & 0 & C_{lr} \end{bmatrix}$$

Now, equating block partitions of equations 3.11.1 and 3.11.2 the compensator state space model matrices are

$$A_k = \begin{bmatrix} A_c & 0 \\ \hat{B}_{lr}C_c & \hat{A}_{lr} - \hat{B}_{lr}g_{lr} - H_{kf}\hat{C}_{lr} \end{bmatrix}$$

$$B_k = \begin{bmatrix} B_cK & 0 \\ \hat{B}_{lr}D_cK & -H \end{bmatrix}$$

$$C_k = [\, C_c \quad -g_{lr} \,]$$

$$D_k = [\, D_c \quad 0 \,]$$

3.12 Discrete Time System

The controller is to be implemented in digital form and two means of obtaining the discrete time equivalent are described here.

1) The controller state space model of section 3.11 can be written in equivalent discrete time form, for sample period, T

$$x_{t+1} = \Phi\, x_t + \Gamma\, u_t$$

$$y_t = C\, x_t$$

with Φ and Γ determined as

$$\Phi = \exp(A_k T) \qquad \Gamma = \int_0^T \exp(A_k \eta)\, d\eta\, B_k \qquad 3.12.1$$

2) Evaluate the discrete time LQR and Kalman filter gains and substitute these in the compensator state space description of section 3.11, the system component matrices being the discrete time equivalents of the plant model, determined using equations 3.12.1.

The discrete time LQR problem is formulated as minimizing the summation

$$J = \Sigma\{x^T Q\, x + u^T R\, u\}$$

subject to the constraint of the linear system

$$x_{t+1} = \Phi\, x_t + \Gamma\, u_t$$

$$y_t = C\, x_t$$

Where the discrete time (dt) weighting matrices are selected to yield the same time response as the continuous time (ct) design for small sampling period T, as [12],

$$Q_{dt} = Q_{ct} T$$

$$R_{dt} = [R_{ct} + \frac{1}{3} B^T Q_{ct} B T^2] T \qquad 3.12.2$$

with T being the sample period and the continuous time weighting matrices are as determined in section 3.5.2.

In order to introduce minimal effect (phase) due to discretization, the sample period is chosen arbitrarily small as T = 0.01 seconds (or sample rate of 100Hz).

Similarly, the Kalman filter discrete time solution is determined by aid of the duality with the LQR solution, namely

$$Q_{LQR} \Rightarrow \Gamma \Xi \Gamma^T$$

$$R_{LQR} \Rightarrow V$$

Following the approximations of equations 3.12.2 for the discrete time equivalent weightings, get

$$\Xi_{dt} = (\Gamma \Xi \Gamma^T)_{dt} = \Xi_{ct} T$$

$$V_{dt} = [V_{ct} + \frac{1}{3} B_{ct}^T \Xi_{ct} B_{ct} T^2] T$$

Using these transformations with the discrete time models yields the same inner loop LQG time domain performance controller.

The remaining discretization is that of the lag network. The simplest means of discretizing here, is to write the state space model for the lag network and discretize using equations 3.12.1.

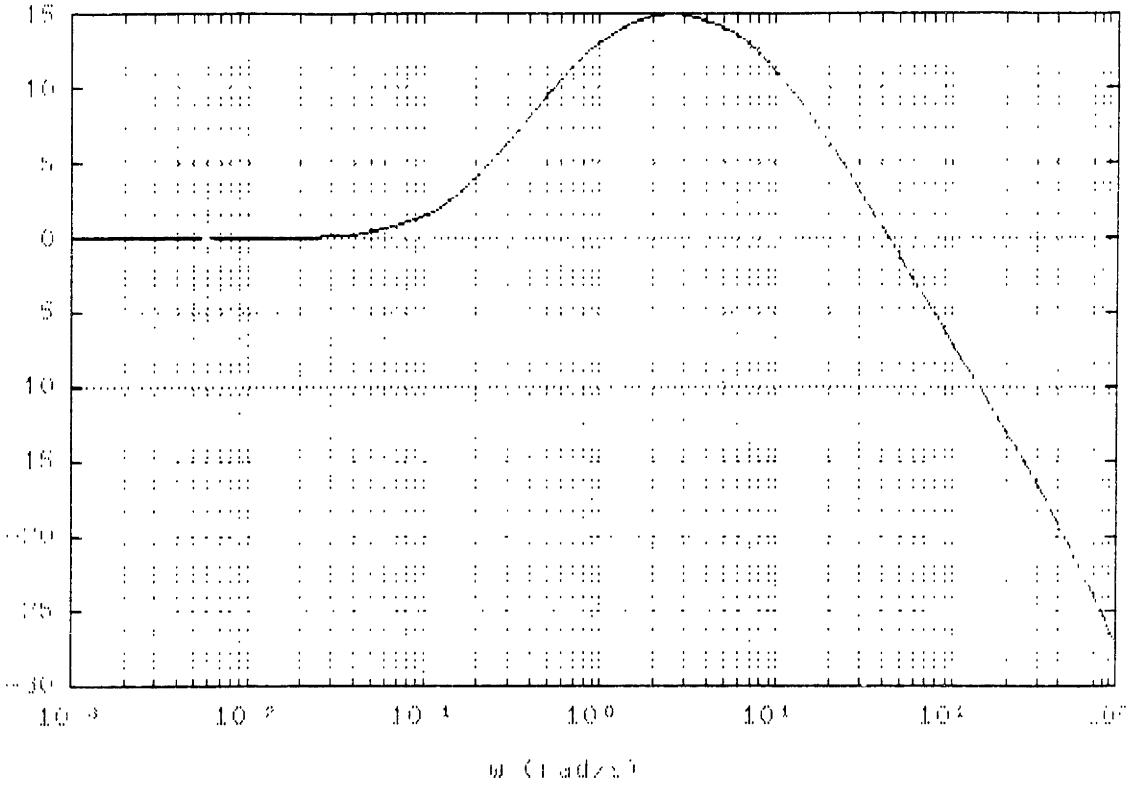

Figure 3.1.1a. LQG/LTR design closed loop Bode plot. Single sensor measuring wheel angular velocity and actuation by wheel torque motor. The poor resonance is a result of the non minimum-phase zero and the fact that in order to fit the LQG/LTR design methodology (defined for square systems) only one state can be measured. For this difficult design problem, we wish to use as much sensor data as possible and thus not discard sensors.

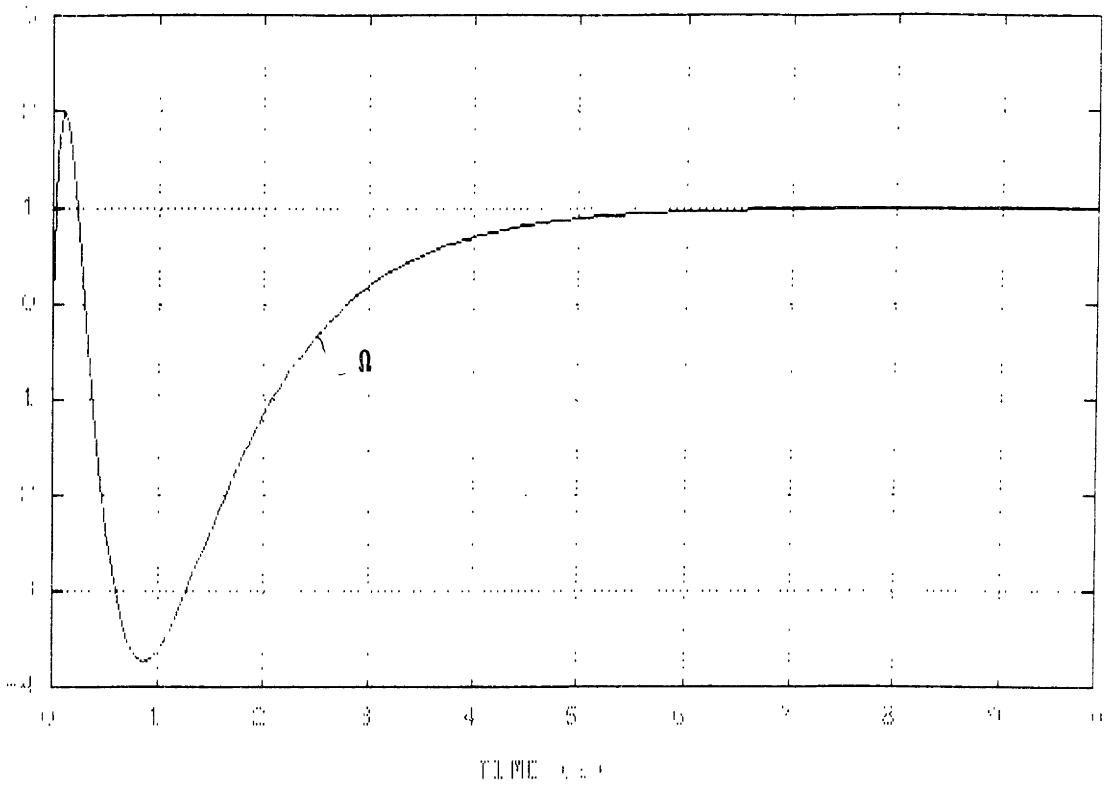

Figure 3.1.1b. LQG/LTR design wheel speed response to step command. The performance is undesirable in the large undershoot. This may certainly be improved if additional sensors are employed.

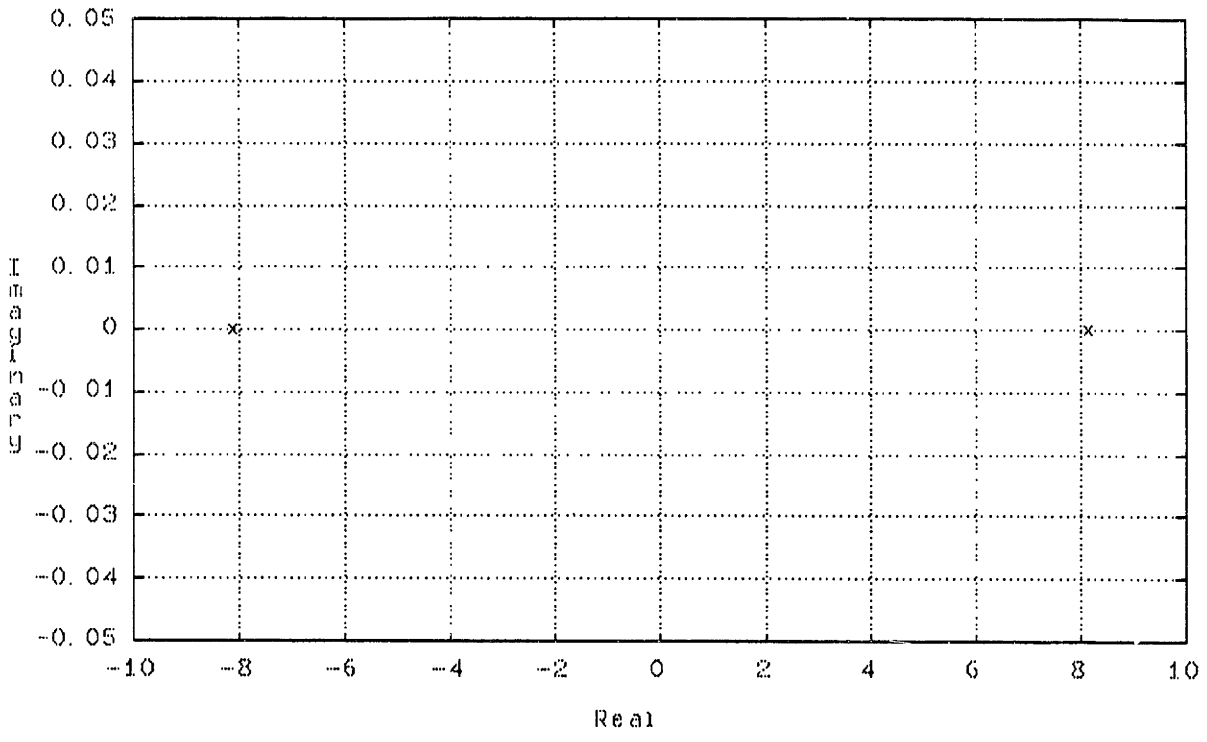

Figure 3.5.2.1 S-Plane plot of open loop reduced order model with system states pitch angle (θ) and pitch rate ($\dot{\theta}$). Using root square locus reasoning, the LQ regulator solution ('expensive control') will place the unstable pole at its mirror image about the imaginary axis. Using cheap control moves one pole closer to the origin, reducing dominant mode frequency.

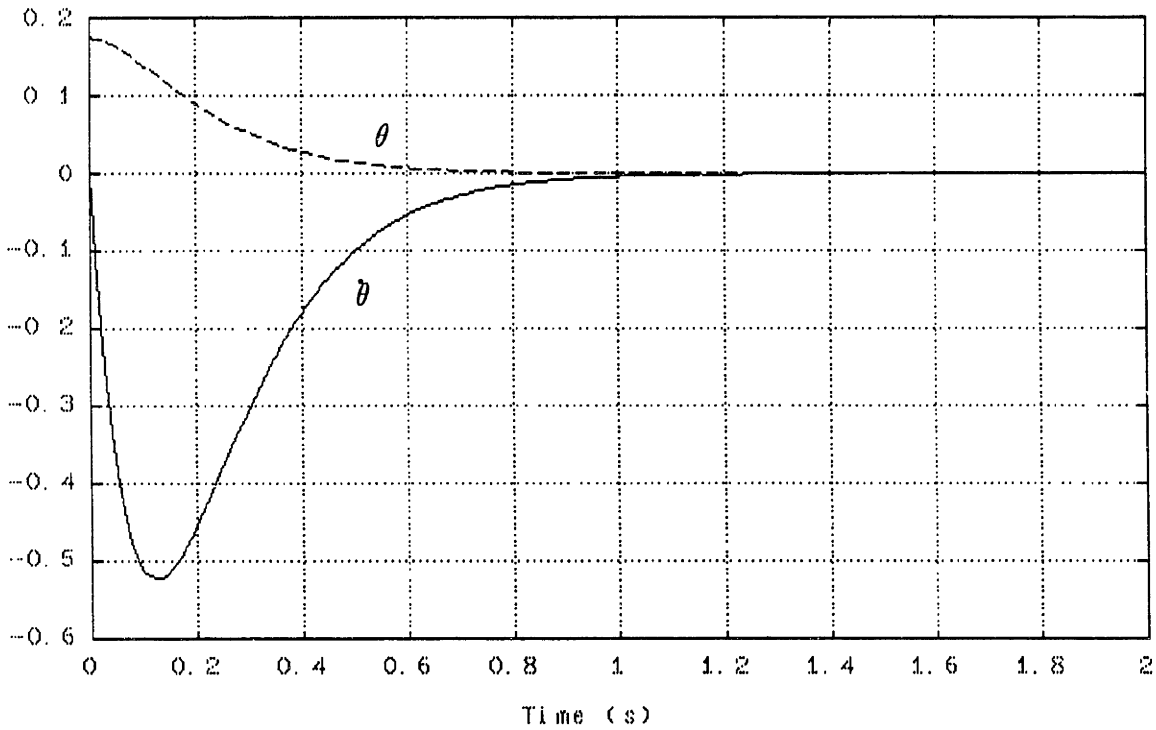

Figure 3.5.2.2. Two state LQ regulator response to initial pitch error of 10^{o} illustrating desirable performance. Units are rad (θ) and rad/s ($\dot{\theta}$). This regulator forms the controller inner loop, but is implemented in typical LQG fashion with a Kalman filter to assist in obtaining good state information with noisy sensors.

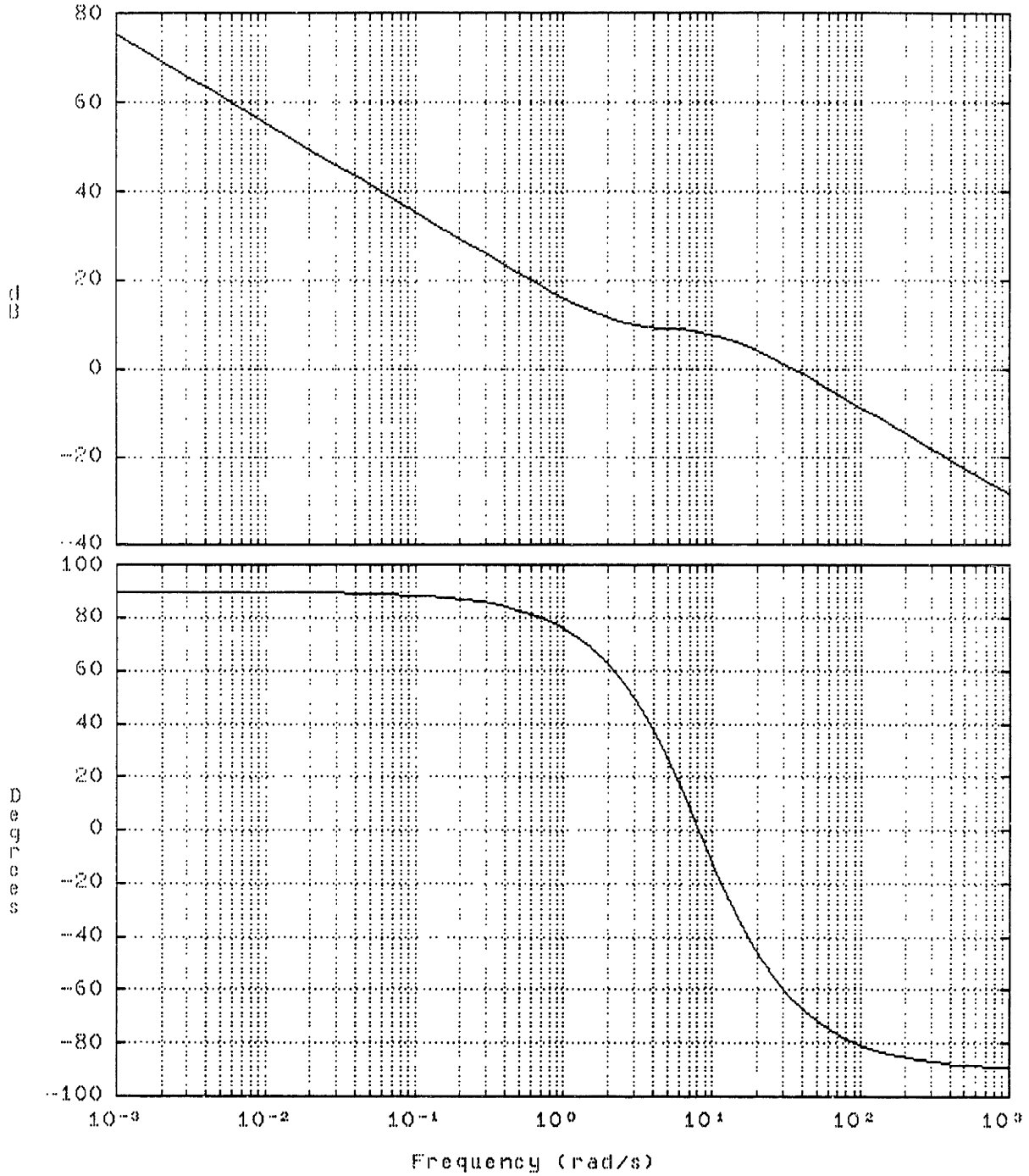

Figure 3.6.1a & b. Bode magnitude and phase plots. Loop transfer function relating motor torque to wheel angular velocity (Ω). The two state inner regulator loop is closed, but does not include a Kalman filter yet. The phase plot is shifted by 180° and clearly illustrates that the non minimum-phase zero phase effect is canceled by the minimum-phase zero at the same frequency.

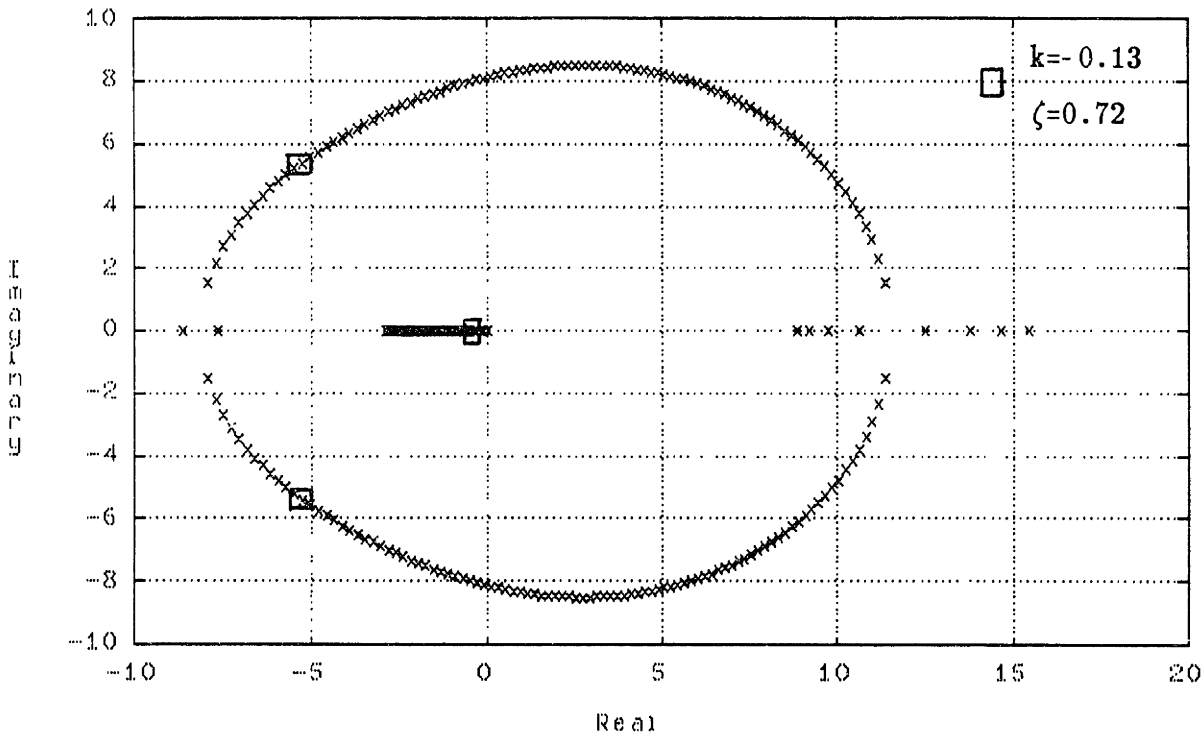

Figure 3.6.2. Negative gain root locus for feedback of wheel speed to motor torque. Note that since the single actuator is used for both inner loop regulation and outer loop control, the inner loop poles move with closing of the outer loop. For good damping (ζ=0.72) of the oscillatory poles, k=-0.13 is selected, but this results in the real pole being of too low frequency. Use of a classical lead-lag network is made to remedy this.

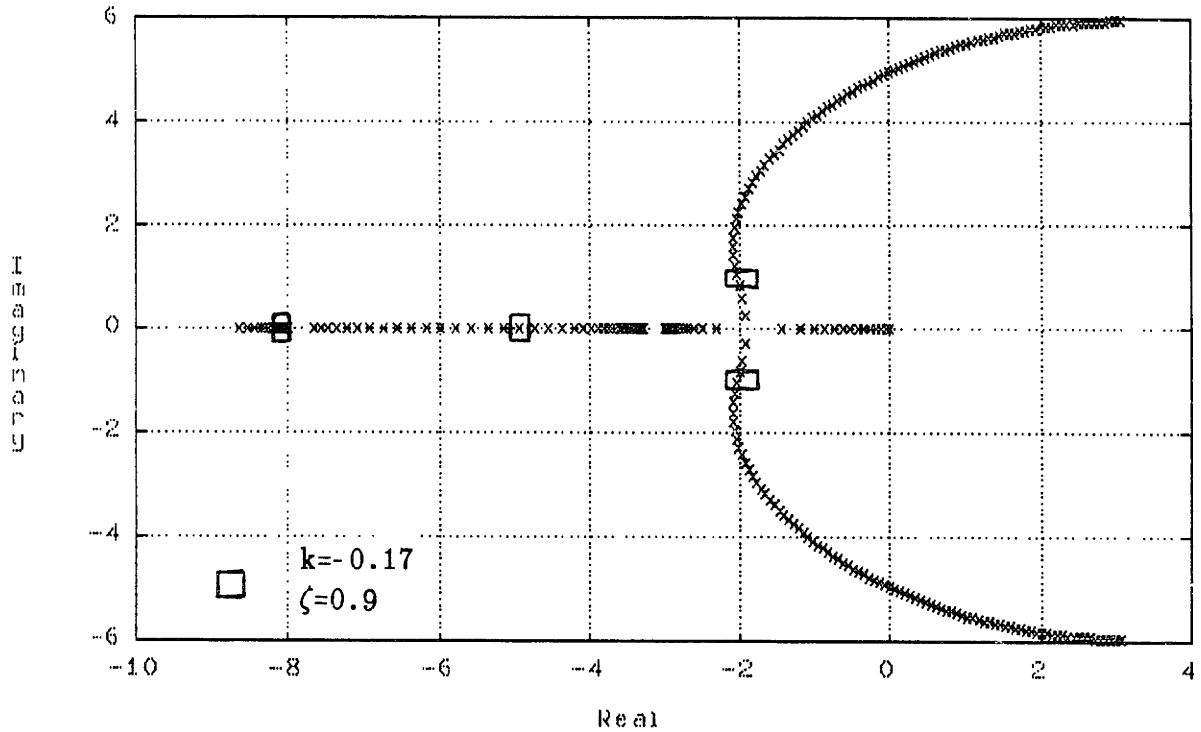

Figure 3.6.3. Root locus closing wheel speed control loop. Lag-lead network included shows improvement of dominant (oscillatory) mode bandwidth for gain of k=-0.17, exhibiting damping of ζ=0.9.

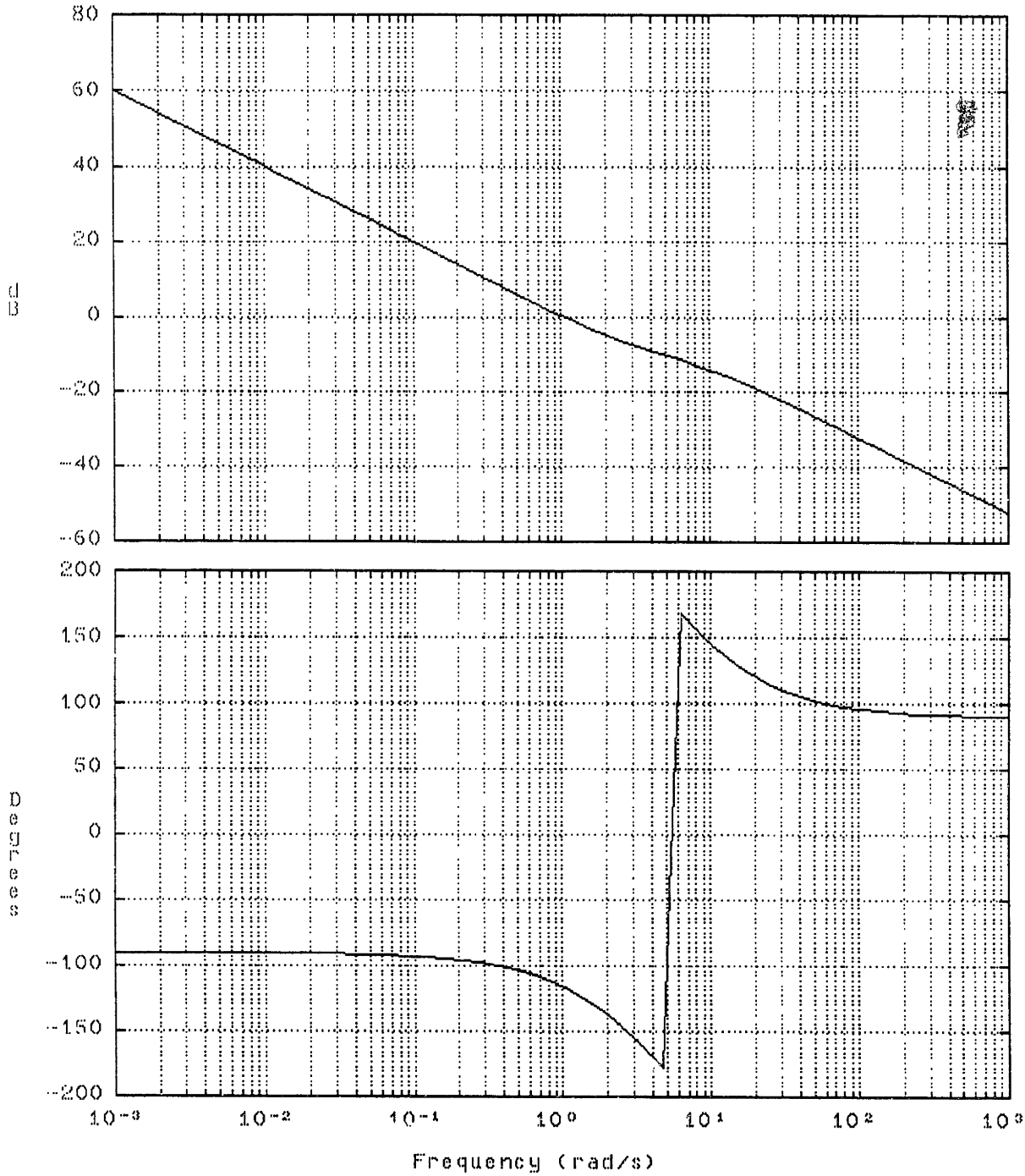

Figure 3.6.4. Bode magnitude and phase plots for lag-lead compensated wheel speed loop transfer function. Comparing this with figure 3.6.1 shows improved loop shape as well as phase. For phase margin of 60°, the crossover frequency is selected at around 1 rad/s.

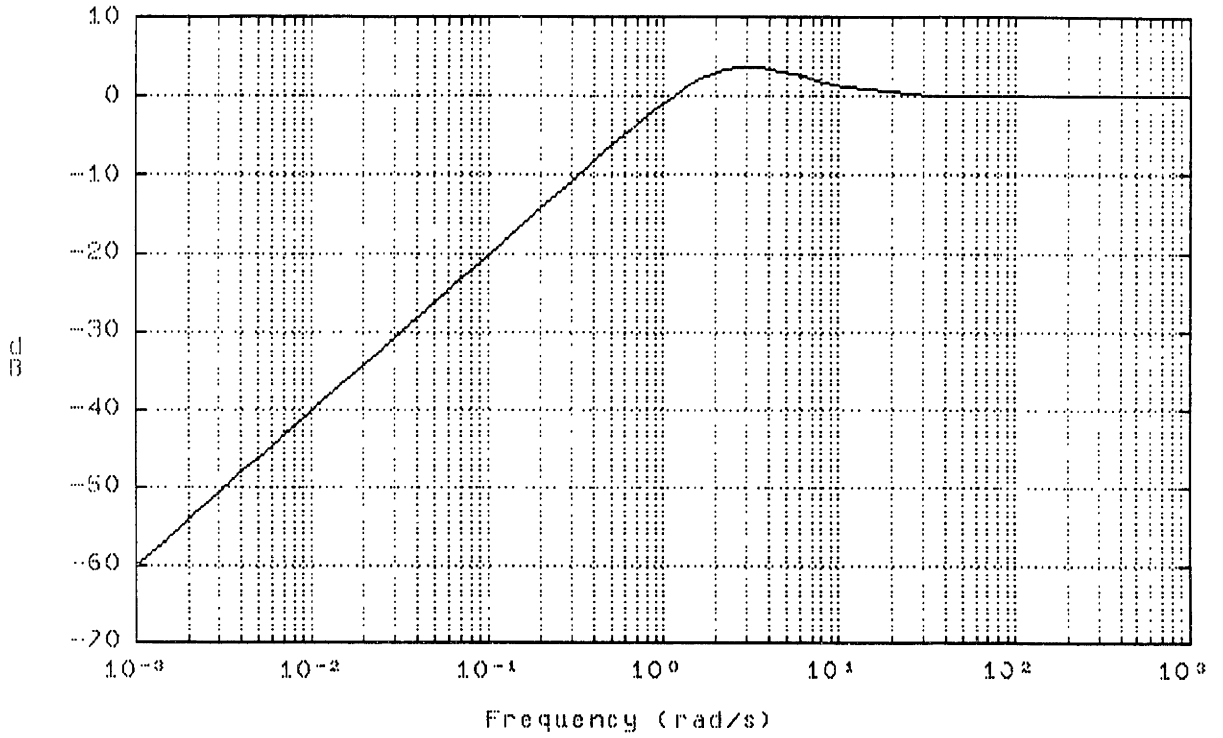

Figure 3.6.5. Wheel speed loop sensitivity relating output disturbance to system output. Amplification of output disturbances occur between 1.4 and 30 rad/s due to non minimum-phase zeros.

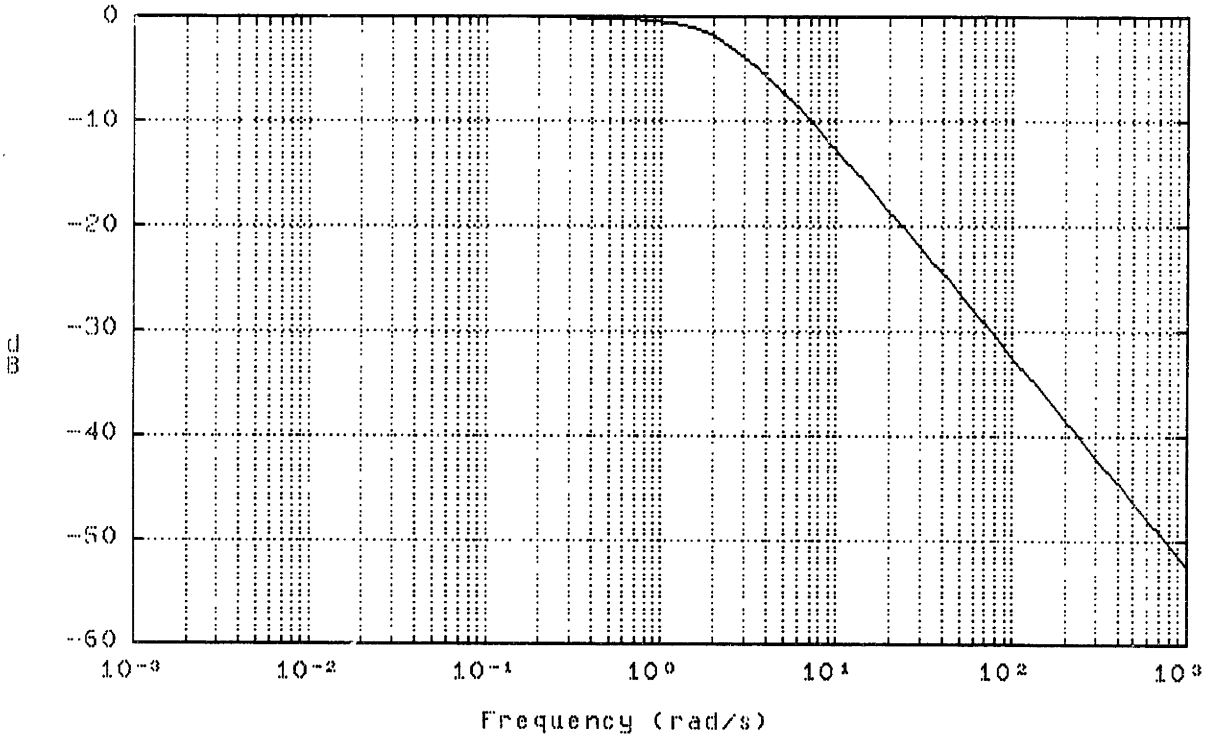

Figure 3.6.6. Bode magnitude plot for wheel speed loop closed. Compare with figure 3.1.1.

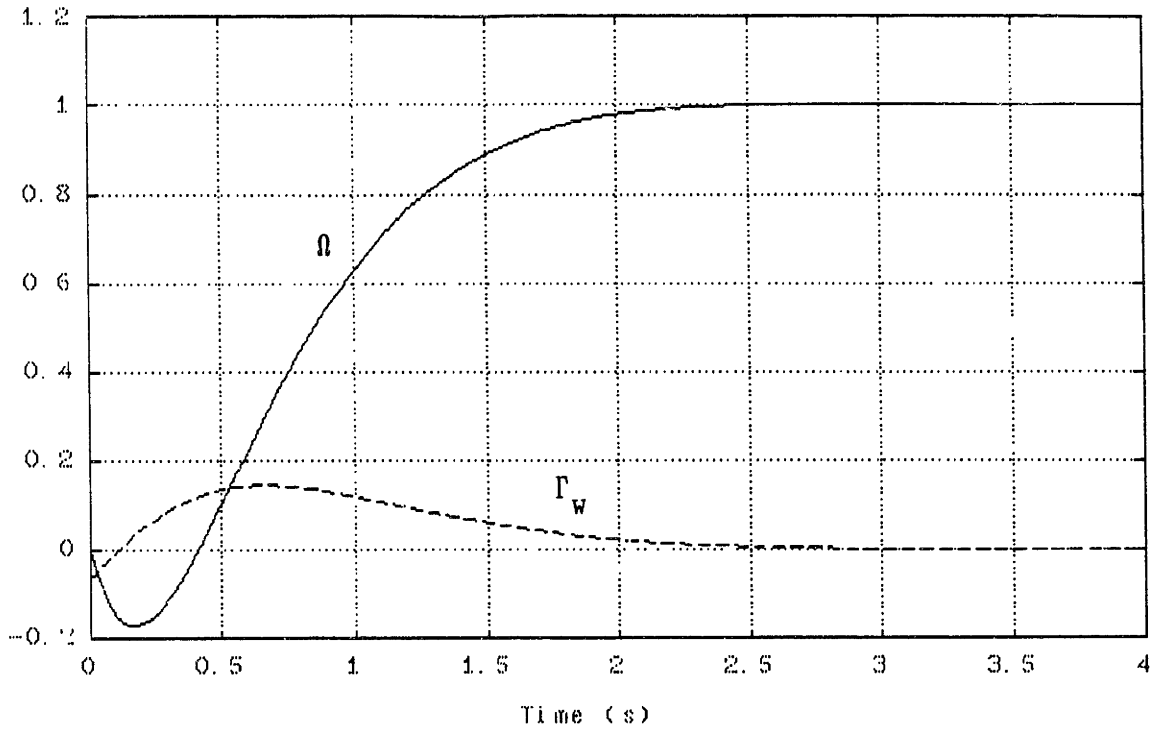

Figure 3.6.7a. Closed loop wheel speed (rad/s) and actuator (Nm) response to step command. The improvement in using sensors for all states is clear in comparison between this and figure 3.1.2.

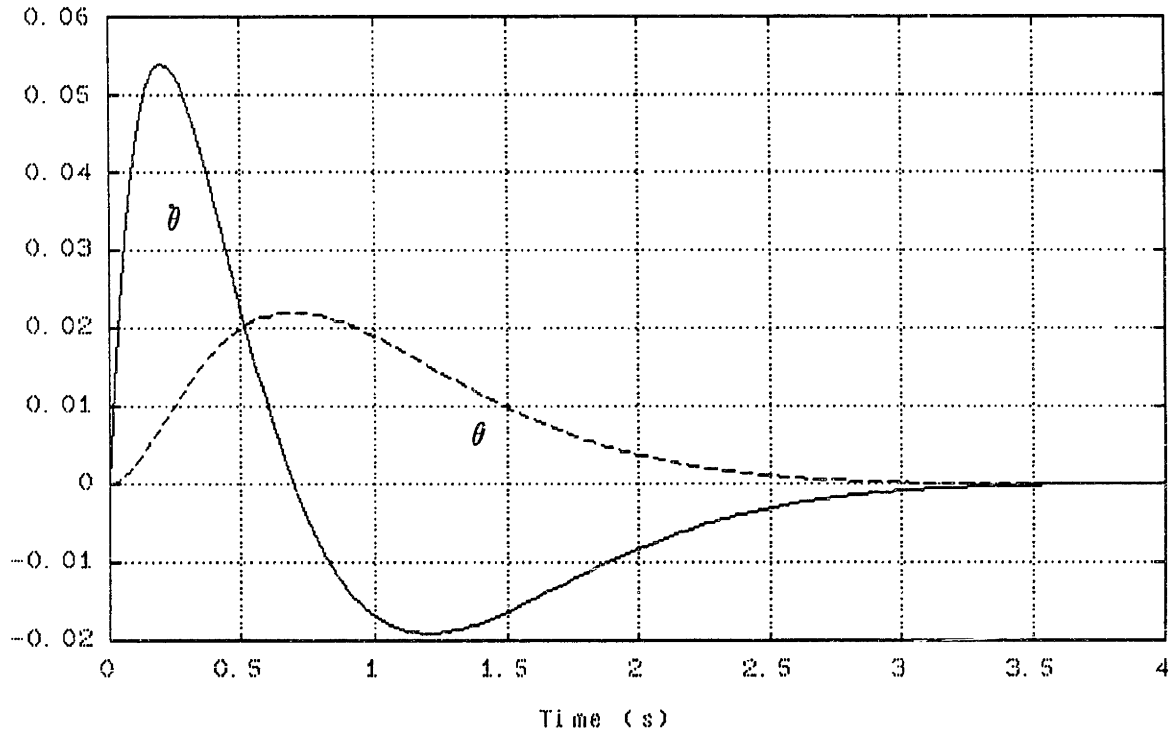

Figure 3.6.7b. Pitch angle and pitch rate response to step wheel speed command. Units in radians and rad/s respectively.

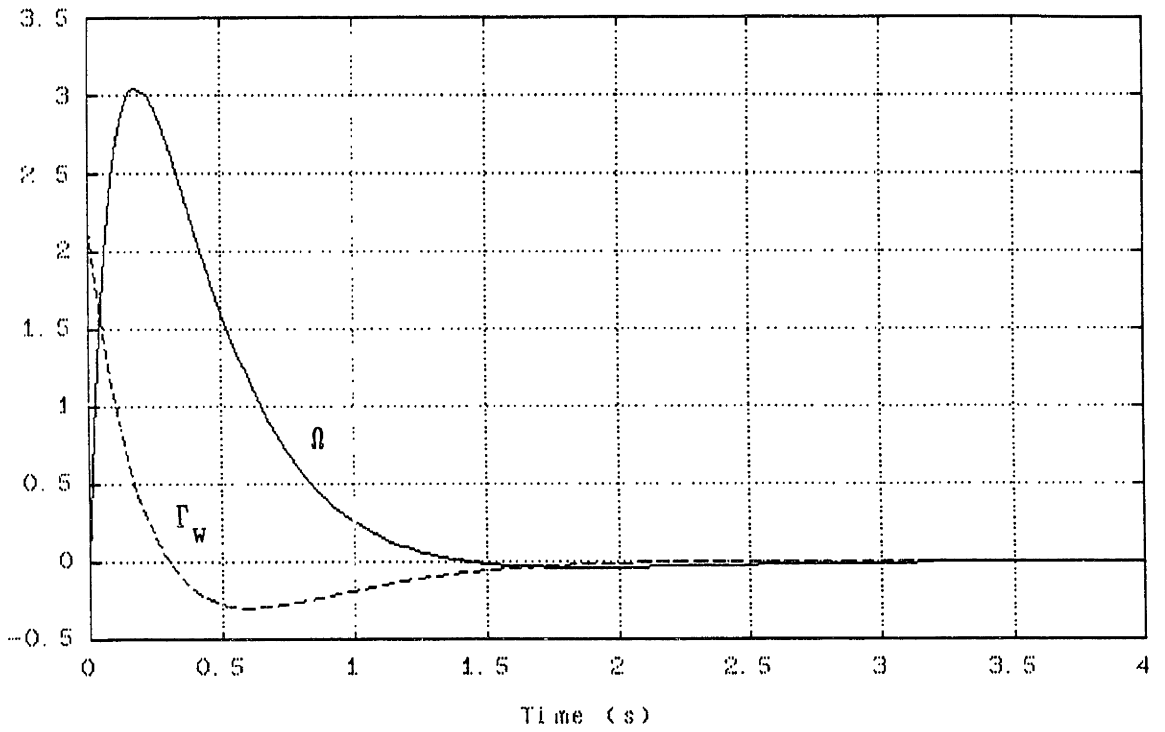

Figure 3.6.8a. Wheel speed (rad/s) and actuator (Nm) response to initial pitch error of 10°.

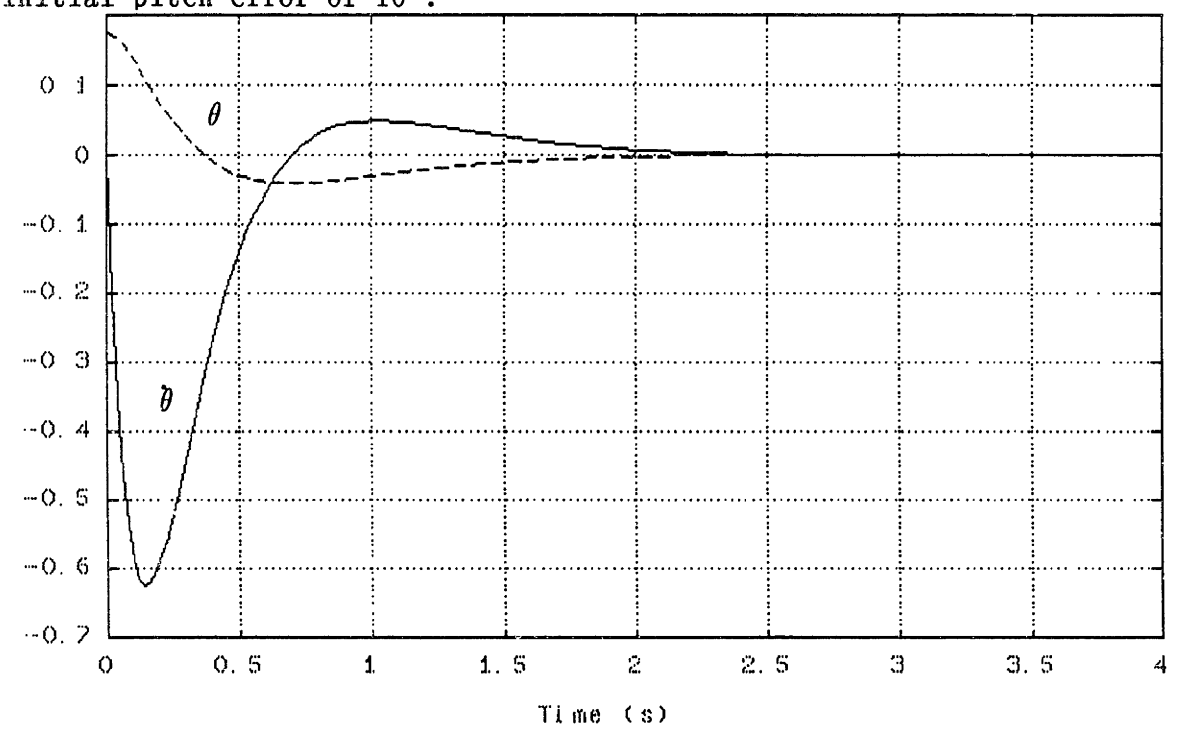

Figure 3.6.8b. Pitch angle and rate response. Comparison with figure 3.5.2.2 shows the effect of the outer loop compensation on the inner loop performance resulting from the single actuator being used to compensate two different bandwidth functions.

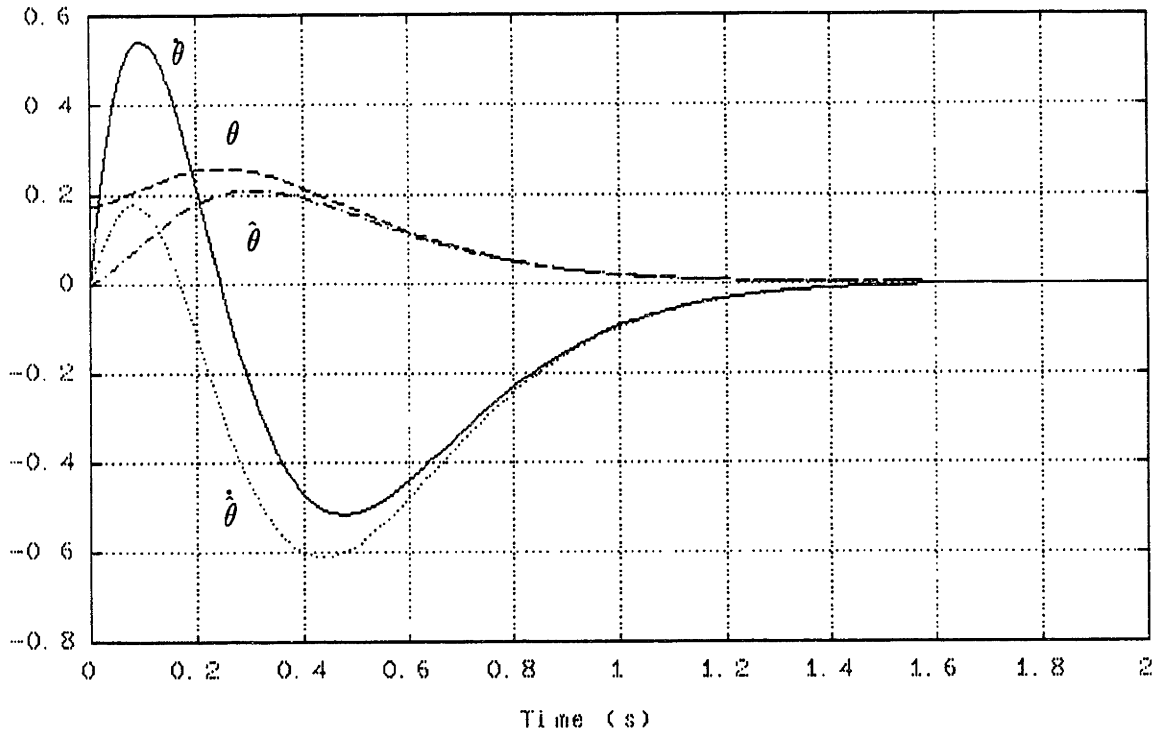

Figure 3.7.2. LQG inner loop (including Kalman filter) response to initial pitch error of 10°. Plotted are filter states $\dot{\hat{\theta}}$ and θ, as well as actual states $\dot{\theta}$ and θ (in units rad/s and rad respectively). The filter states do well in tracking the actual states and the degradation in performance by inclusion of the Kalman filter is minimal as is apparent in comparison with figure 3.5.2.2.

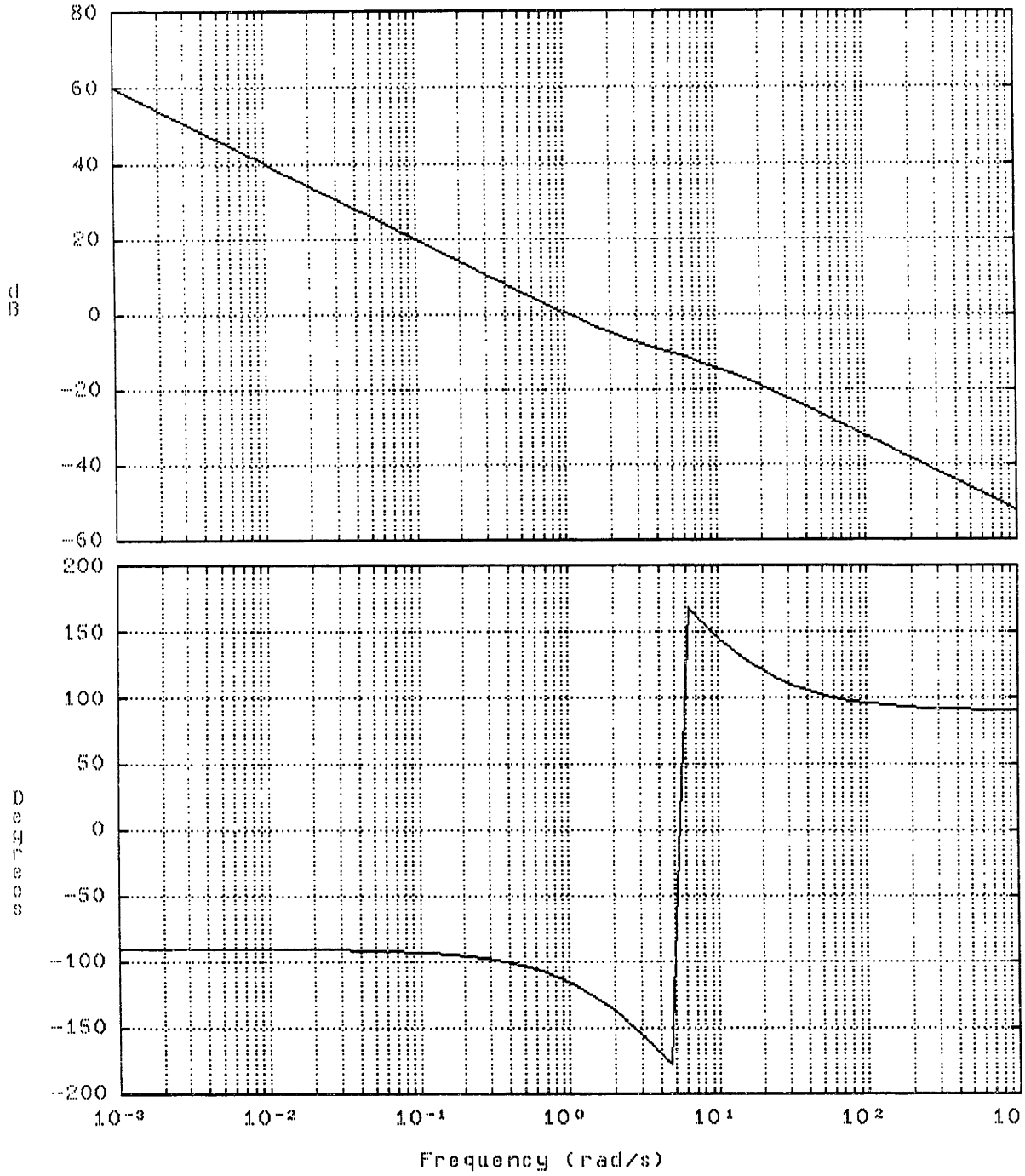

Figure 3.8.2. Bode magnitude and phase plots relating commanded wheel speed to actual wheel speed. This includes the inner LQG regulator loop closed. Comparison with figure 3,6,4 shows that the outer loop as structured is independent of the inner loop Kalman filter.

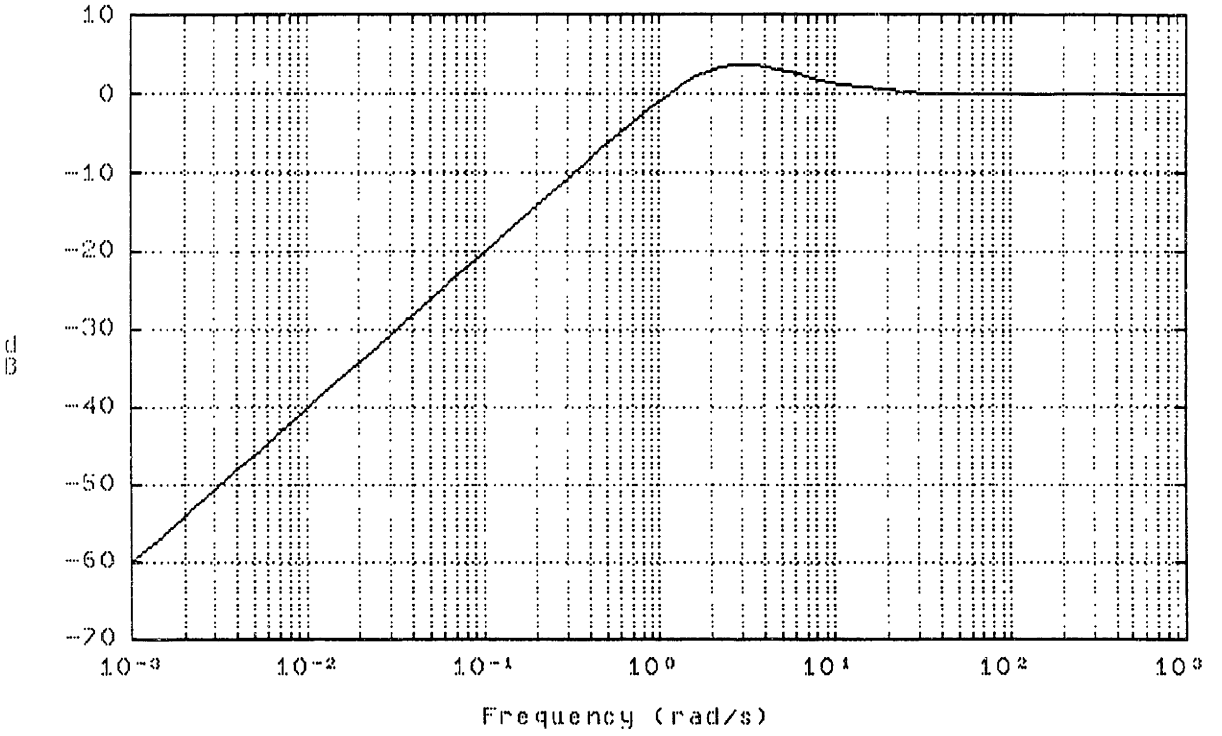

Figure 3.8.3a. Loop sensitivity plot. Inner LQG loop closed.

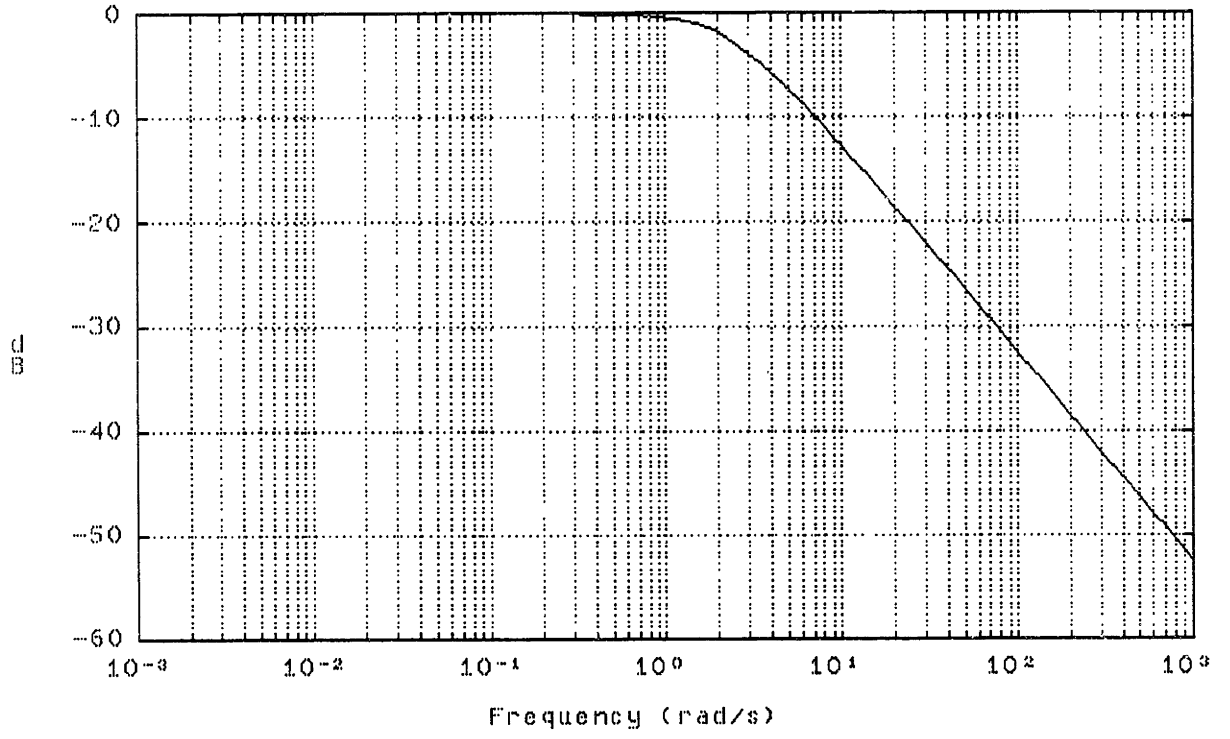

Figure 3.8.3b. Closed loop Bode magnitude plot. Inner LQG loop closed.

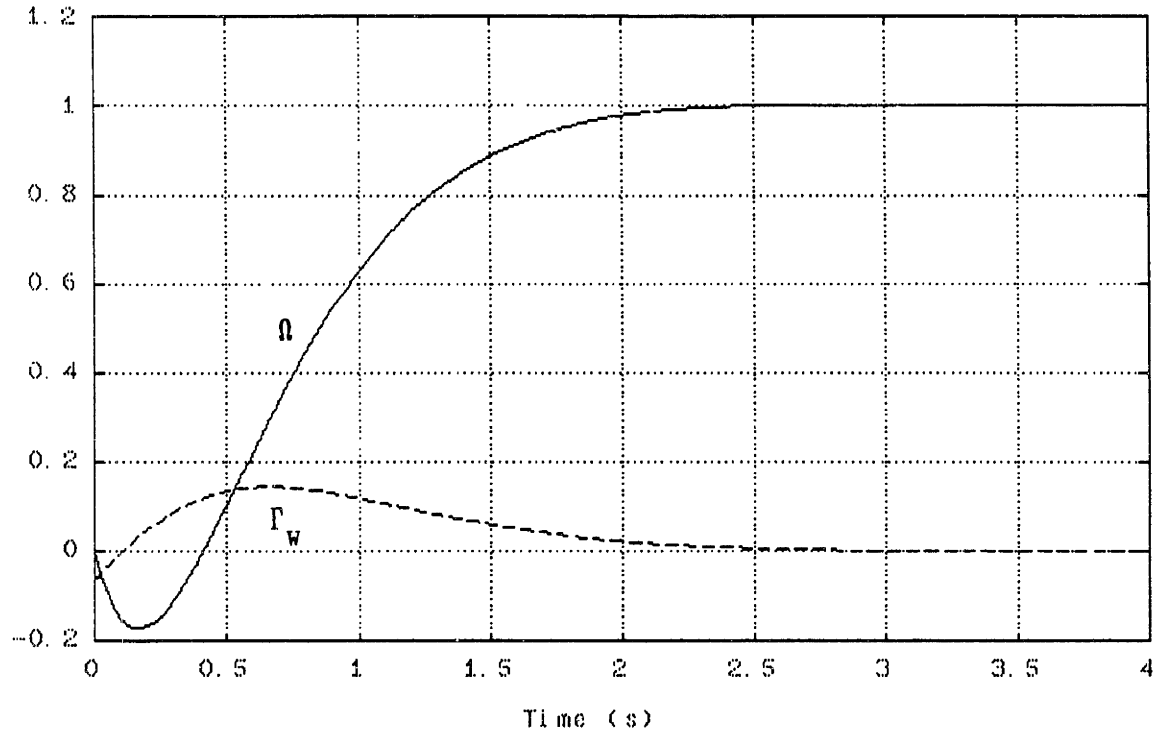

Figure 3.8.4a. Closed loop wheel speed and actuator response to step wheel speed command. Figures 3.8.4a and 3.8.4b represent the system including LQG inner loop closed and outer loop compensated system. These compare well with figure 3.6.7, illustrating the independence of the outer loop on the inclusion of the Kalman filter in the inner loop.

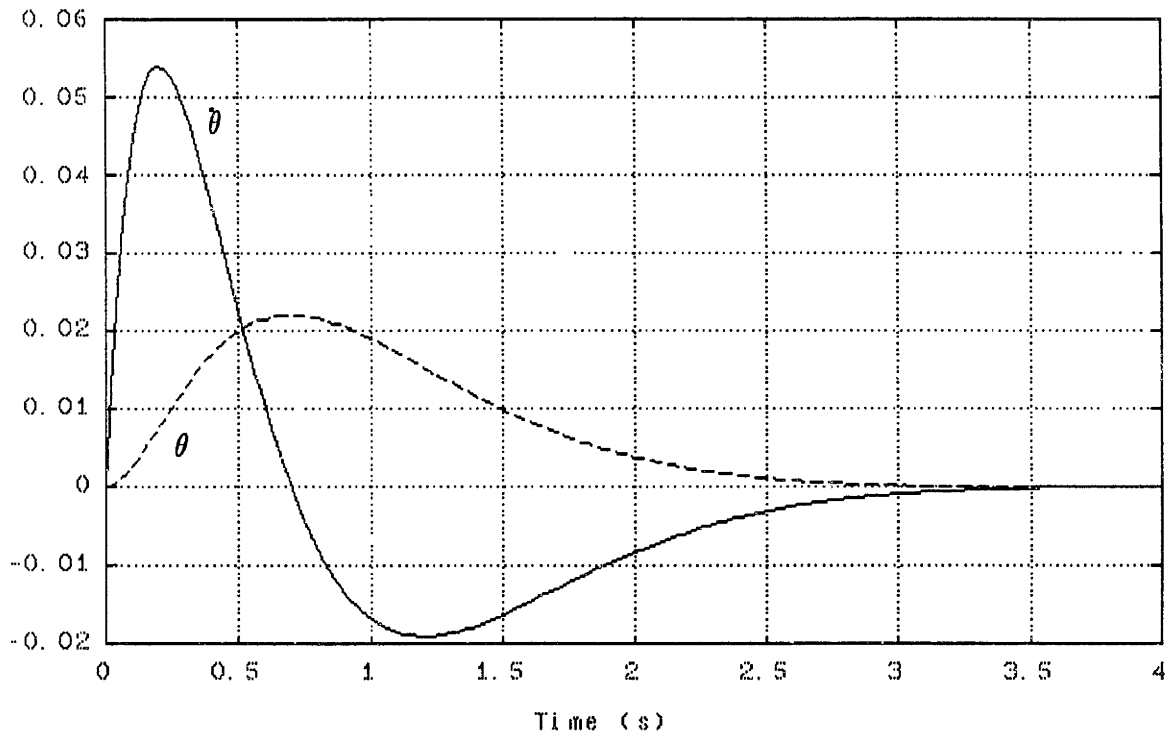

Figure 3.8.4b. Closed loop pitch angle and pitch rate response to step wheel speed command. Units are radians and rad/s respectively.

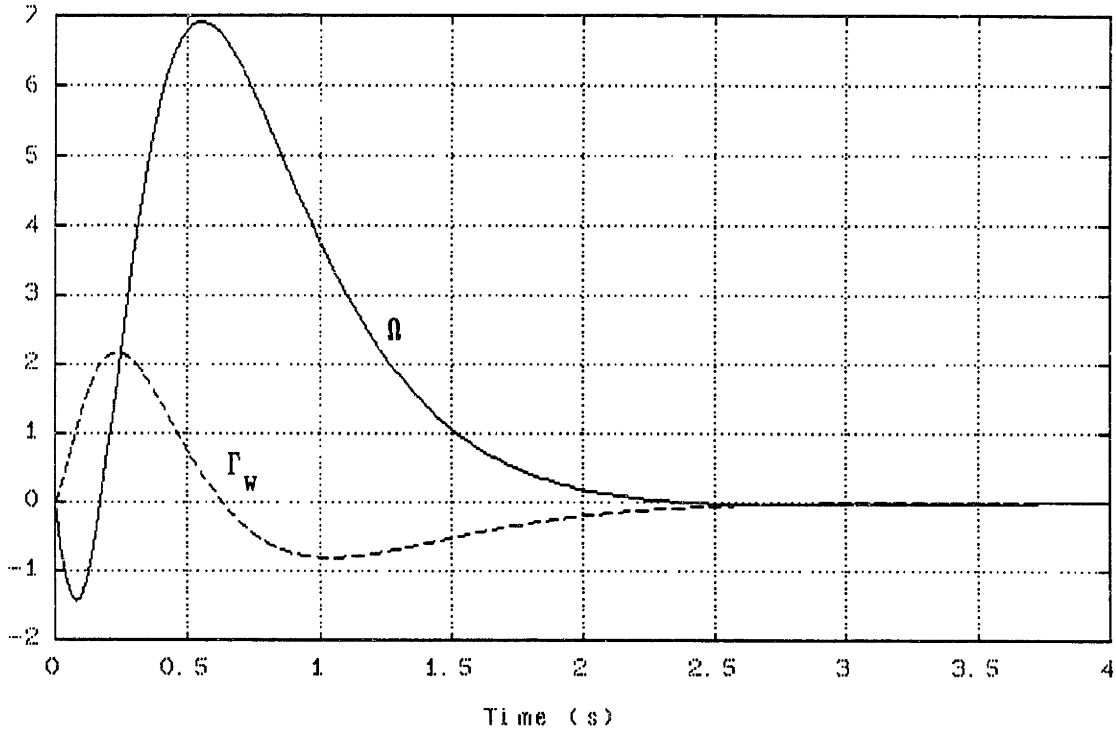

Figure 3.9.2a. Full Closed loop system including LQG inner loop, wheel speed and actuator response to initial pitch angle error of 10°. This for comparison with figure 3.6.8. The effect of the filter is apparent here, since this is effectively inner loop control activity (regulation), as opposed to outer loop command following. In a sense the loop transfer function here is from the desired pitch angle and pitch rate (both desired regulated to zero) to to the actual system outputs, and the filter dynamics show up in this relation.

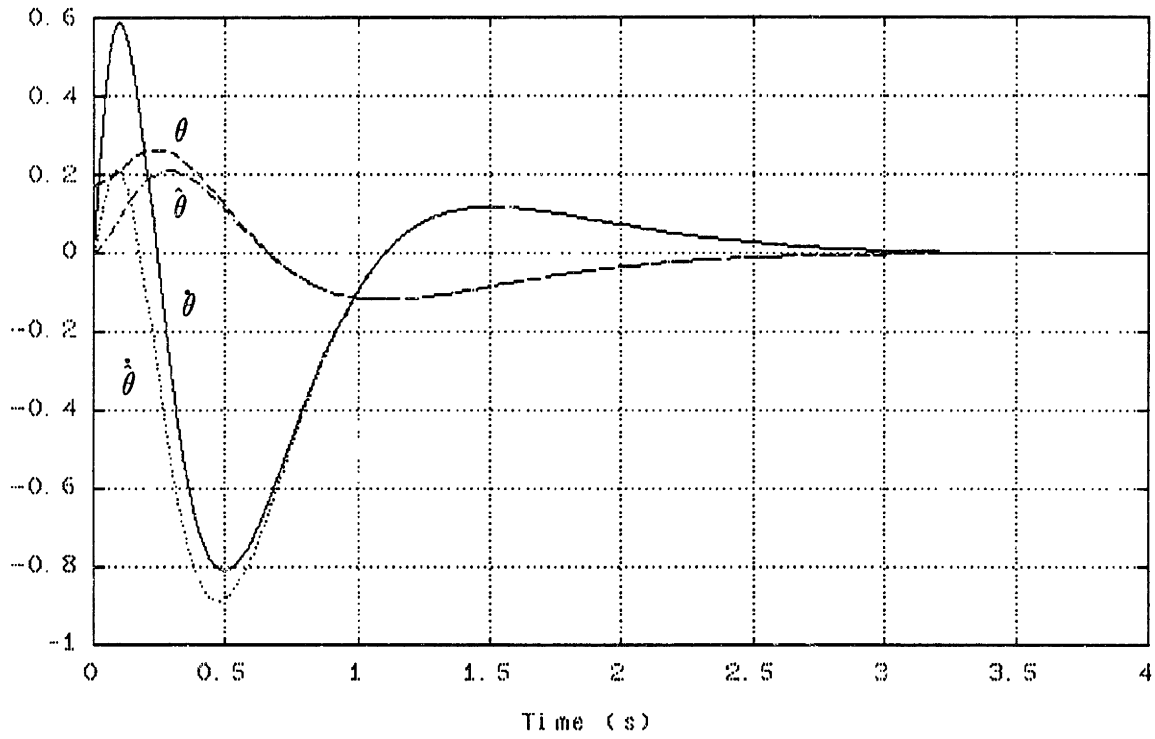

Figure 3.9.2b. Filter estimates and actual pitch angle and pitch rate response. Units are radians and rad/s respectively.

4.0 LATERAL CONTROL DESIGN

4.1 Introduction

The decoupled open loop lateral model is analyzed in this section and the characteristic modes determined. The lateral controller is defined and simulation results are shown to demonstrate the performance of the linear controlled system.

As shown in appendix 1, the lateral and longitudinal systems decouple for zero reference angular velocity of the turntable. Due to the non minimum-phase nature of the lateral system, an unusual implementation of an LQG type structure is used, as in the longitudinal controller. An algebraic proof for a single input single output system as well as multi input multi output systems is given in appendix 2 as justification for the specific result obtained in this structure.

4.2 Open Loop Lateral Dynamics Model

The lateral system state space model as derived in appendix 1 is repeated here for the state vector $x=[\dot{\varphi}\ \varphi\ \dot{\psi}\ \dot{\eta}]^T$ and control input vector $u=[\Gamma_t\ \ F\ ]^T$, where Γ_t and F are turntable torque and friction respectively. A description of the friction model is given in section 6.2. In this chapter, we ignore these nonlinear friction effects, but include viscous friction in yaw (see the term $-f_{\dot{\psi}}$ in stiffness matrix), in the linear

controller design. The linear controller forms a structure for generating the correct commands for stabilization, but is to be implemented in a nonlinear bang-bang form as discussed in Chapter 6.

For the lateral system equations

$$\mathbf{M}\,\ddot{x}(t) + \mathbf{K}\,x(t) + B_u u(t) = 0$$

with

$$\mathbf{M} = \begin{bmatrix} \begin{bmatrix} -(m_w r_w^2 + m_f(r_w + r_f)^2 + I_1^W) \\ -(m_t(r_w + l_t)^2 + I_1^F + I_1^T) \end{bmatrix} & 0 & 0 & 0 \\ 0 & -1 & 0 & 0 \\ 0 & 0 & -(I_3^W + I_3^F + I_3^T) & -I_3^T \\ 0 & 0 & -I_3^T & -I_3^T \end{bmatrix}$$

$$\mathbf{K} = \begin{bmatrix} 0 & \begin{bmatrix} (m_w r_w + m_f r_f)g \\ +(m_f r_w + m_t(r_w + l_t))g \end{bmatrix} & \begin{bmatrix} r_w(m_w r_w + m_f(r_w + r_f))\Omega_o \\ +(r_w m_t(r_w + l_t) + I_2^W)\Omega_o \end{bmatrix} & 0 \\ 1 & 0 & 0 & 0 \\ -I_2^W\Omega_o & 0 & -f_{\dot{\psi}} & 0 \\ 0 & 0 & 0 & 0 \end{bmatrix}$$

(Note that the viscous friction coefficient $f_{\dot{\psi}}$ is positive)

$$B_u = \begin{bmatrix} 0 & 0 \\ 0 & 0 \\ 0 & 1 \\ -n_t & 0 \end{bmatrix}$$

Notice that the implication of the actuation being a reaction wheel type of input is the state $\dot{\psi}$ is not directly influenced by input torques to the turntable, but via the state $\dot{\eta}$. This could obviously be rewritten, eliminating the turntable angular velocity state by substitution of the $\ddot{\eta}$ equation into that for $\ddot{\psi}$. This is, however, unnecessary since in arriving at the state space form, multiplication of the inverse of the mass matrix with the control distribution matrix, B_u gives the correct distribution of input torques to the frame and turntable.

The state space form is determined as

$$\begin{aligned} \ddot{x}(t) &= -M^{-1}K\, x(t) - M^{-1}B_u u(t) \\ &= A\, x(t) + B\, u(t) \end{aligned}$$

Using the parameters for the model as in appendix 3 and nominal wheel speed of 2 rad/s yields the following numerical values for the state space model

$$A = \begin{bmatrix} 0 & 10.9 & 0.45 & 0 \\ 1 & 0 & 0 & 0 \\ -0.21 & 0 & 0.064 & 0 \\ 0.21 & 0 & -0.064 & 0 \end{bmatrix}$$

$$B = \begin{bmatrix} 0 & 0 \\ 0 & 0 \\ 94.7 & 2.63 \\ -154.7 & -2.63 \end{bmatrix}$$

Note that the friction F (see figure 6.2.1) is modeled as a negative quantity, since it is an external force which opposes rotation of the frame. Since we measure all states, the measurement matrix is

$$C = I_{4\times4} \qquad (I_{4\times4} \equiv 4\times4 \text{ identity matrix})$$

4.3 Controllability and Observability

4.3.1 Observability

Evaluation of the observability matrix given by

$$O_b = [C^T \quad A^T C^T \ldots\ldots\ldots\ldots (A^T)^{n-1} C^T] \qquad (n \equiv \text{system order})$$

and checking the rank of O_b shows it to be full rank, as could be expected, since we measure all states. The system is

completely observable.

4.3.2 Controllability

In this section we evaluate the controllabilty of the system with all friction effects ignored.

The controllability of the system can be evaluated in a number of ways. We use firstly the modal form to determine reachability of each mode from turntable torque and secondly check for rank deficiency of the controllability matrix C_c where, for the system matrices as defined in 4.1

$$C_c = [B \quad AB \cdots\cdots A^{(n-1)}B] \qquad n \equiv \text{order of system}$$

The modal form of the state response to forced input is determined as [4]

$$x(s) = \sum_{k=1}^{m} [sI - A]^{-1} u_k(s)$$

$$= \sum_{i=1}^{n} \sum_{k=1}^{m} \frac{1}{(s - \lambda_i)} v_i w_i^T u_k(s)$$

where v_i and w_i^T are right and left eigenvectors respectively of the open loop system associated with the i'th eigenvalue λ_i and $u_k(s)$ is the Laplace transform of the k'th input.

Evaluation of this (modal) form using standard eigen analysis software (MATLAB or $MATRIX_x$) indicates (erroneously) that all modes are controllable from the single input Γ_t, the turntable torque, which might lead one to believe that the system is completely controllable, whilst the first method shows the controllablity matrix C_c to be of reduced rank and hence the system to be not completely controllable.

The modal form result is counter intuitive, since it is clear that in a frictionless system using 'reaction wheel' actuation, it is impossible to control both the action and reaction independently. It is only possible to obtain a desired action and the reaction has to be within the constraints of the system and thus dependant directly on the action.

This is a typical problem encountered in solving for the eigenstructure of a system having repeated eigen values. The solution to the posed eigenvalue problem, for example the left eigenstructure problem

$$[\lambda_i I - A]v_i = 0$$

where λ_i is one of a set of repeated eigenvalues, yields an n-dimensional plane as the solution to this linear algebra problem which is clearly not correct for a physical system. The correct solution is easily determined using standard software by 'fooling' the software and perturbing one of the state space

A-matrix parameters slightly (on the order of 10^{-3} perturbation). This yields the correct eigenvector solution.

The important result is that the system is not completely controllable if no friction is modeled. Including yawing friction (viscous friction) between the tyre and the surface yields a completely controllable system as intuitively expected since this changes the means of actuation to be no longer reactionary.

This result also yields insight into how to independently control the turntable speed in a low bandwidth sense i.e. impose a restraining torque which is always much less than the stiction, to retard rotation of the turntable which might arise due to control.

4.4 Open Loop Plant Dynamics

The eigenstructure of the open loop plant below shows the presence of an integrator, an unstable-stable pair of equal frequency and a low frequency stable pole. The eigenvalues and eigenvectors of these modes are as follows

$$\lambda_1 = -3.29 \qquad v_1 = \begin{bmatrix} 0.95 \\ -0.29 \\ 0.06 \\ -0.06 \end{bmatrix}$$

$$\lambda_2 = 3.29 \qquad v_2 = \begin{bmatrix} 0.95 \\ 0.29 \\ -0.06 \\ 0.06 \end{bmatrix}$$

$$\lambda_3 = -0.065 \qquad v_3 = \begin{bmatrix} 0.002 \\ 0.03 \\ -0.71 \\ 0.71 \end{bmatrix}$$

$$\lambda_4 = 0.0 \qquad v_3 = \begin{bmatrix} 0.0 \\ 0.0 \\ 0.0 \\ 1.0 \end{bmatrix}$$

Closer examination of the mode shapes indicates that the two poles at -3.29 and +3.29 rad/s respectively represent the inverted pendulum effect in roll. The pole at -.065 is representative of the yawing motion of the unicycle and is not a pure integrator since we have included viscous friction in the yawing equation of motion. In forced motion. the ratio of turntable to frame rotation rate is determined by the inertia ratio of these two elements, since we have not modeled any friction effects between the turntable and the frame. The integrator represents purely the rotation of the turntable independant of the frame, again since we have not modeled friction effects between these two elements this is

not a stable pole.

4.5 Root Locus as Function of Wheel Angular Velocity

The lateral dynamics are strongly dependant on the angular velocity of the wheel by means of the gyroscopic coupling between roll and yaw which arises when the forward rolling wheel undergoes yawing or rolling motion. This is demonstrated in figure 4.5.1 which shows the s-plane location of the open loop lateral system dynamics as a function of wheel angular velocity.

As is shown later, this effect necessitates implementation of a gain scheduled control algorithm in order to account for the linear controller not being able to control the system adequately at wheel velocities differing significantly from the design value so that a time varying (parameter dependant) control structure is necessary. This is discussed further in chapter 5.

4.6 Transmission Zeros

As we wish to control only the heading of the lateral system in a command following sense, the other states all being regulated to zero, we consider only this square system when evaluating the transmission zeros.

In section 3.2 reference is made to the fact that nonsquare systems do not in general have any transmission zeros [10] and this is shown by the following reasoning for this single input, four output system.

By definition, the transmission zero represents, specifically for the single input multi output case, a frequency of exponential input for which there is no response in any of the output channels (in the multi input multi output case, this includes a requirement on the directionality of the combined inputs as well as the plant initial condition).

Considering the four transfer functions from the turntable torque input to each of the outputs $\dot{\varphi}$, φ, $\dot{\psi}$ and $\dot{\eta}$

$$\frac{\dot{\varphi}(s)}{\Gamma_t(s)} = \frac{42.9\ s^2}{s(s + 0.065)(s + 3.29)(s - 3.29)}$$

$$\frac{\varphi(s)}{\Gamma_t(s)} = \frac{42.9\ s}{s(s + 0.065)(s + 3.29)(s - 3.29)}$$

$$\frac{\dot{\psi}(s)}{\Gamma_t(s)} = 94.7\frac{s(s + 3.3)(s - 3.3)}{s(s + 0.065)(s + 3.29)(s - 3.29)}$$

$$\frac{\dot{\eta}(s)}{\Gamma_t(s)} = -154.7\frac{(s - 0.025)(s + 3.296)(s - 3.296)}{s(s + 0.065)(s + 3.29)(s - 3.29)}$$

it is clear there exist no common zeros to all the above transfer functions and hence we deduce that the system has

no transmission zeros.

4.7 Reduced Order Inner Loop Regulator

As in the longitudinal system, the system is essentially of two time scales and thus lends itself to a controller structured around a 'fast' inner loop and 'slow' outer loop. A reduced order model is used in this section to define the inner loop regulator.

Since the measurements are noisy, it is sensible to use an LQG structure to obtain good state estimates for regulation. All the inner loop states are to be regulated as opposed to command following, which makes the possible structure specially suited to a variation in the standard LQG structure. This leads to the command following outer loop being independent of the Kalman filter dynamics in the inner loop and is shown in detail in appendix 2.

4.7.1 Variation of LQG Structure

The closed inner loop structure is shown in figure 4.7.1.1. The subscrpt 'lr' denotes lateral reduced order model, to distinguish from the full order model of section 4.1

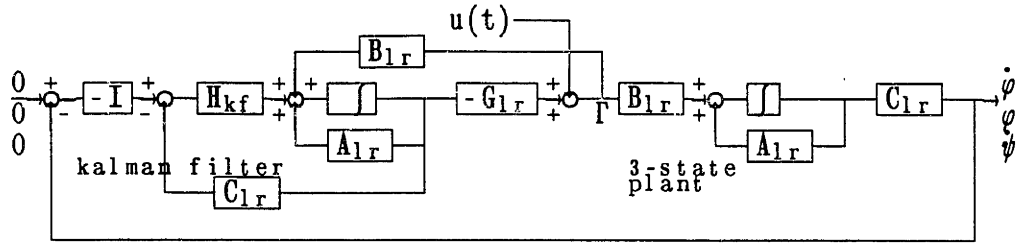

Figure 4.7.1.1 Inner LQG regulator loop

In the inner loop we wish to regulate the roll rate, roll angle and yaw rate and these are the states of the reduced order lateral model. The input to the plant, $\Gamma_t(t)$, is the turntable torque and by the nature of the model, this is the natural place to break the regulator loop when appending the outer loop dynamics i.e. the integration of yaw rate to yield heading angle. This is so since the heading command generates a commanded torque to the turntable and this influences the status of the inner loop in the sense of input disturbances to the reduced order plant. The interesting result is that the filter dynamics do not show up in the outer loop transfer function relating the 'external' (outer loop) input u(t) and the output $y(t) = [\dot{\varphi}\ \varphi\ \dot{\psi}]^T$. See appendix 2.

This approach is used in both the longitudinal and lateral controllers which are both 'non-square' and as such do not fit into the LQG/LTR ballpark. It is of course possible to reduce the number of measurements of the 'design plant' in order to

fit the LQG/LTR approach, but it is senseless to throw away information contained in these measurements specifically seen in the light of the difficulty of the control problem. Only in the case of measurements providing redundant information would this be feasible.

Using this method of synthesis thus defines an inner loop of desirable characteristics about which any design methodology can be applied to design the outer loop compensation. For example, the outer loop may be multivariable and if dimensionality of the compensator is not too much of an issue, an LQG structure could be implemented in order to be sure of optimal outer loop state estimates being used in the controller.

4.7.2 Design of Inner Loop

In this section we apply the methodology defined in 4.7.1 to the lateral controller. The inner loop is designed about the reduced order plant which, similar to the longitudinal controller inner loop, contains the inverted pendulum type dynamics and the yaw motion dynamics. The state space model describing these dynamics for the reduced order state vector $x(t)=[\dot{\varphi}\ \varphi\ \dot{\psi}]^T$ and input Γ_t (turntable torque) is

$$A_{lr} = \begin{bmatrix} 0 & 10.9 & 0.45 \\ 1 & 0 & 0 \\ -0.21 & 0 & 0.064 \end{bmatrix}$$

$$B_{lr} = \begin{bmatrix} 0 \\ 0 \\ 94.7 \end{bmatrix}$$

with measurement matrix the identity matrix of order 3×3 since we measure all states.

4.7.2.1 Reduced Order Regulator

We design the linear quadratic regulator to stabilize the inner loop and to minimize the quadratic cost functional

$$J = \int_0^\infty \{ x^T(t)Qx(t) + u^T(t)Ru(t) \}dt$$

The feedback gains are determined for the steady state solution as

$$G_{lr} = R^{-1}B_{lr}^T P$$

with P the solution (steady state) to the control algebraic Riccati equation [4, 12]

$$-P A_{lr} - A_{lr}^T P - Q + P B_{lr} R^{-1} B_{lr}^T P = 0$$

This yields a closed loop regulator with all the desirable characteristics of the LQR solution in gain margins of 1/2 to ∞ in each channel independently and simultaneously, phase margins of at least between -60° and $+60^\circ$ in each channel independently and simultaneously and closed loop high frequency roll-off of -20dB per decade.

The inner loop is to act as a regulator in the sense that outer loop commands generate disturbances to the inner loop and these are desired to be 'rejected' as efficiently as possible. This is the perfect setting for the input disturbance rejection characteristics of the LQ regulator which guarantee, for the cheap control problem (control weighting $\rightarrow 0$) and minimum-phase systems, perfect input disturbance rejection [4]. The reduced order system here is non-square (one input and three outputs) and has no transmission zeros, but we use the expensive control problem, so perfect disturbance rejection is not achieved, however, it is optimal in a least squares sense for the weightings selected.

For the state weighting

$$Q = I_{3\times 3}$$

and control weighting

$$R = 100$$

rather arbitrarily selected as expensive control weightings, the LQR gain matrix is

$$G_{lr} = [1.99 \quad 6.58 \quad 0.17]$$

yielding closed loop poles at

$$\lambda_1 = -9.45 \text{ rad/s}$$
$$\lambda_2 = -3.54 \text{ rad/s}$$
$$\lambda_3 = -3.09 \text{ rad/s}$$

Clearly the solution has yielded closed loop pendulum mode poles located close to the stable open loop pole and the unstable pole has moved to its mirror image about the imaginary axis as is expected using root square locus reasoning. One of the poles around -3 rad/s would move closer to the origin as the control weighting is reduced, thus reducing the effective bandwidth of the closed loop system, hence the choice of the expensive control solution.

Figure 4.7.2.1.1 shows an initial condition time simulation of the regulator for initial value of ten degrees in roll angle error. Figure 4.7.2.1.2 shows the Bode magnitude plot for the

transfer function relating turntable torque to yaw rate. Note that since this transfer function has dc gain of 97.4, the magnitude is raised approximately 20dB. This is the loop shape (closed inner loop) which we wish to retain when incorporating the Kalman filter in the feedback loop.

4.7.2.2 Kalman Filter

The Kalman filter is essentially in the feedback loop of the LQG structure as implemented here. For the plant

$$\dot{x}(t) = A_{lr}x(t) + B_{lr}u(t) + B_{lr}\xi(t)$$

and measurement

$$y(t) = C_{lr}x(t) + v(t)$$

Where $\xi(t)$ and $v(t)$ are assumed to be zero mean Gaussian white noise of constant intensities Ξ and V respectively.

The optimal steady state least squares estimator for this linear time invariant system is of the structure

$$\dot{\hat{x}}(t) = \hat{A}_{lr}\hat{x}(t) + H_{kf}(y(t) - \hat{C}_{lr}\hat{x}(t)) + \hat{B}_{lr}u(t)$$

$$= (\hat{A}_{lr} - H_{kf}\hat{C}_{lr})\,\hat{x}(t) + H_{kf}y(t) + \hat{B}_{lr}u(t)$$

In the absence of noise data for the process and sensor noise of the system, we select the covariance matrices as follows. Essentially, the rate sensors are considered ten times (arbitrarily) noisier than the inclinometer and the process noise.

Process covariance

$$\Xi = 1$$

Sensor covariance

$$V = \begin{bmatrix} 10 & 0 & 0 \\ 0 & 1 & 0 \\ 0 & 0 & 10 \end{bmatrix}$$

The steady state state error covariance Σ, is the steady state solution to the Filter algebraic Riccati equation

$$\dot{\Sigma} = A\,\Sigma + \Sigma\,A^T + L\,\Xi\,L^T - \Sigma\,C^T V^{-1} C\,\Sigma$$

yielding filter gains

$$H_{kf} = \Sigma\,C^T V^{-1}$$

$$= \begin{bmatrix} 3.47 & 10.43 & 0.38 \\ 1.04 & 3.16 & -0.007 \\ 0.38 & -0.07 & 30.02 \end{bmatrix}$$

The closed loop dynamics are (eigenvalues of $[\hat{A}_{lr} - H_{kf}\hat{C}_{lr}]$)

λ_1 = -29.95 rad/s

λ_2 = -3.38 rad/s

λ_3 = -3.25 rad/s

Since the filter has three inputs and one output, it has no transmission zeros.

4.8 Outer Loop Closure

4.8.1 The LQG Inner Loop Closed

The LQG inner loop regulator structure including the turntable angular velocity state ($\dot{\eta}$) is shown in figure 4.8.1.1 and the transfer function defined here relates input $r_c=[0\ 0\ 0\ 0]^T$ to the output of the plant $[\dot{\varphi}\ \varphi\ \dot{\psi}\ \dot{\eta}]^T$

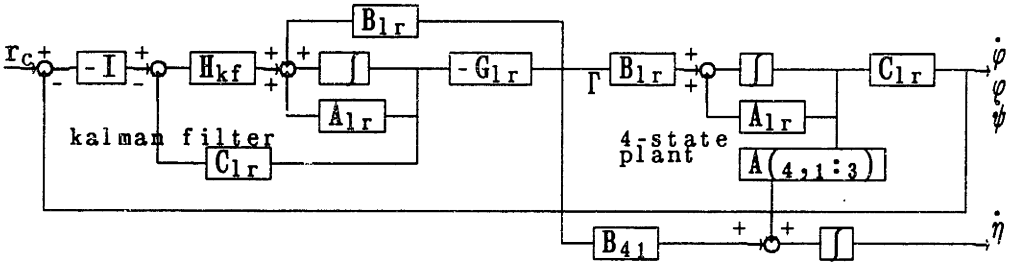

Figure 4.8.1.1 LQG Inner Loop Regulator Block Diagram.

The seven state (3 filter states and four plant states including $\dot{\eta}$) open loop state space model for figure 4.8.1.1 is

$$\begin{bmatrix} \dot{\hat{x}}(t) \\ \dot{x}(t) \\ \ddot{\eta}(t) \end{bmatrix} = \begin{bmatrix} [\hat{A}_{lr} - \hat{B}_{lr}G_{lr} - H_{kf}\hat{C}_{lr}] & 0 & 0 \\ -B_{lr}G_{lr} & \begin{bmatrix} A_{lr} & A(:,4) \\ A(4,1:3) & A(4,4) \end{bmatrix} \end{bmatrix} \begin{bmatrix} \hat{x}(t) \\ x(t) \\ \dot{\eta}(t) \end{bmatrix}$$

$$+ \begin{bmatrix} -H_{kf} & 0 \\ 0 & 0 \\ 0 & 0 \end{bmatrix} r_c$$

Where 'A' and 'B' without subscripts refer to the system matrices of section 4.2, superscript $\hat{}$ refers to the Kalman filter.

For measurement of all four states

$$y(t) = \begin{bmatrix} \dot{\varphi}(t) \\ \varphi(t) \\ \dot{\psi}(t) \\ \dot{\eta}(t) \end{bmatrix} = [\, 0_{4\times3} \quad I_{4\times4}] \begin{bmatrix} \hat{x}(t) \\ x(t) \\ \dot{\eta}(t) \end{bmatrix}$$

The closed loop dynamics matrix is then simply

$$A_{7cl} = A_{7ol} - B_7C_7$$

Where the subscript '7' refers to the seven state open loop model as defined here.

The closed inner LQG loop (i.e. including Kalman filter) transfer function relating turntable torque and yaw rate ($\dot{\psi}$) Bode magnitude plot is shown in figure 4.8.1.2 and comparison with figure 4.7.2.1.2 shows that the presence of the Kalman filter has not influenced this transfer function at all, as predicted in section 4.7.1. The transfer function is

$$\frac{\dot{\psi}(s)}{\Gamma_t(s)} = \frac{97.74(s+29.95)(s+3.25)(s+3.38)(s+3.30)(s-3.30)s}{(s+29.5)(s+3.25)(s+3.38)(s+9.45)(s+3.54)(s+3.09)s}$$

$$= \frac{97.74(s+3.30)(s-3.30)}{(s+9.45)(s+3.54)(s+3.09)}$$

Where the filter error dynamics appear in both the numerator and the denominator and hence pole zero cancellation occurs. This, together with the controllability matrix structure as set out in section 4.3.2, also indicates that the filter error dynamics are uncontrollable from the input $\Gamma(t)$. The integrator in this transfer function is the turntable rotation mode and as discussed in section 4.3.2, this mode is uncontrollable, hence the differentiator in the transfer function showing pole zero cancellation of this mode.

In order to see the effect of the filter on the inner loop regulation performance, initial condition simulations for an initial bank angle error of ten degrees are shown in figures 4.8.1.3 a, b & c. Comparing these with figure 4.7.2.1.1 shows that the LQG regulator response is degraded (slower than the LQ

regulator) but is still very good with peak values and transient behaviour quite similar to the system without the Kalman filter. The Kalman filter states of figure 4.8.1.3a track the plant states of figure 4.8.1.3b very well, so the performance of the filter appears good.

The Kalman filter thus influences the system mainly in that it obtains better estimates of the states for full state feedback in the inner LQG regulator loop and in an optimal sense (minimizing least square errors, if our guesses at the noise covariances are not too far wrong) as opposed to simply employing low pass filtering in each channel to eliminate noise, at the cost of phase loss and no assistance in obtaining better estimates from the sensors.

This is a very desirable feature in that some form of filtering is necessary on these sensor channels, so if this is transparent in the outer loop of interest, all the better.

4.8.2 Positive Feedback in Heading Loop

The model is now augmented with an integrator, representing integration of the yaw rate to yield heading angle as we would like to maintain heading in a relatively low bandwidth function to counter the drift due to turntable torque commands required for maintaining balance of the unicycle. The system block diagram is given in figure 4.8.2.1 and the state space model is

determined as follows

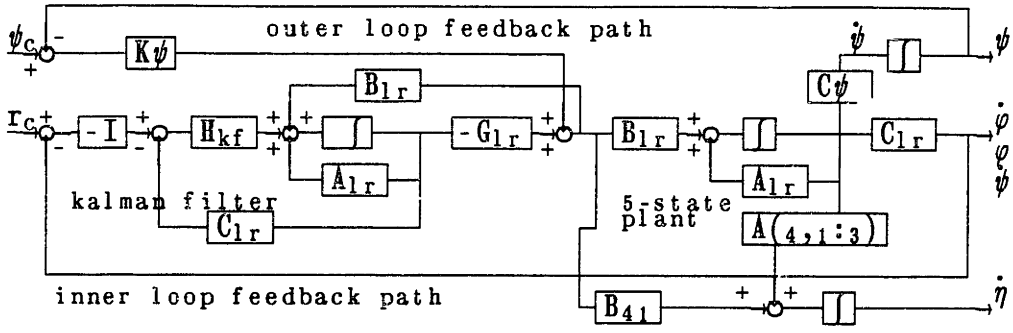

Figure 4.8.2.1 Complete Lateral Closed Loop Block Diagram.

The full system with inner LQG loop closed and outer heading loop open state space model is

$$\begin{bmatrix} \dot{\hat{x}}(t) \\ \dot{x}(t) \\ \ddot{\eta}(t) \\ \dot{\psi}(t) \end{bmatrix} = \begin{bmatrix} [\hat{A}_{1r} - \hat{B}_{1r}G_{1r} - H_{kf}\hat{C}_{1r}] & H_{kf}C_{1r} & 0 & 0 \\ -B_{1r}G_{1r} & \begin{bmatrix} A_{1r} & A(:,4) \\ A(4,1:3) & A(4,4) \end{bmatrix} & 0 & 0 \\ -B(4,1)G_{1r} & & 0 & 0 \\ 0 & [0\ 0\ 1] & 0 & 0 \end{bmatrix} \begin{bmatrix} \hat{x}(t) \\ x(t) \\ \dot{\eta}(t) \\ \psi(t) \end{bmatrix}$$

$$+ \begin{bmatrix} \hat{B}_{1r} \\ B_{1r} \\ B(4,1) \\ 0 \end{bmatrix} K_{\psi}\psi_c$$

with measurement

$$y(t) = \psi(t) = [0_{1\times 7}\ 1]\ x(t)$$

The closed loop dynamics matrix is

$$A_{cl} = A_{ol} - B_{ol}C_{ol}$$

The numerical transfer function form for this case (wheel speed of 2 rad/s) is determined as

$$\frac{\psi(s)}{T_t(s)} = \frac{97.74(s+29.95)(s+3.25)(s+3.38)(s+3.30)(s-3.30)s}{(s+29.5)(s+3.25)(s+3.38)(s+9.45)(s+3.54)(s+3.09)(s)(s)}$$

$$= \frac{97.74(s+3.30)(s-3.30)}{(s+9.45)(s+3.54)(s+3.09)s}$$

Clearly the presence of the non minimum-phase transmission zero will pull the integrator into the right half plane for negative feedback, so positive feedback is used in closing the heading loop. Feedback gain of K_{ψ}=-0.06 (Nms/rad) is chosen for this loop and the open loop transfer function is shown in figure 4.8.2.2 a & b.

The net phase contribution of the two zeros around 3.3 rad/s is zero since one is non minimum-phase. The two poles of the inner loop regulator contribute approximately 90° phase lag (at this frequency) and this combined with the 90° phase lag due to the integrator, is the cause of the poor phase at this frequency if we were to use negative feedback and positive loop gain. The loop transfer function is of desirable shape as regards high dc gain for good command following and disturbance rejection and

no resonant modes, with good high frequency roll-off to guard against excitation of unmodeled high frequency dynamics.

The closed loop transfer function is

$$\frac{\psi(s)}{\Gamma_t(s)} = \frac{97.74(s+30)(s+3.3)(s+3.4)(s+3.3)(s-3.3)s}{(s+30)(s+3.3)(s+3.4)(s+10)(s+3.3)(s+1.1+j0.7)(s+1.1-j0.7)s}$$

$$= \frac{97.74(s+3.30)(s-3.30)}{(s+10.49)(s+3.33)(s+1.13+j0.7)(s+1.13-j0.7)}$$

Since the filter error dynamics are uncontrollable from the outer loop, these poles remain fixed when closing the heading loop. The effect of the need for positive feedback (negative gain $K\psi$ in figure 4.8.2.1) is clearly illustrated in the presence of the two stable oscillatory (well damped) poles, instead of unstable poles which result from positive gain $K\psi$. The root locus plot of figure 4.8.2.3 illustrates this.

The closed loop Bode magnitude plot is shown in figure 4.8.2.4, and closed loop step heading command simulations are shown in figure 4.8.2.5 a, b & c. The time responses illustrate the non minimum-phase behaviour of the system. The small motor torques required by the linear controller are clearly too small to overcome yawing friction between the wheel and the surface and this is motivation for the implementation of the lateral controller in the form of a bang-bang controller. Details of this are given in chapter 6.

4.9 Compensator State Space Model

For purposes of implementing the controller in digital form, we need to define the state space model of the compensator with all feedback paths open. The cascaded form of the open loop compensated system is shown in figure 4.9.1.

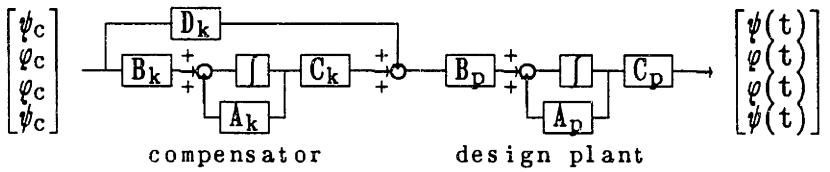

Figure 4.9.1 Cascaded compensator and plant

This is the desired form since the closed loop compensated system is simply obtained by defining the closed loop form of this state space model. Consider then, referring to figure 4.8.2.1, the state space description with all feedback loops (ψ $\dot{\varphi}$, φ, $\dot{\psi}$ loops) open.

$$\begin{bmatrix} \dot{\hat{x}}(t) \\ \dot{x}(t) \\ \ddot{\eta}(t) \\ \dot{\psi}(t) \end{bmatrix} = \begin{bmatrix} [\hat{A}_{lr} - \hat{B}_{lr}G_{lr} - H_{kf}\hat{C}_{lr}] & 0 & 0 & 0 \\ -B_{lr}G_{lr} & \begin{bmatrix} A_{lr} \\ A(4,1:3) \end{bmatrix} & \begin{bmatrix} A(:,4) \\ A(4,4) \end{bmatrix} & \begin{matrix} 0 \\ 0 \end{matrix} \\ -B(4,1)G_{lr} & & & \\ 0 & [0\ 0\ 1] & 0 & 0 \end{bmatrix} \begin{bmatrix} \hat{x}(t) \\ x(t) \\ \dot{\eta}(t) \\ \psi(t) \end{bmatrix}$$

$$+ \begin{bmatrix} H_{kf} \\ 0 \\ 0 \\ 0 \end{bmatrix} \begin{bmatrix} \hat{B}_{lr} \\ B_{lr} \\ B(4,1) \\ 0 \end{bmatrix} K_{\psi} \begin{bmatrix} \psi_c \\ \varphi_c \\ \varphi_c \\ \dot{\psi}_c \end{bmatrix} \qquad 4.9.1$$

with measurement matrix

$$y(t) = \begin{bmatrix} 0_{4\times3} & \begin{bmatrix} [Clr] & 0_{3\times1} & 0_{3\times1} \\ 0_{1\times3} & 0_{1\times1} & 1_{1\times1} \end{bmatrix} \end{bmatrix} \begin{bmatrix} \hat{x}(t) \\ x(t) \\ \dot{\eta}(t) \\ \psi(t) \end{bmatrix} \qquad 4.9.2$$

The state space model for the cascaded system of figure 4.9.1 is

$$\begin{bmatrix} \dot{x}_k(t) \\ \dot{x}(t) \end{bmatrix} = \begin{bmatrix} A_k & 0 \\ B_pC_k & A_p \end{bmatrix} \begin{bmatrix} x_k(t) \\ x(t) \end{bmatrix} + \begin{bmatrix} B_k \\ B_pD_k \end{bmatrix} r_c \qquad 4.9.3$$

with $r_c = [\psi_c \ \dot{\varphi}_c \ \varphi_c \ \dot{\psi}_c]^T$, the commanded input to the system, and measurements

$$y(t) = [0 \quad C_p] \begin{bmatrix} x_k(t) \\ x(t) \end{bmatrix} \qquad 4.9.4$$

Now, matching blocks of the partitioned matrices of 4.9.1 with 4.9.3 and 4.9.2 with 4.9.4, yields the state space model for the compensator

$$A_k = [\, A_{lr} - B_{lr}G_{lr} - H_{kf}C_{lr}]$$

$$B_k = [-H_{kf} \quad B_{lr}K_{\psi}]$$

$$C_k = [-G_{lr}]$$

$$D_k = [\ 0_{1\times 3} \quad K_\psi]$$

4.10 Discrete Time Compensator

The discrete time controller is determined as in section 3.12 method (2), but since we have a time varying plant in the lateral model, not only do the LQ and Kalman filter gains vary with wheel angular velocity, but also the plant model. This requires a slightly different approach than for the longitudinal system. This is discussed in the following chapter on gain scheduling the discrete time controller.

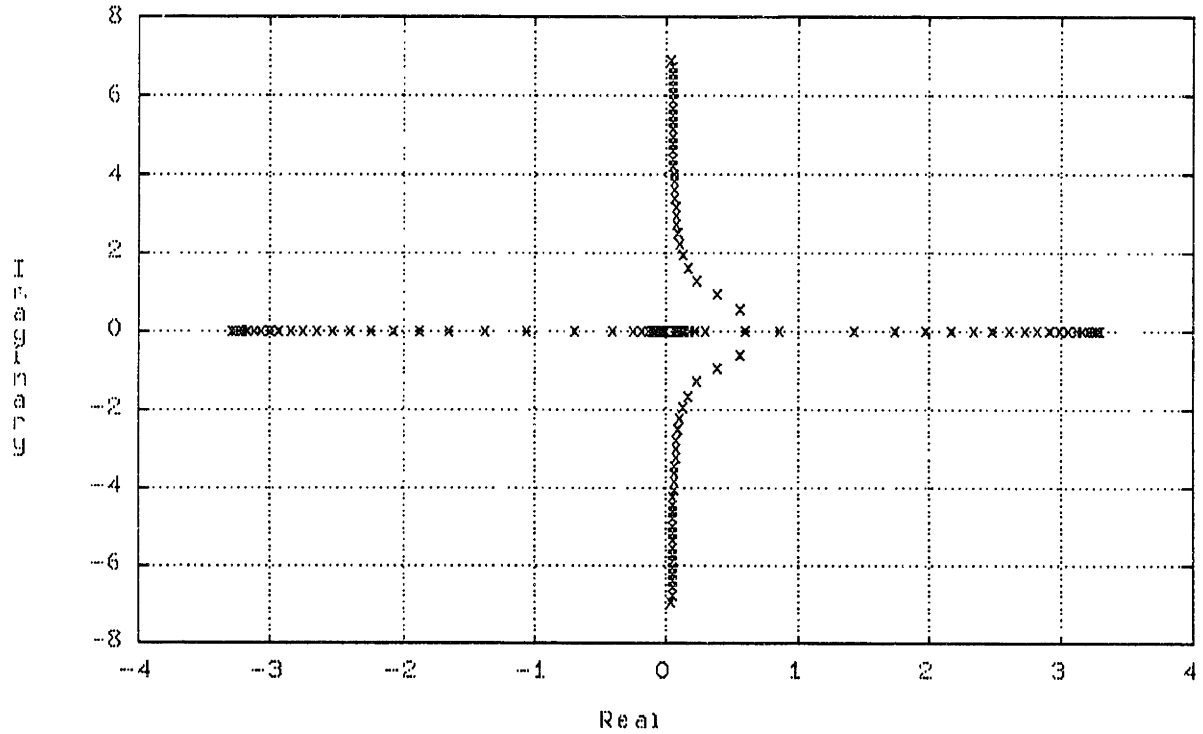

Figure 4.5.1. Root locus of lateral open loop dynamics as function of wheel speed. The stabilizing of the pendulum mode with increased wheel speed in roll is entirely due to greater gyroscopic restoring moments existing at higher wheel angular velocities. This mode stabilization is synonymous with that demonstrated by a rolling disk at high speed.

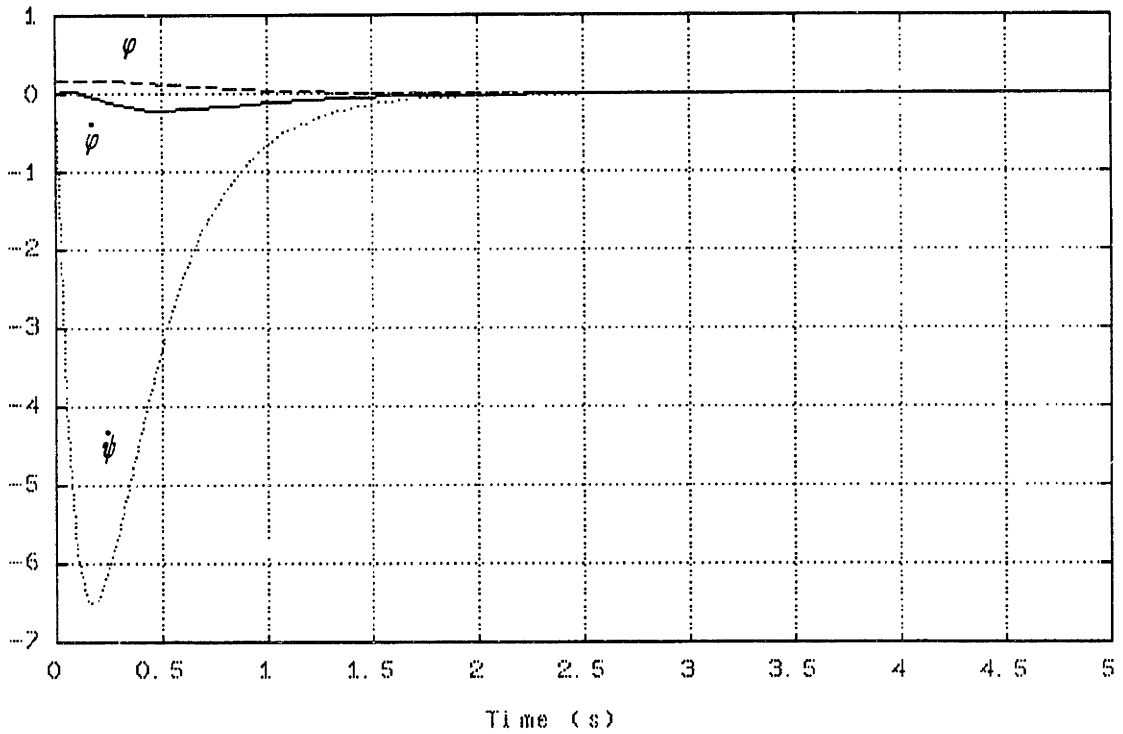

Figure 4.7.2.1.1. Inner loop LQ regulator (excluding Kalman filter) response to initial roll error of 10°. Units are radians and rad/s. The inner loop serves to regulate errors in roll angle, roll rate and yaw rate, emulating human unicyclist behavior when executing a heading change, which typically involves pulse heading changes- the roll angle, roll rate and yaw rate errors being regulated to zero in an inner loop sense.

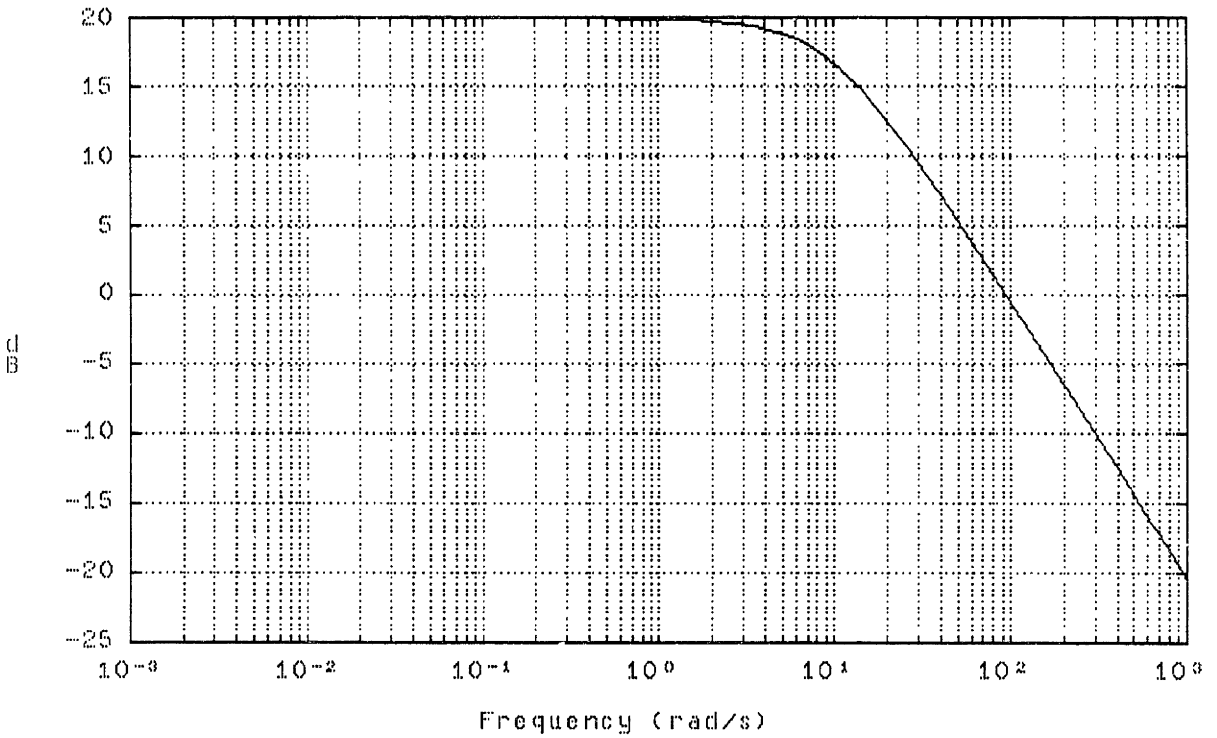

Figure 4.7.2.1.2. Bode magnitude plot for LQ inner loop closed. The transfer function relates turntable torque to yaw rate. This loop transfer function is retained when the Kalman filter is included in the inner loop (see figure 4.8.1.2.). Note 20 dB gain at low frequencies- this occurs since we are breaking the regulator loop at the unusual location in the plant input.

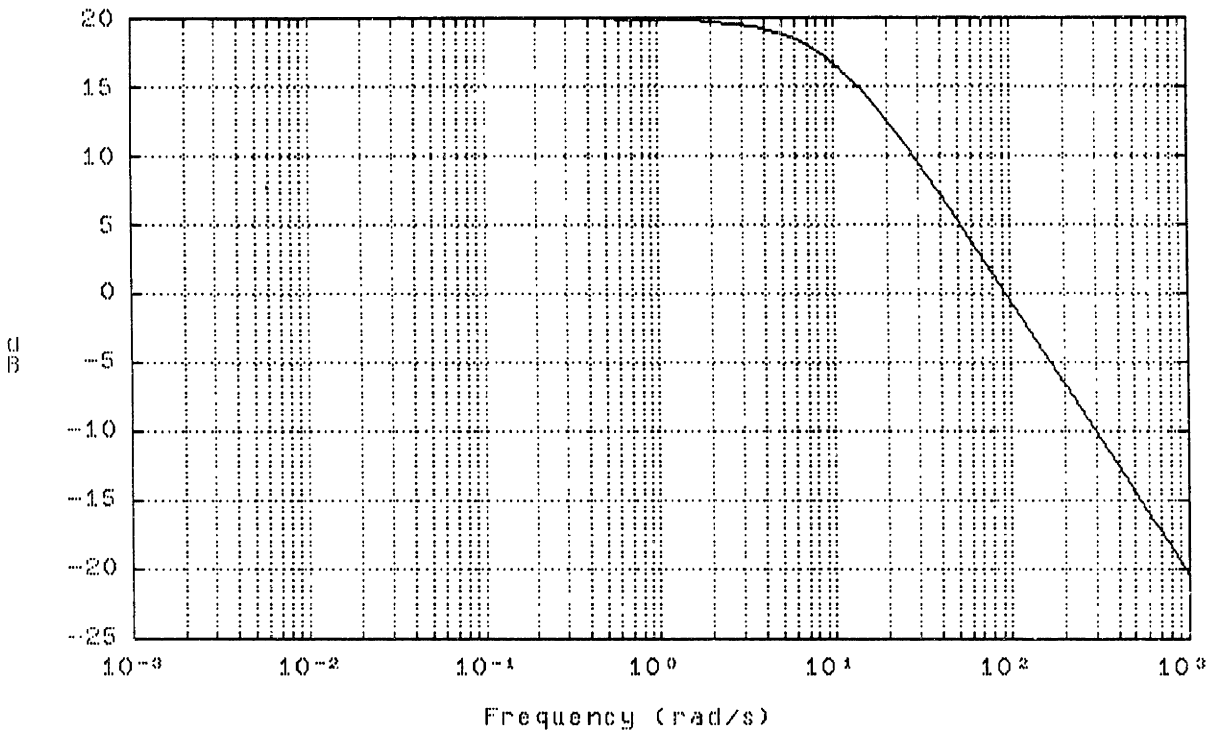

Figure 4.8.1.2. Bode magnitude plot for inner LQG loop closed. The inner loop includes a Kalman filter in the typical LQG structure and this does not affect the outer loop transfer function as is apparent in comparison with figure 4.7.2.1.2.

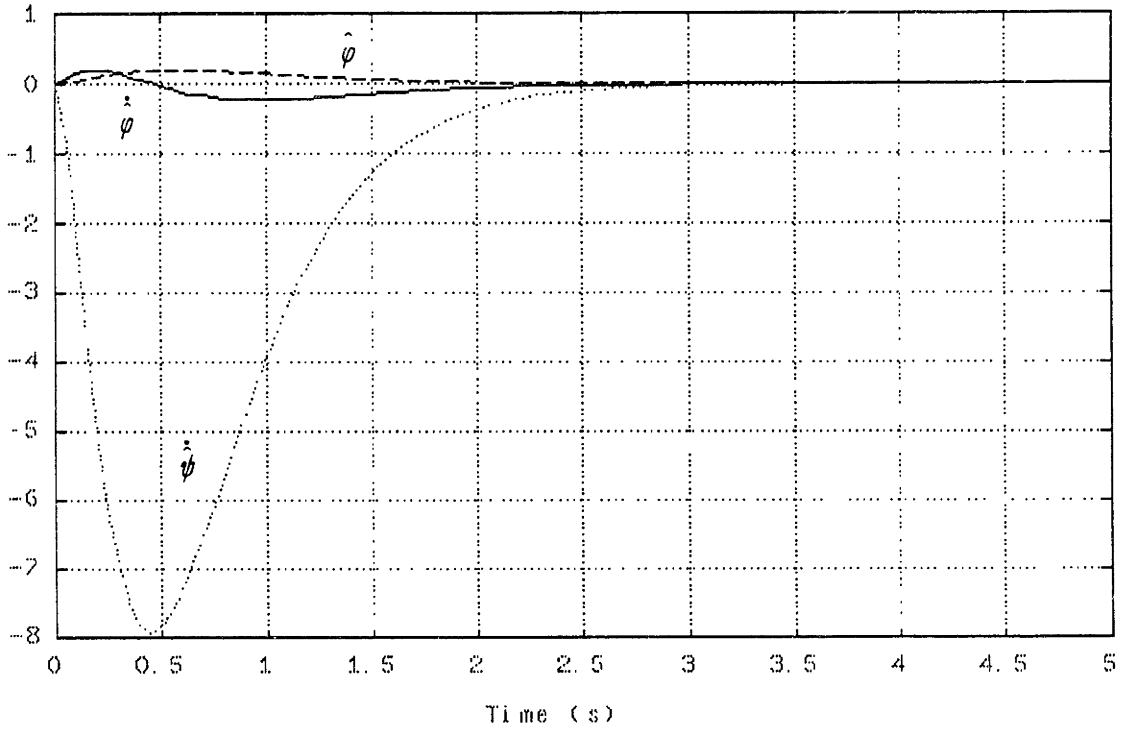

Figure 4.8.1.3a. LQG inner loop regulator response to initial roll error of 10°. Estimates of roll angle, roll rate and yaw rate states plotted with units radians and rad/s. Comparison with figure 4.7.2.1.1 shows almost negligible difference in performance. The true states are plotted in figure 4.8.1.3b for comparison.

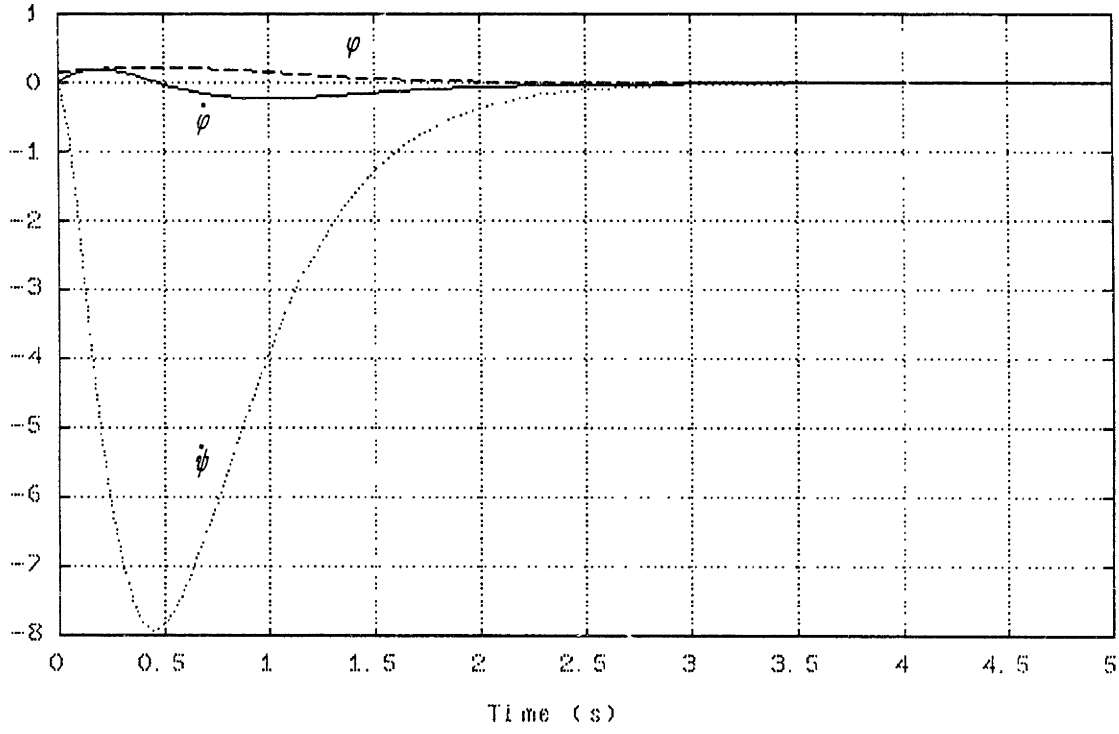

Figure 4.8.1.3b. True states response to initial condition as specified in figure 4.8.1.3a. Comparison with this figure shows good tracking of the states by the Kalman filter estimates.

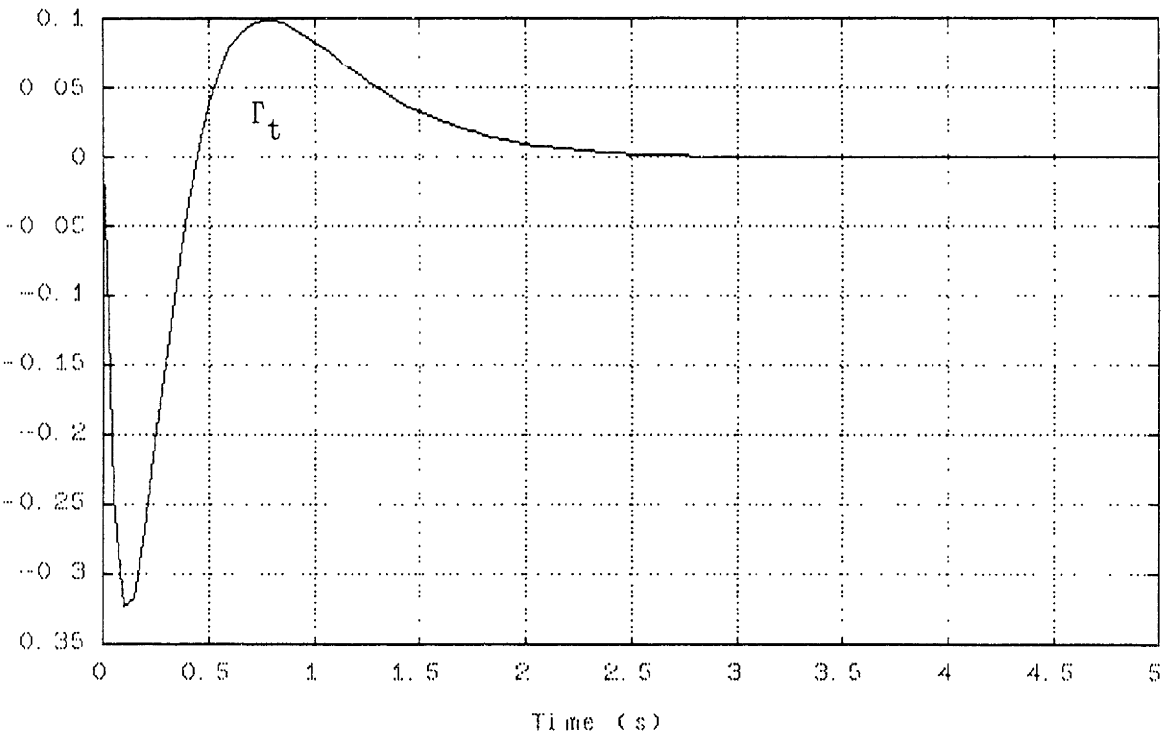

Figure 4.8.1.3c. Actuator activity for initial condition simulation. Note the small amplitudes. These represent motor torque and the gearing on the turntable amplifies this by ratio 36:1. These amplitudes are too small to overcome coulomb friction (stiction and kinematic friction) effects hence the implementation of this controller in a bang-bang setting.

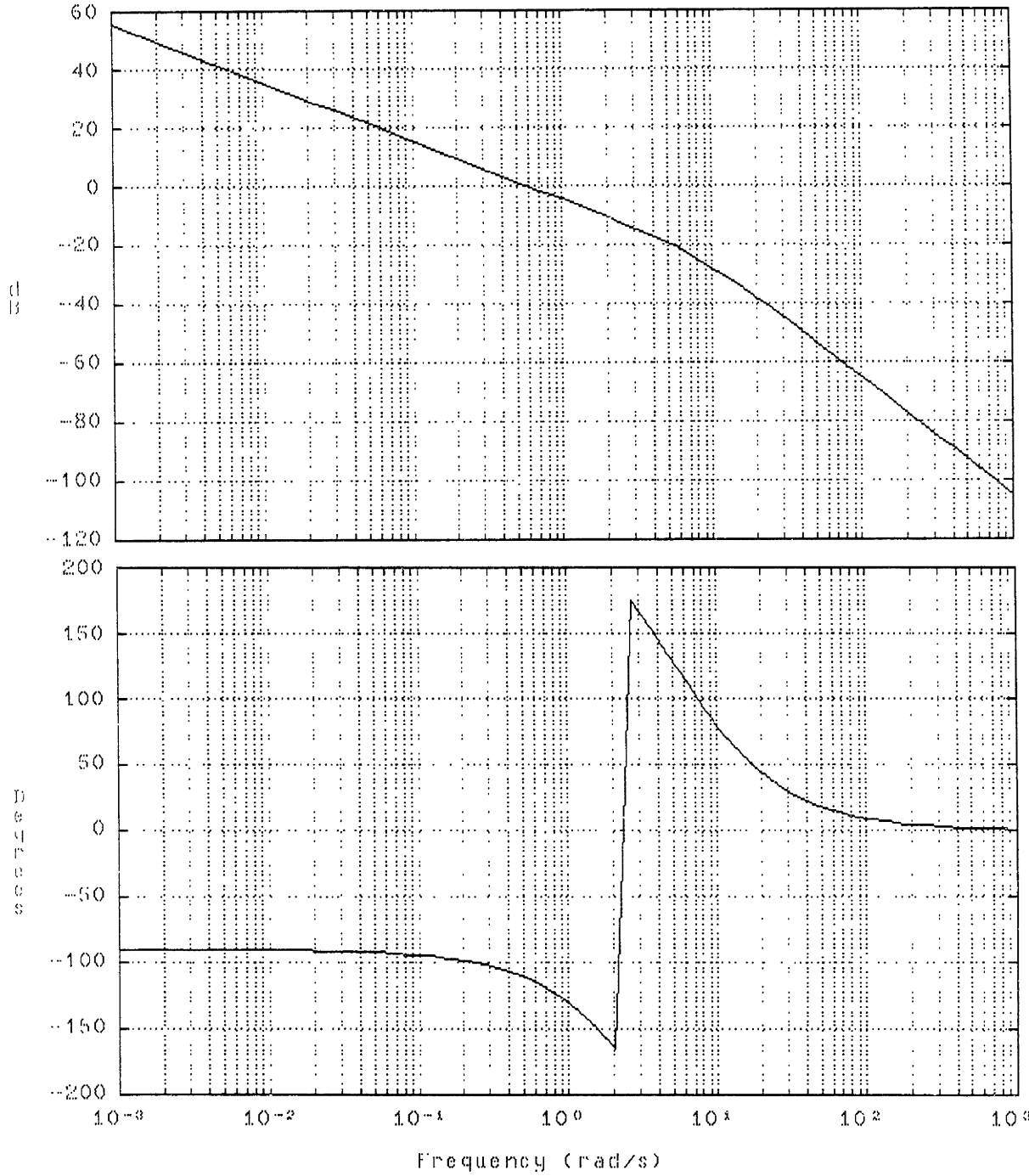

Figure 4.8.2.2. Bode magnitude and phase plots. Open outer loop relating commanded heading to plant heading, with inner LQG loop closed. The loop shape is desirable for good command folowing, output disturbance rejection and attenuation of sensor noise and has good phase margin.

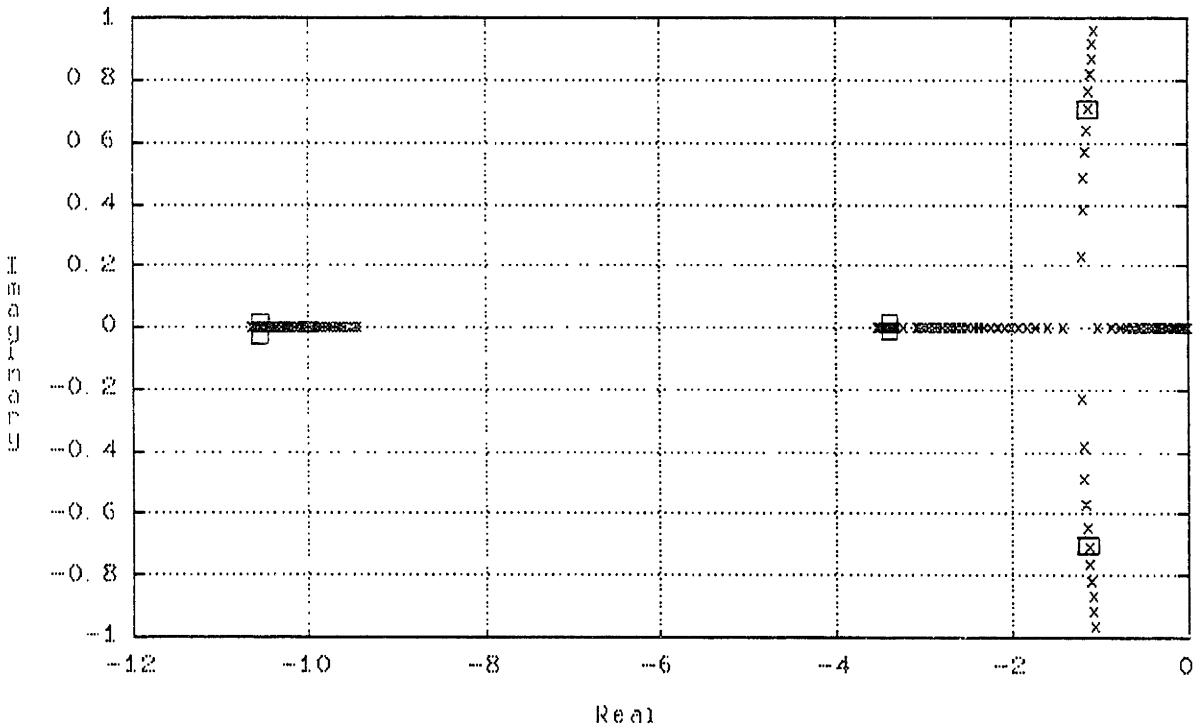

Figure 4.8.2.3. Heading loop root locus (negative gain). The heading loop gain is selected negative to prevent the integrator moving into the right half plane toward the non minimum-phase zero near 3.3 rad/s. Closed loop poles are at -10.64 rad/s, -3.33 rad/s and an oscillatory pair at -1.13±j0.7 rad/s respectively.

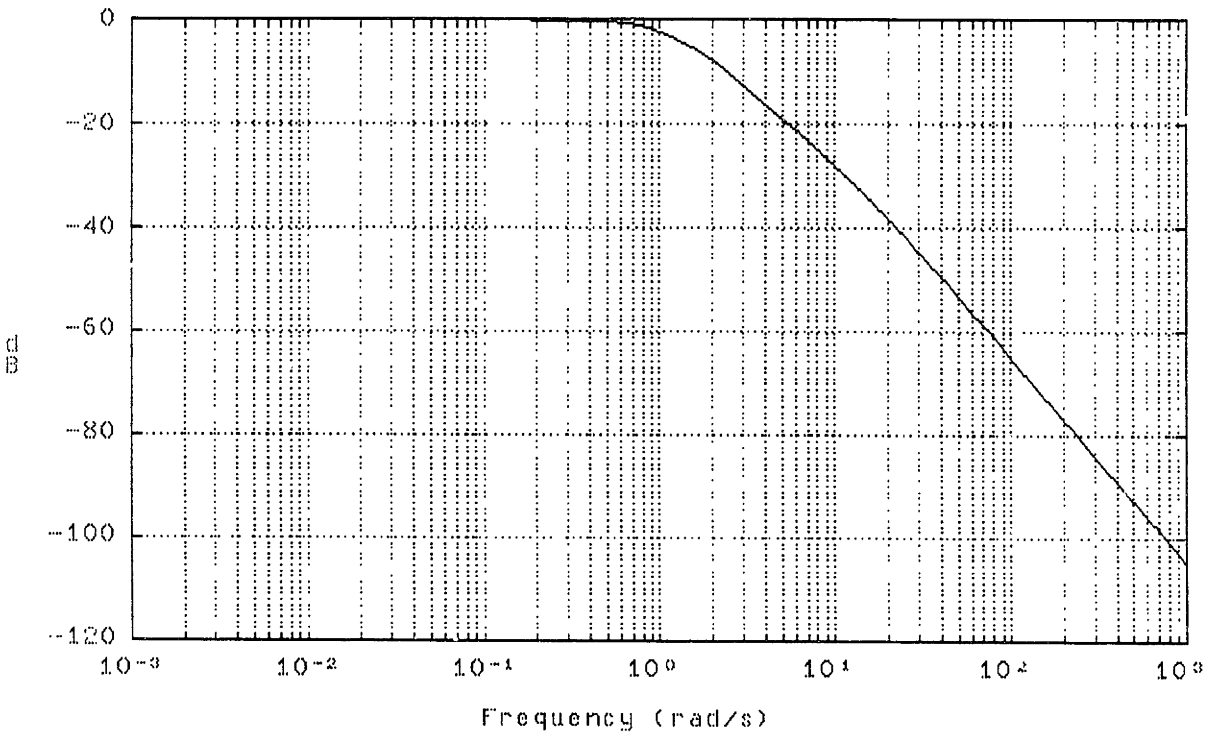

Figure 4.8.2.4. Bode magnitude plot. Outer heading loop closed and inner LQG regulator loop closed. Bandwidth is approximately 0.4 rad/s, i.e. one decade below the frequency of the non minimum-phase zero. This could be designed to have higher bandwidth, but the loop sensitivity would show amplification of output disturbances over a significant frequency range, which is undesirable. This is directly attributable to the non minimum-phase zero.

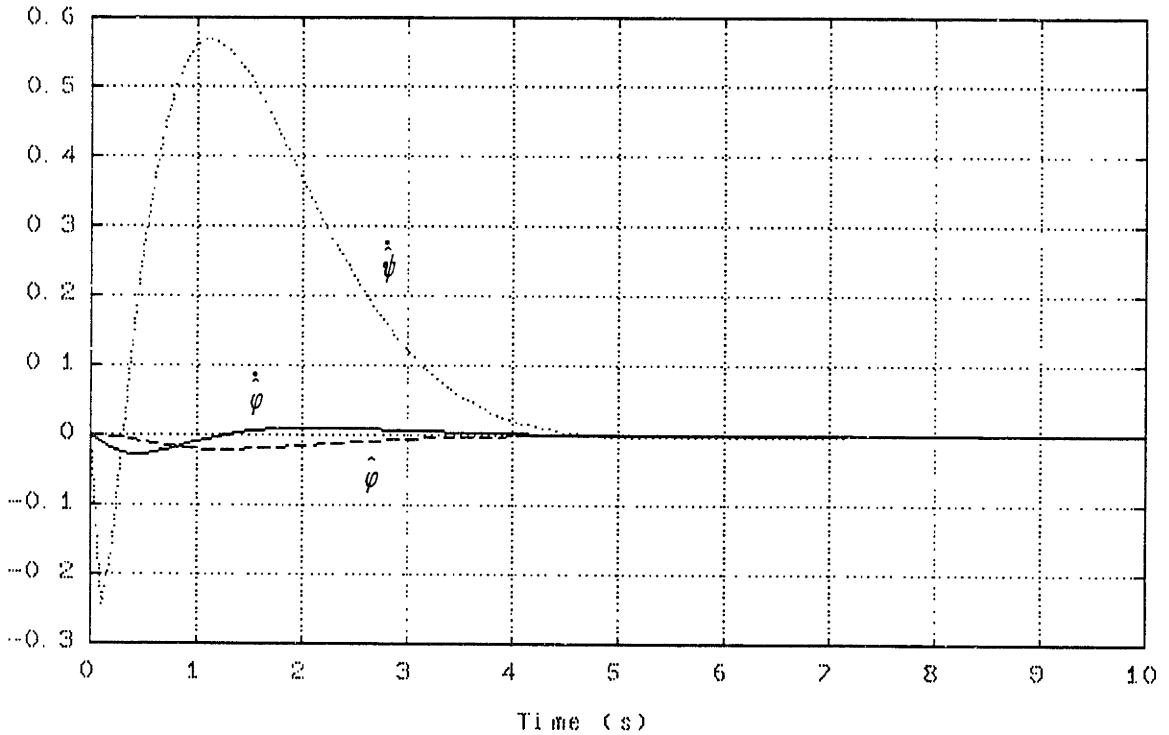

Figure 4.8.2.5a. Simulation response of closed loop system to step heading command. Estimator states in units of radians and rad/s respectively. Comparison with figure 3.8.2.5b shows excellent tracking of plant states.

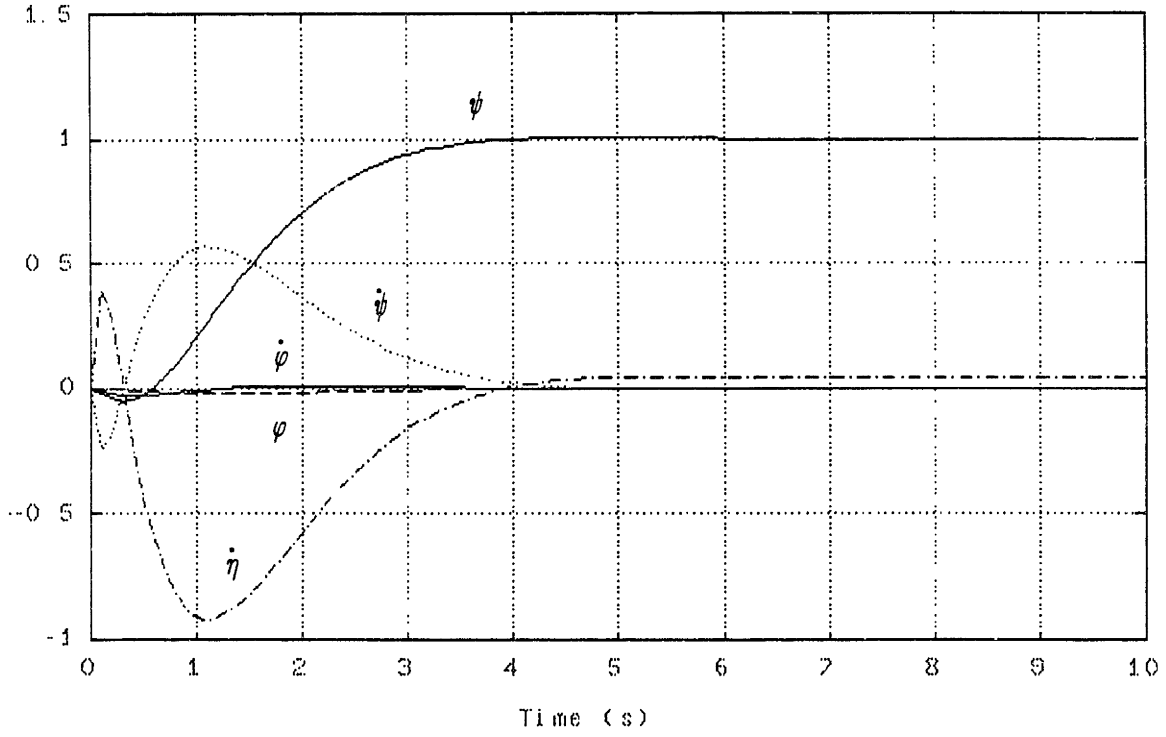

Figure 4.8.2.5b. True system states response to step heading command. Units are radians and rad/s. Notice the steady state error in turntable angular velocity. This is since we have not modeled any friction in the turntable drive-train and also have no means of controlling this state independently in the frictionless model. If the stiction (breakaway friction) value is well known, a slow loop (requiring torque actuation much smaller than the stiction value) may be closed around turntable speed to regulate this.

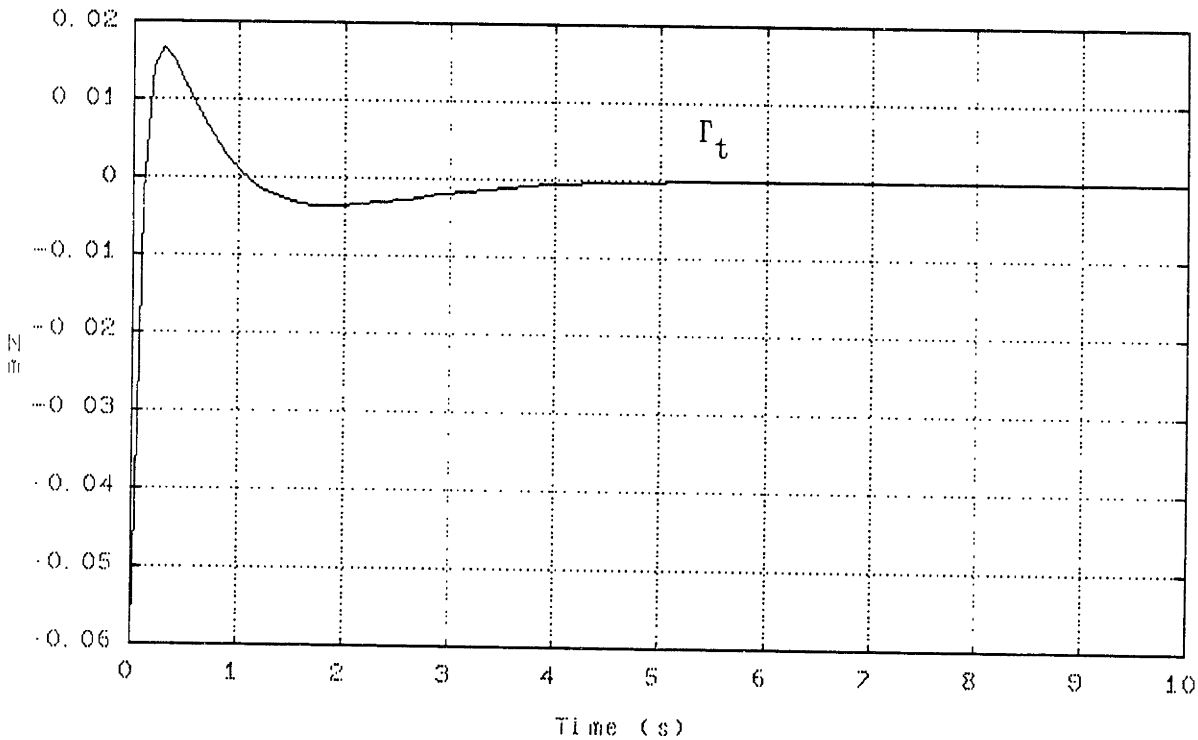

Figure 4.8.2.5c. Turntable actuator activity for step heading command. Again, these are motor torques, so the torque experienced by the system is 36 (the gear ratio on the turntable is 36:1) times greater. These values are still too small to overcome friction and we deal with this by applying pulsewidth modulated torque commands of large amplitude (significantly larger than friction) in a bang-bang type implementation. This is discussed in chapter 6.

5.0 GAIN SCHEDULING THE DISCRETE TIME CONTROLLER

5.1 Introduction

As indicated in section 4.10, the lateral model is of time varying nature, requiring a gain scheduled controller since no one controller as designed in chapter 4 will suffice over a large enough range of wheel speeds.

Here we look more carefully at the nature of the time variation and define methods for dealing with this. Since the system varies according to a single parameter, the dynamic model can be written as a function of this in discrete time.

As a result of this time variation of the plant it is of course necssary to have time varying LQ regulator and Kalman filter gains to yield consistent performance over the operatimg region. Thus, the LQ and Kalman filter gains are evaluated over a large number of operating points and then least squares polynomial fits of each element as a function of wheel angular velocity ($\Omega(t)$) are defined in order to compensate for the necessary time varying nature of these gains.

5.2 The Time Varying Model

5.2.1 Continuous Time Model

The continuous time lateral model in standard state space form $\dot{x}(t)=Ax(t) + Bu(t)$ for the state vector $x(t)=[\dot{\varphi}(t)\ \varphi(t)\ \dot{\psi}(t)\ \dot{\eta}(t)]^T$ is determined by carrying out the symbolic inversion of the mass matrix of the lateral decoupled system as specified in section 4.2, to yield

$$A = \begin{bmatrix} 0 & \frac{-k_{12}}{m_{11}} & \frac{-k_{13}}{m_{11}} & 0 \\ 1 & 0 & 0 & 0 \\ \frac{-m_{44}k_{31}}{den} & 0 & 0 & 0 \\ \frac{m_{43}k_{31}}{den} & 0 & 0 & 0 \end{bmatrix}$$

$$B = \begin{bmatrix} 0 \\ 0 \\ \frac{-m_{34}}{den} \\ \frac{m_{33}}{den} \end{bmatrix}$$

with

$$m_{11} = -(m_w r_w^2 + m_f(r_w + r_f)^2 + m_t(r_w + l_t)^2 + I_1^W + T_1^F + I_1^T)$$

$$m_{33} = -(I_3^W + I_3^F + I_3^T)$$

$$m_{44} = -I_3^T$$

$$m_{43} = m_{34} = -I_3^T$$

$$den = I_3^T(I_3^W + I_3^F)$$

$$k_{12} = (m_w r_w + m_f(r_w + r_f) + m_t(r_w + l_t))g$$

$$k_{13} = (m_w r_w^2 + m_f r_w(r_w + r_f) + m_t r_w(r_w + l_t) + I_2^W)\Omega_o$$

$$k_{31} = -I_2^W \Omega_o$$

Clearly, the only coefficients which are affected by a change in wheel angular velocity, are A(1,3) and A(3,1) for the continuous time system nodel and the relation is linear, however this linearity is not necessarily preserved in the discrete form.

5.2.2 Discrete Time Model

The discrete time model, discretized according to the method as outlined in section 3.12, has nine state transition matrix (Φ) elements which are time varying and the control distribution matrix (Γ) has two.

The means of determining this is simply to evaluate the state transition matrix and control distribution (discrete time)

matrix at a number of typical values of wheel angular velocity (Ω) and look at the trends shown by the individual coefficients, a rather brute force approach, but effective for this specific system. Only one of these varies in a significantly quadratic sense, the others all being essentially linear.

Using a least squares curve fit to these data, we obtain the following expressions for the time varying elements of thes matrices.

$$\Phi(3,1) = -1.0523 \times 10^{-3}\Omega$$

$$\Phi(4,1) = 1.0523 \times 10^{-3}\Omega$$

$$\Phi(5,1) = -5.2621 \times 10^{-6}\Omega$$

$$\Phi(3,2) = -5.7347 \times 10^{-5}\Omega$$

$$\Phi(4,2) = 5.7347 \times 10^{-5}\Omega$$

$$\Phi(5,2) = -1.9117 \times 10^{-7}\Omega$$

$$\Phi(1,3) = 2.2324 \times 10^{-3}\Omega$$

$$\Phi(2,3) = 1.1163 \times 10^{-5}\Omega$$

$$\Phi(4,3) = 1.1747 \times 10^{-6}\Omega^2 + 1.9464 \times 10^{-9}\Omega + 6.4452 \times 10^{-4}$$

$$\Gamma(1,1) = 1.0576 \times 10^{-3}\Omega$$

$$\Gamma(2,1) = 3.5254 \times 10^{-6}\Omega$$

These expressions are all really simple and as such could easily be implemented in code with minimal cost in terms of CPU time of the microcontroller.

5.3 The Time Varying Controller

The controller is a model based compensator and thus incorporates the time varying plant dynamics as specified in section 5.2.2. In addition, the LQ regulator and Kalman filter gains are time varying and since these are generated via a highly nonlinear function in the Riccati equation, these do not follow nice linear paths, but are nonetheless continuous functions suited to least squares curve fitting. A typical example is shown in figure 5.3.1, where the regulator gain g1 is plotted as a function of wheel angular velocity for both the data points as well as the curve fit.

Following the approach as in section 5.2.2, generating data at a number of typical operating points and solving for the regulator and filter gains at each condition according to the

procedure as outlined for the discrete time case in section 3.12, the folowing polynonials describe the value of the respective gain elements as functions of wheel angular velocity (rad/s).

The LQ regulator gain matrix has three elements

$$G_{lr} = [g1 \quad g2 \quad g3]$$

and the Kalman filter gain matrix has nine elements

$$H_{kf} = \begin{bmatrix} h1 & h2 & h3 \\ h4 & h5 & h6 \\ h7 & h8 & h9 \end{bmatrix}$$

The polynomials determined by least squares fit are

$$g1 = -8.806\times10^{-9}\Omega^9 + 9.051\times10^{-7}\Omega^8 - 3.992\times10^{-5}\Omega^7 + 9.879\times10^{-4}\Omega^6 - 1.506\times10^{-2}\Omega^5 + 0.146\,\Omega^4 - 0.905\,\Omega^3 + 3.466\,\Omega^2 - 7.699\,\Omega + 8.743$$

$$g2 = -2.907\times10^{-8}\Omega^9 + 2.988\times10^{-6}\Omega^8 - 1.318\times10^{-4}\Omega^7 + 3.261\times10^{-3}\Omega^6 - 4.973\times10^{-2}\Omega^5 + 0.483\,\Omega^4 - 2.989\,\Omega^3 + 11.44\,\Omega^2 - 25.42\,\Omega + 28.86$$

$$g3 = 3.794\times10^{-6}\Omega^2 + 1.737\times10^{-5}\Omega + 0.16$$

$$h1 = -9.48\times10^{-7}\Omega^3 + 6.048\times10^{-5}\Omega^2 + 1.795\times10^{-4}\Omega + 3.742\times10^{-2}$$

$$h2 = 5.6\times10^{-7}\Omega^3 - 3.261\times10^{-5}\Omega^2 - 1.744\times10^{-4}\Omega + 8.7432\times10^{-2}$$

$$h3 = -1.183\times10^{-5}\Omega^2\ 1.635\times10^{-3}\Omega - 4.275\times10^{-4}$$

$$h4 = 0.0114$$

$$h5 = 0.0265$$

$$h6 = -5\times10^{-4}$$

$$h7 = -1.132\times10^{-5}\Omega^2 + 1.663\times10^{-3}\Omega - 2.762\times10^{-3}$$

$$h8 = 5.975\times10^{-6}\Omega^2 - 8.156\times10^{-4}\Omega - 5.014\times10^{-2}$$

$$h9 = -8.123\times10^{-6}\Omega^2 - 4.843\times10^{-5}\Omega + 0.255$$

The controller structure is shown in figure 5.3.2 for the discrete time system

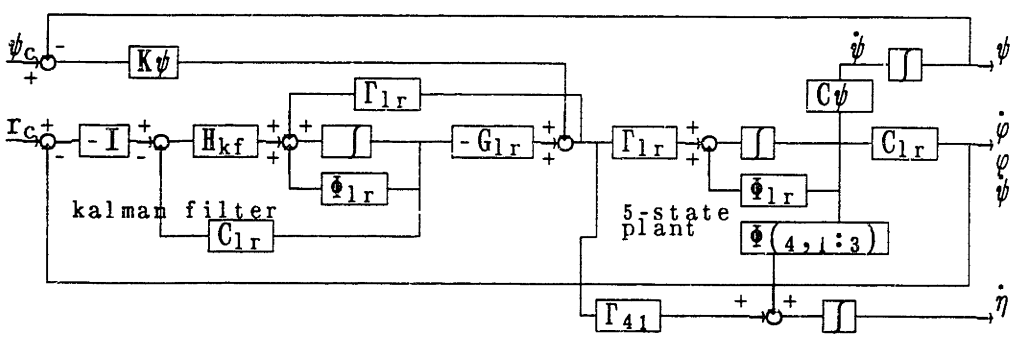

Figure 5.3.2 Discrete Time Lateral Closed Loop Block Diagram.

The subscript 'lr' refers to the reduced order (3-state) model used for design of the inner LQG regulation loop and specifically refers to the model determined by reducing the state vector to $x_{lr}=[\dot{\psi} \quad \varphi \quad \ddot{\psi}]^T$. Note that figure 5.3.2 refers to a five state plant, the extra state being simply the integral of yaw rate to yield heading angle.

By the very fact that we deem it necessary to use gain scheduling due to the non-robustness of the controllers to varying wheel speed, it is of quite significant importance to obtain good data as regards this parameter and in order to achieve this, it may be necessary to low pass filter this measurement as suggested in section 3.10, or even run a Kalman filter around the inner LQG loop (i.e. run an estimator in the outer wheel angular velocity loop), which would turn out to be of third order since as shown in appendix 2, the inner LQG loop Kalman filter dynamics may be ignored when considering only the outer loop, and the plant is third order when wheel speed is included. This will of course lead to a compensator of order five (three in outer loop and two in inner LQG loop), however, this does not pose any problems for us in implementation, so it is a feasible idea.

Simulations showing the performance of the gain scheduled controller in discrete time are shown if figure 5.3.3. The gains are continuously updated at each data sample point which is nominally selected at 0.01 seconds period

(sample rate 100 Hz). The simulation results look good, but the important issue is that the measurement of wheel angular velocity (Ω) is assumed perfect as is the model (in the sense of unmodeled high frequency dynamics) in the simulations, which is definitely not the case in the real world.

5.4 Stability of Gain Scheduled system

We have absolutely no guarantees as regards the stability of this scheme and make no claims to this end. As mentioned in chapter 4, we could consider the system as moving in a linearized time invariant sense from one stabilized point to an adjacent stabilized point and that the direction in which it starts out from each point is such as to incur minimal least squares penalty according to the LQG regulator and filter cost functions.

Of course one sure way to evaluate the scheme is to test it in the real world and these results should be available in the near future.

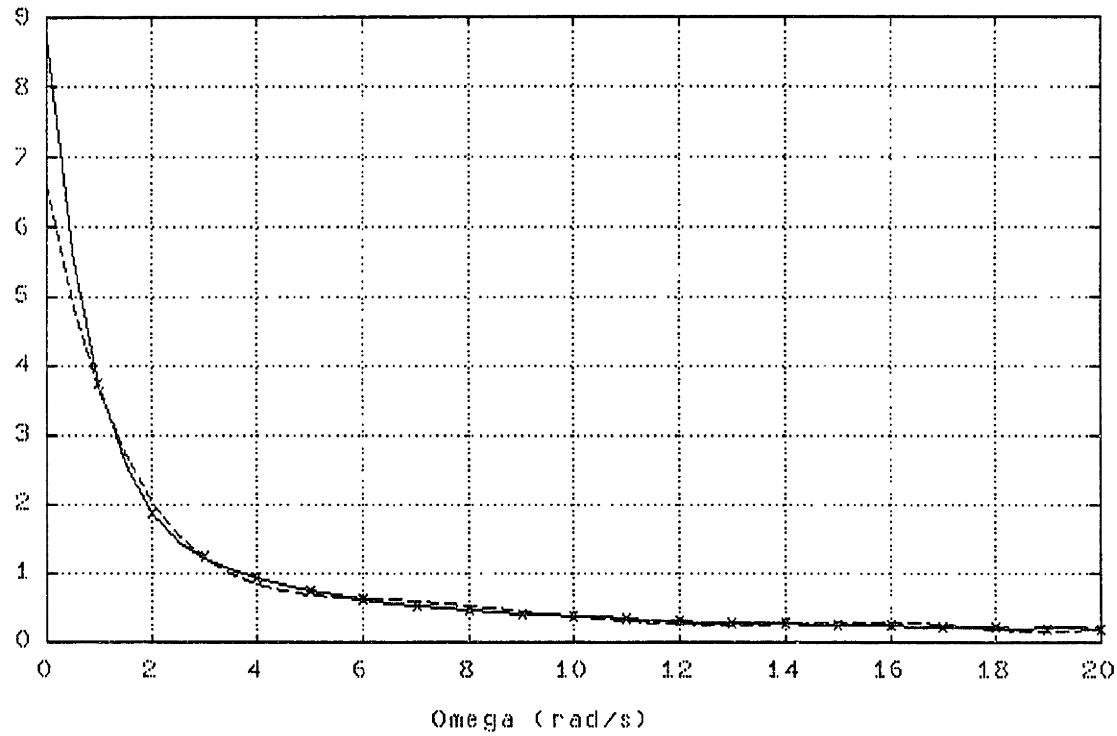

Figure 5.3.1. Regulator gain g1 variation with wheel angular velocity. The discrete data points (*) represent the value as determined by the controller design at the specific wheel speed. The continuous line represents the least squares curve fit for the ninth order polynomial and the dashed curve (- -) represents a seventh order polynomial fit. Clearly the seventh order fit is inadequate.

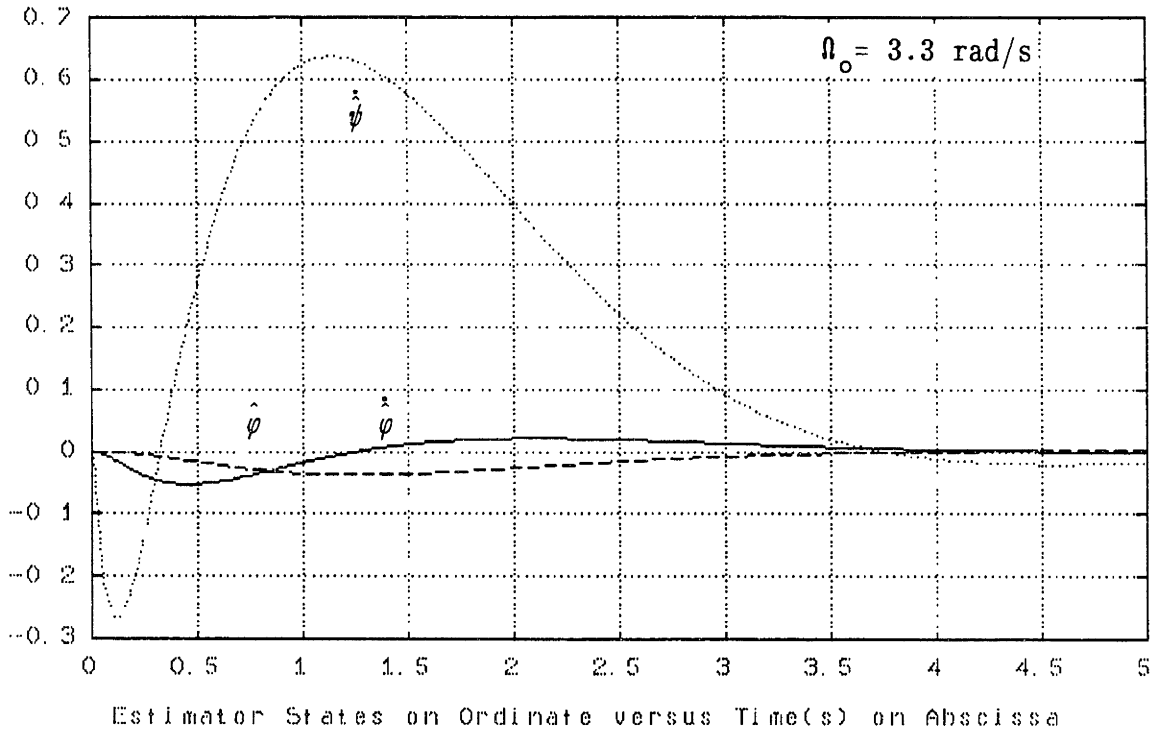

Figure 5.3.3a. Discrete time simulation of step heading command with gain scheduled controller. Inner loop Kalman filter estimates of roll angle, roll rate and yaw rate shown. The controller gains are updated at every time increment (100 Hz frequency). Comparison with figure 4.8.2.5 shows that in simulation, the gain scheduling has not affected performance at all.

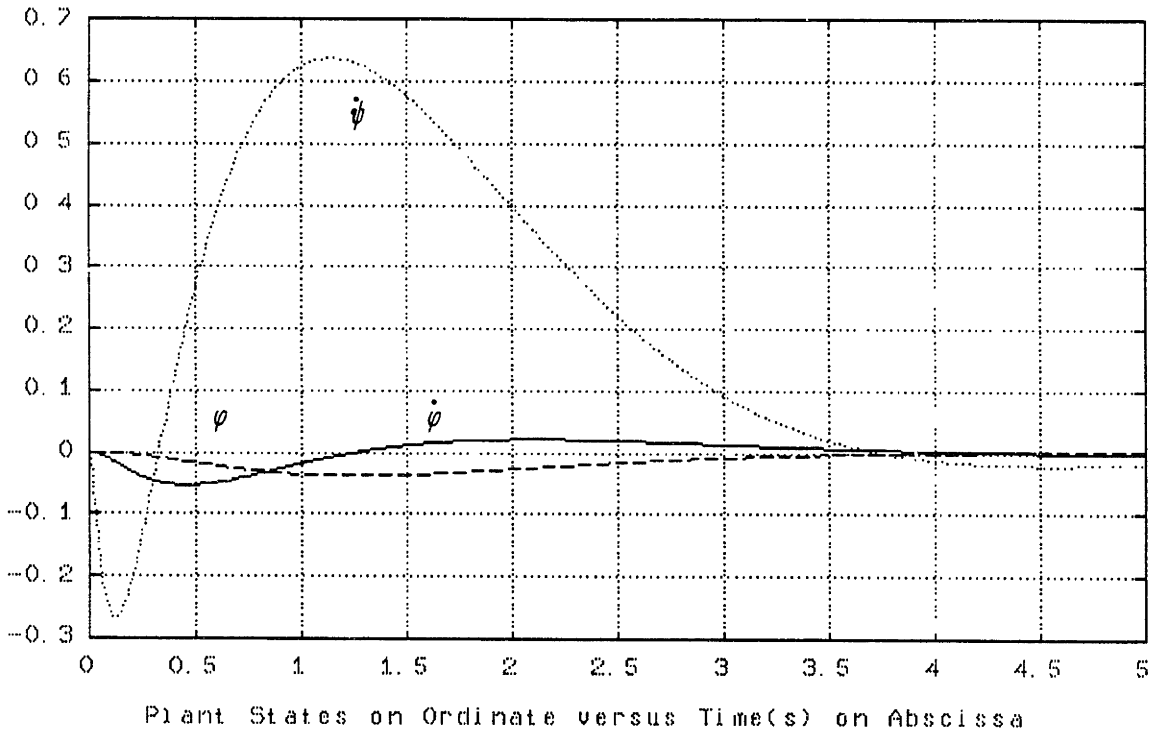

Figure 5.3.3b. Inner loop plant states roll angle, roll rate and yaw rate for step heading command. The estimated states accurately reflect similar time histories to these, as shown in figure 5.3.3a.

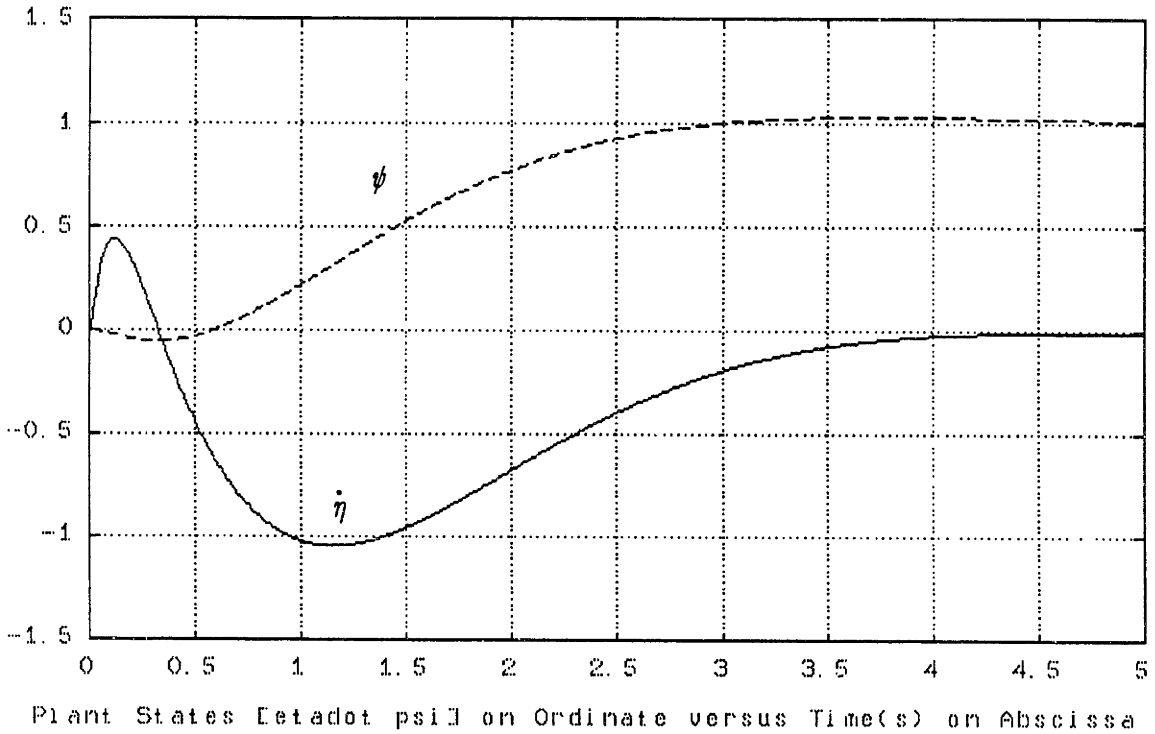

Figure 5.3.3c. Heading and turntable angular velocity response to step heading command for the gain scheduled controller.

6.0 PULSEWIDTH MODULATED BANG-BANG ADAPTIVE CONTROLLER

6.1 Introduction

Since the friction between the wheel and the surface is very 'condition dependent' for example tyre pressure and surface state markedly influence the nature and magnitude of the friction, it is desirable to have the controller capable of dealing with this situation. To this end we define an adaptive controller which could of its own accord determine the friction (in yawing motion) magnitude, but dependent on a pre-specified form or model.

In order to overcome the problem of stiction, we implement the lateral controller in the form of a bang-bang controller, the amplitude of actuation being larger than the estimated stiction such that the unicycle always breaks free of this restraining moment when commanded.

6.2 Friction Model

We model the friction in three forms. The equations of motion as derived in appendix 1 take into account the linear form of friction i.e. viscous friction which might be present between the wheel and the surface and all other forms of friction are lumped into the externally working friction term F. The viscous friction term models a form of yaw damping and is an opposing

moment in yaw which is a linear function of the yaw rate. The second form is stiction or static friction (breakaway friction) which is assumed to be a constant value and essentially represents a deadband of torque action on the system in that no motion occurs in yaw before the external action torque exceeds the magnitude of the stiction moment. Thirdly, we model a constant with yaw rate kinematic friction, which is thus independent of yaw rate and a function of the surface condition. Figure 6.2.1 shows a schematic diagram of the complete friction model.

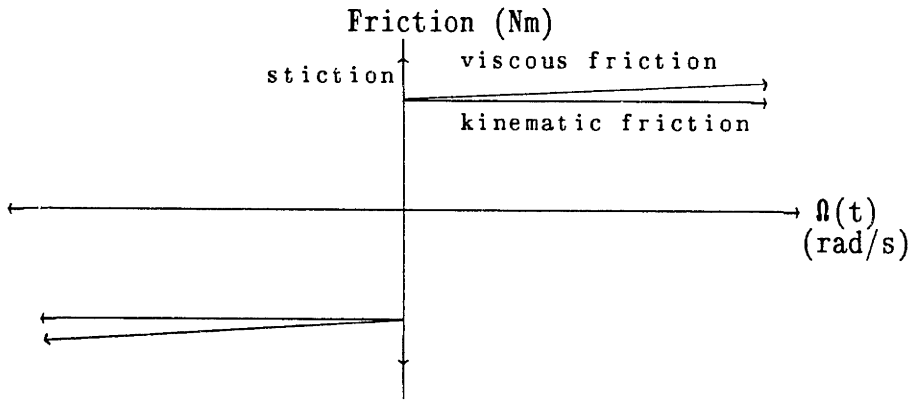

Figure 6.2.1 Yawing motion friction model

6.3 Pulsewidth Modulated Bang-Bang Controller Structure

The linear controllers we have thus far designed have the best chance of success if the unicycle in the real world is as closely as possible modeled by the linear equations of motion

as derived. To this end, we aim to identify the main source of potential deviation from the linear model. This is obviously the friction problem as defined in section 6.2 above and the obvious solution is to try and define some scheme such that as far as the linear control system is concerned, this nonlinearity is not apparent in the sense that the response of the unicycle to turntable torque commands should as close as possible be what is expected in the logic of the controller.

This implies defining a scheme which converts the commanded (by the controller) torques into an expected yaw acceleration, assuming that the longitudinal controller is successful in achieving its task of reducing pitch motion errors to zero. Referring to figure 6.3.2, the block defined as 'actuator' should essentially yield the expected accelerations desired by the controller in yawing motion.

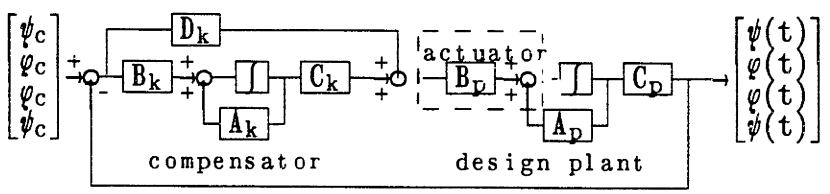

Figure 6.3.2 Location of 'actuator' block.

Assuming the pitch controller is successful and since we do not ever command steady turn rates (rather, heading is commanded) the roll rates and roll errors can be assumed small, the

lateral yawing motion may be described by a single simple equation

$$\ddot{\psi}(t) = K_t \Gamma_t - [\text{friction effects}]$$

where K_t represents inertia effects and is the associated element in the control distribution matrix of the linear model. Γ_t is the turntable torque assumed instantaneously achieved since the time constant (in torque) of the DC motor used is negligible. The linear controller, however, expects yaw acceleration governed approximately by the equation (other small terms are neglected)

$$\ddot{\psi}(t) = K_t \Gamma_t$$

Clearly, the difference in actual response and linear expected response is due to the friction effects and we could obtain estimates of the friction by measuring the yaw rate and comparing this with the expected rate. Thus

$$\dot{\psi}_{expected} - \dot{\psi}_{actual} = \int_{t_i}^{t_f} \{ K_t \Gamma_t + [\text{friction effects}] - K_t \Gamma_t \} \, dt$$

or, considering the differential over a small interval in time Δt

$$\frac{\dot{\psi}_{expected} - \dot{\psi}_{actual}}{\Delta t} \approx - [\text{friction effects}]$$

This offers a means of estimating the friction effects, but the estimate must occur over a short time period and the assumption regarding the fast torque motor response may be inaccurate over short time intervals. A better approach would be to do estimation while the system has no actuator torques active. In this case the governing equation of motion is simply

$$\ddot{\psi}(t) = -[\text{friction effects}]$$

the negative sign indicating the effect of friction is to derease the yaw rate. Now it is simpler to consider a period of time over which the turntable torque actuator has no command and take measurements of the yaw rate at the beginning and the end of this period. The estimate of friction effects is then

$$\frac{\dot{\psi}_{initial} - \dot{\psi}_{final}}{\Delta t} \approx -[\text{friction effects}]$$

which is dependant on good measurements of $\dot{\psi}$ and has one less source of error in that since no turntable torque is active, this does not also have to be determined as is necessary in the previous suggested approach.

6.4 Bang-Bang Control

The requirement we have imposed upon ourselves by the second method of friction effects estimation is that the lateral

system has to run open loop for a short period of time whilst measurements are made to drive the estimator. This fits very nicely into the framework of a discrete time bang-bang pulsewidth modulated strategy. We define three time scales: 1) define Δt_c as the time period over which the torque command to the turntable is held constant and 2) define T to be the sample period of the discrete time controller, with $\Delta t_c > T$ and 3) define Δt_t as the time period of fixed amplitude torque application to exert an equivalent (to the linear controller required value) torque impulse on the system.

The magnitude of the torque command (Γ_c) to remain constant over the interval Δt_c is determined by the controller based on the latest measurements and the product of this value and Δt_c determines the impulse which will be applied to the system by this command.

$$I_m = \Gamma_c \Delta t_c \quad \text{(Newton meter seconds)}$$

Consider the actuator which applies torques of fixed magnitude, Γ_f, then the duration of this torque required to yield the same impulse (Newton meter seconds) to the system is

$$\Delta t_t = \frac{I_m}{\Gamma_f}$$

$$= \frac{\Gamma_c \Delta t_c}{\Gamma_f} \quad \text{(seconds)}$$

A timing diagram showing the relation between the 3 time intervals as defined here is given in figure 6.4.1

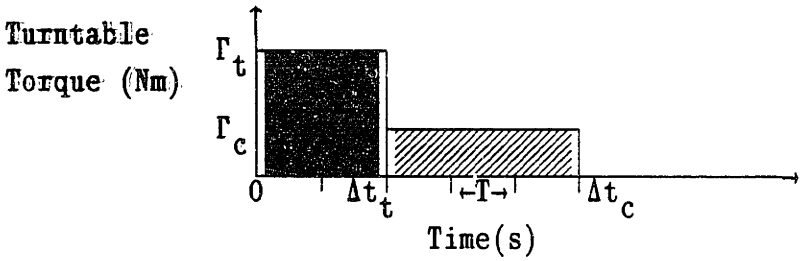

Figure 6.4.1 Timing Diagram for Pulsewidth Modulation

In figure 6.4.1, the area under the curves represent the equivalent torque impulse applied to the system for the constant torque inputs. As defined above, the interval Δt_c represents the interval of constant applied torque and Δt_t the time interval required to yield the same impulse with larger amplitude. The interval $(\Delta t_c - \Delta t_t)$ is the interval over which the torque command is set to zero and is thus also the interval over which yaw rate measurements are used to obtain an estimate of the friction.

The time interval Δt_c must be selected large enough such that it does not excite the unmodeled dynamics of the drive train and the motor should be able to achieve the selected rate of torque commands. The trade-off is to ensure that this interval is short enough so as not to allow the unicycle to attain irrecoverable roll or pitch errors between actuation.

The discretization interval T, as shown indicates the fact that

the applied constant torque may only exist over integer multiples of T, thus it is apparent that the unicycle will settle into a stable limit-cycle induced by the controller since it can never achieve the infinitesimally small torque impulses required to maintain an unnoticeably small amplitude limit cycle, unless we use amplitude modulation together with pulsewidth modulation.

6.5 Compensating for Friction

Now we have a controller structure which obtains on-line estimates of the total friction effective in yawing on the unicycle and we use this information to define compensatory values in the commanded torque to overcome these effects.

Consider the friction as estimated

$$F = I_3\left(\frac{\dot{\psi}_{initial} - \dot{\psi}_{final}}{\Delta t_c - \Delta t_t}\right)$$

where I_3 represents the moment of inertia about the yaw axis of the unicycle wheel and frame. Bearing in mind the fact that we are trying to ensure that the response of the system is as expected by the linear controller it is obvious that the friction needs to be compensated for. This is easily achieved assuming that the friction estimate is relatively accurate and then increasing the commanded torque by this amount.

In the bang-bang controller framework, this implies increasing the time Δt_t (amplitude is constant) as follows. Let the friction compensated time interval be Δt_f, then assuming that the friction is essentially consistant of kinematic friction and is thus constant, get

$$\Gamma_t \Delta t_f = (\Gamma_c + F) \Delta t_c$$

or

$$\Delta t_f = \frac{(\Gamma_c + F) \Delta t_c}{\Gamma_t}$$

6.6 Implementation

Simulation results of this adaptive, bang-bang control algorithm are shown in figure 6.6.1. In these simulations, the discretization of the system is done for a sample period of 0.01 seconds and the time interval Δt_c= 0.05 seconds, with torque amplitude of one Newton meter (motor torque). Various amplitude torque values and time intervals Δt_c, were simulated, the only requirements being that the torque value be significantly greater than the stiction , but smaller than motor saturation torque, and the main difference in performance is the magnitude of the limit cycle which results. Also, Δt_c must be small enough (Δt_c=0.1 seconds simulations showed no degradation in performance) to prevent errors too large for

system recovery developing, i.e. Δt_c should be small compared to system time constants. Typical values of stiction are assumed to be approximately 1.5 times greater than the kinematic friction [13] and since we estimate the kinematic (or dynamic) friction, the controller knows roughly what the stiction value is.

6.6.1 Limit Cycle Amplitude

The limit cycle which results from the bang-bang controller, has amplitude directly related to the amplitude of the peak torque value used in the bang-bang structure. Also, the frequency of the cycle is obviously the inverse of the time period over which commands are held constant. Thus

$$F_{lc} = \frac{1}{\Delta t_c} \quad (Hz)$$

For the system in a stable limit cycle, the impulse applied to the system is determined as

$$I_{lc} = (\Gamma_t - F)\,\Delta t_t - F\,(\Delta t_c - \Delta t_t)$$

$$= (I_3^W + I_3^F)\,(\dot{\psi}_1 - \dot{\psi}_2) \qquad 6.6.1.1$$

Where $\dot{\psi}_1$ and $\dot{\psi}_2$ are the initial and final yaw rates, evaluated at the beginning of the impulse application time and time period Δt_c later, respectively and F is the friction in yaw assumed to be kinematic friction since a yaw rate exists (hence no static friction) and these rates are small enough to neglect viscous friction in this analysis. By the nature of the limit cycle, the yaw rate at the start of Δt_c is exactly the negative of the final value at the end of the interval Δt_c, or

$$\dot{\psi}_2 = -\dot{\psi}_1$$

Using this in 6.6.1.1,

$$\Gamma_t \Delta t_t - F \Delta t_c = 2\dot{\psi}_{1c}(I_3^W + I_3^F)$$

Now the amplitude of the limit cycle is determined by integrating over one half cycle (Δt_c), thus

$$\psi_{1c} = \frac{1}{(I_3^W + I_3^F)2} \int_{\Delta t_c} (\Gamma_t \Delta t_t - F \Delta t_c)$$

$$\doteq \frac{1}{(I_3^W + I_3^F)2} [\Gamma_t \Delta t_t^2 - F \Delta t_c^2]$$

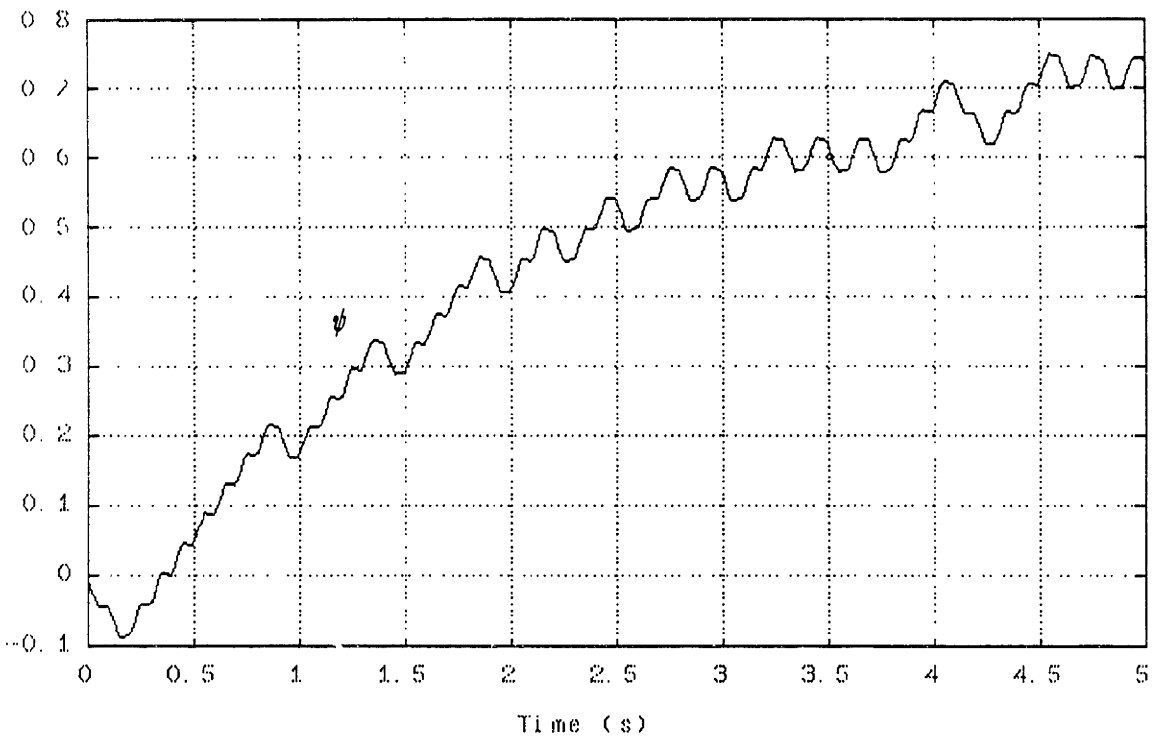

Figure 6.6.1a. Gain scheduled bang-bang controller. Heading response to step command. This is representative of typical human unicyclist control. The 'global' heading change is accomplished in a series of discrete incremental heading changes. This simulation used fixed turntable motor torque amplitude of 1 Nm and time interval Δt_c of 0.05 seconds. The discretization sample rate is 100 Hz.

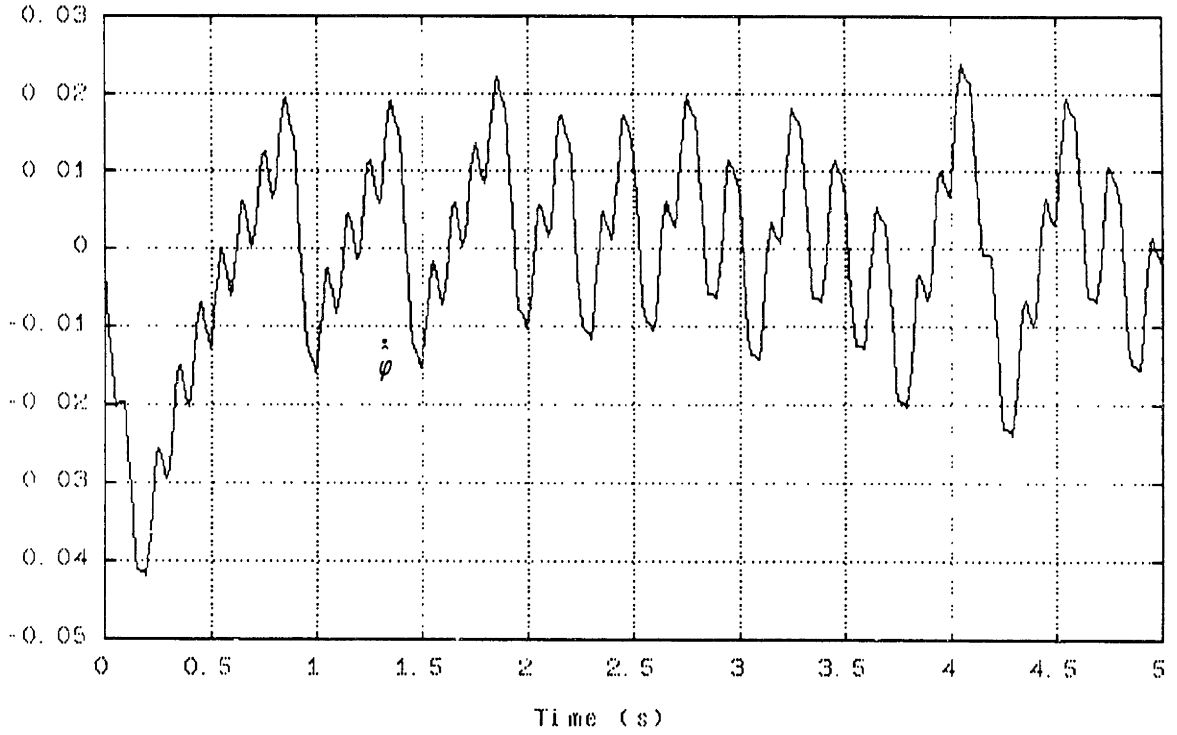

Figure 6.6.1b. Bang-bang controller. Estimated roll rate (rad/s).

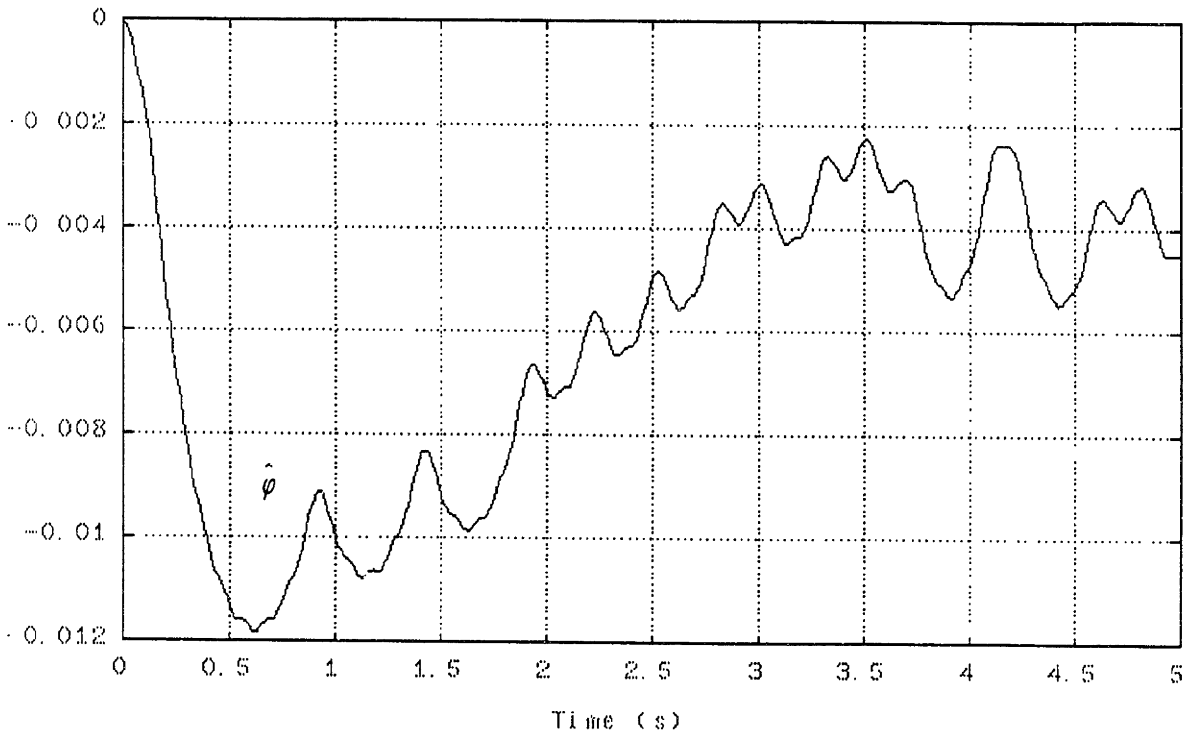

Figure 6.6.1c. Bang-bang controller. Estimated roll angle (radians).

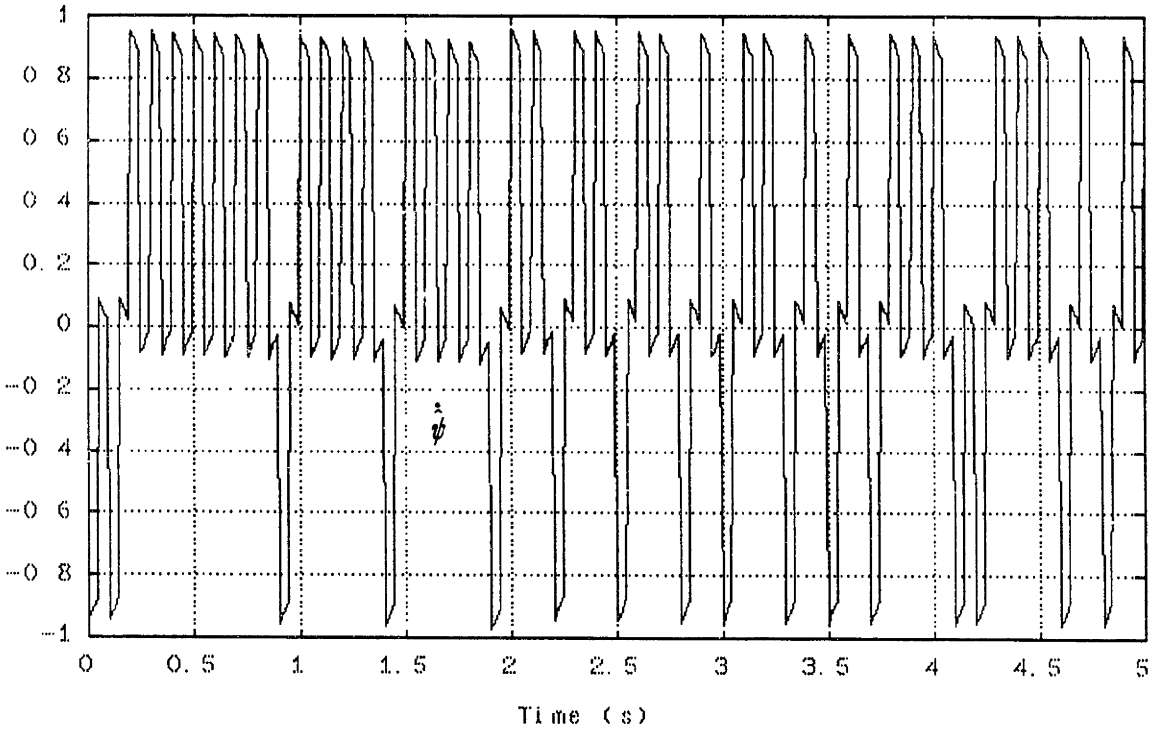

Figure 6.6.1d. Estimated yaw rate (rad/s). The Kalman filter estimates of figures 6.6.1 b through d show excellent tracking of the actual plant states shown in e through g.

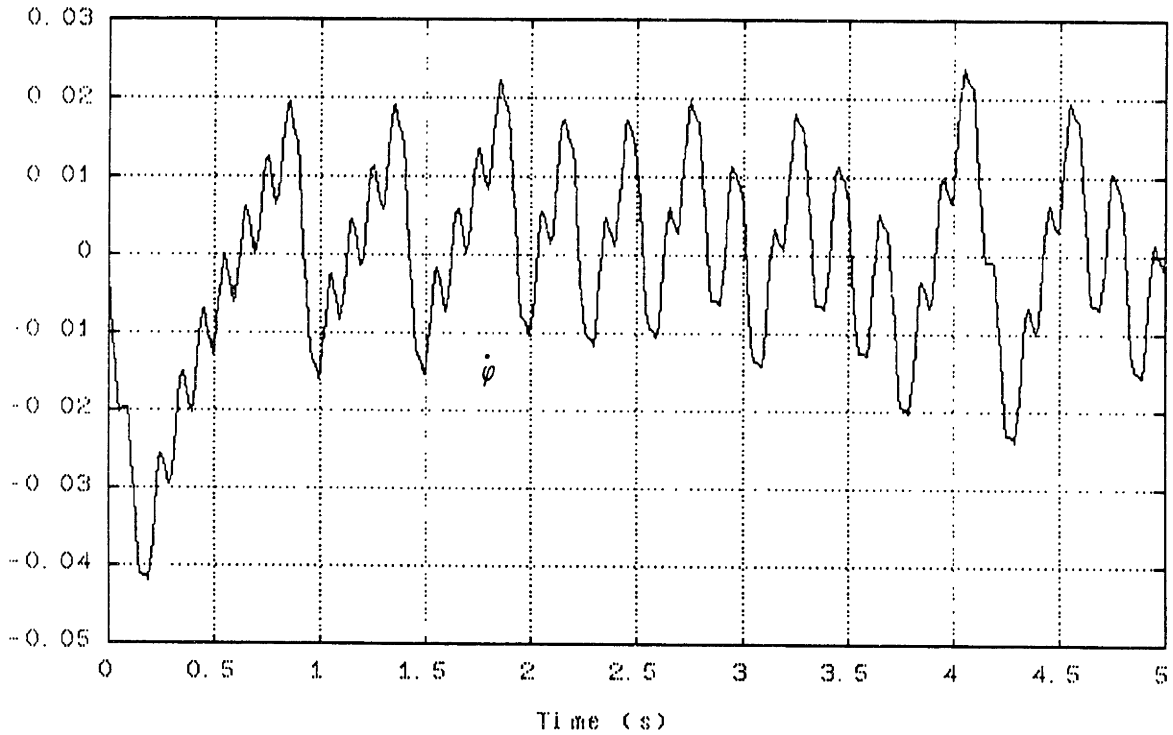

Figure 6.6.1e. Bang-bang control. Roll rate (rad/s) response.

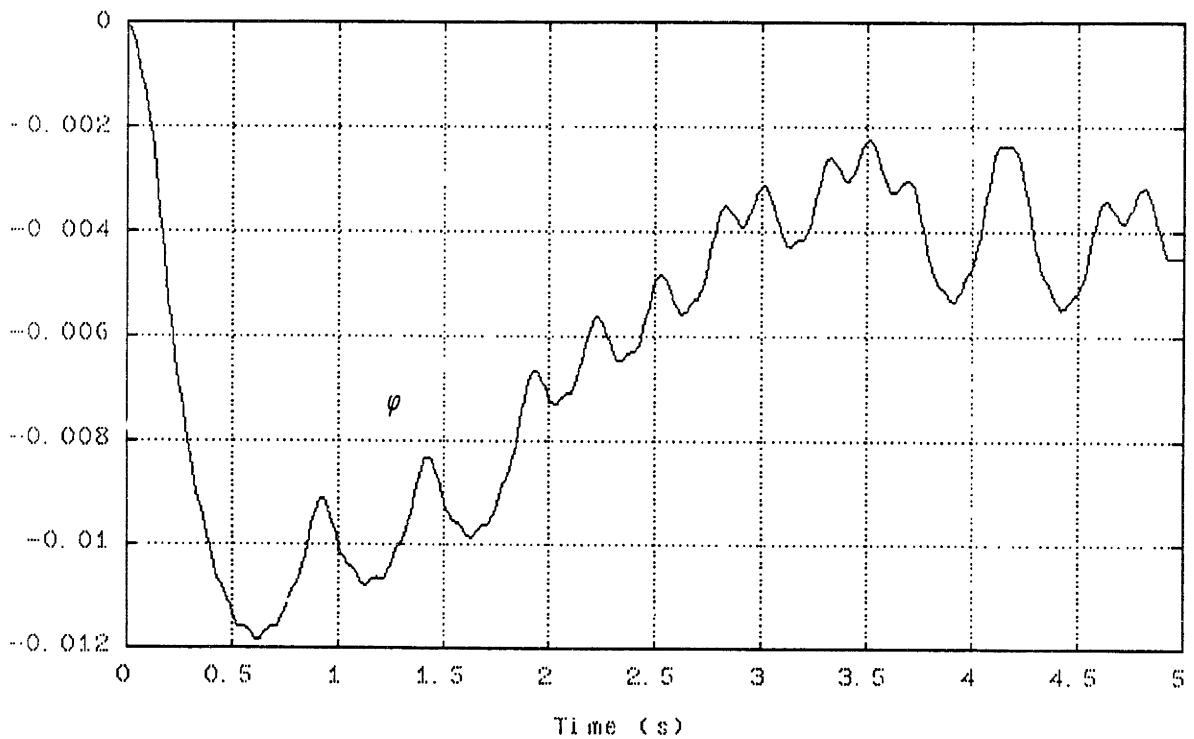

Figure 6.6.1f. Bang-bang control. Roll angle (rad) response.

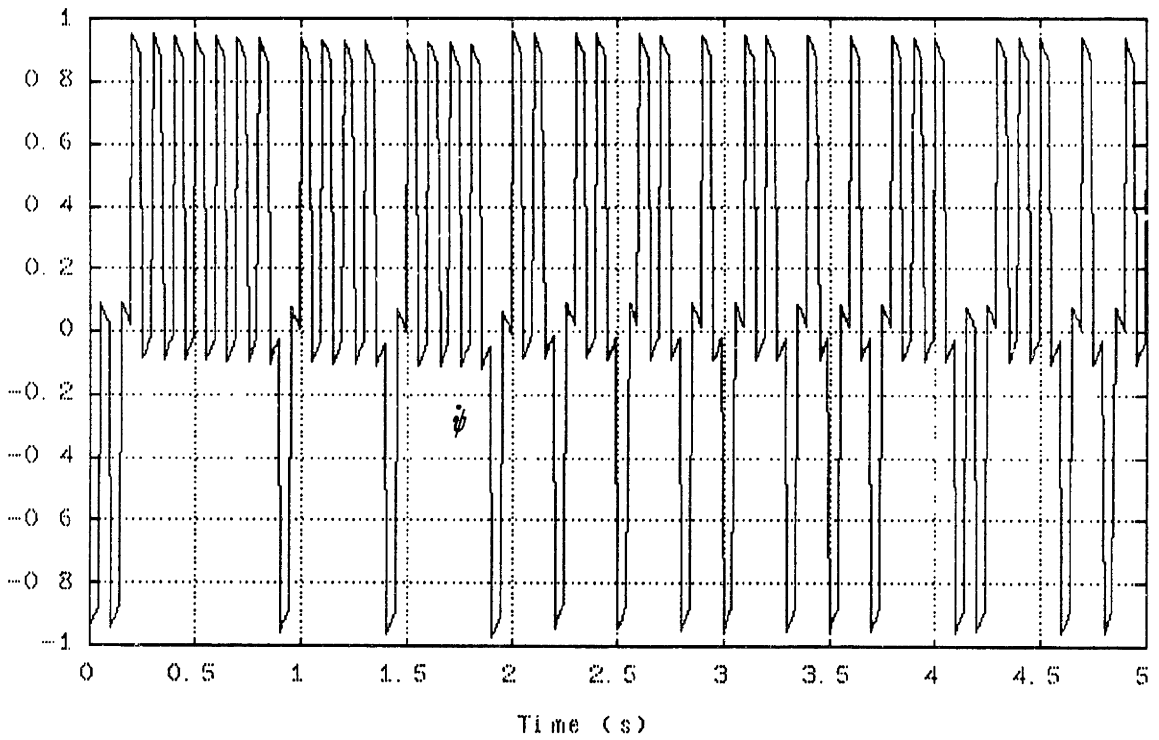

Figure 6.6.1g. Plant yaw rate response (rad/s). Pulse torque commands are applied and estimation of kinematic frictiom occurs whilst applied turntable torque is set to zero. The gradient of the response between pulses is proportional to this friction.

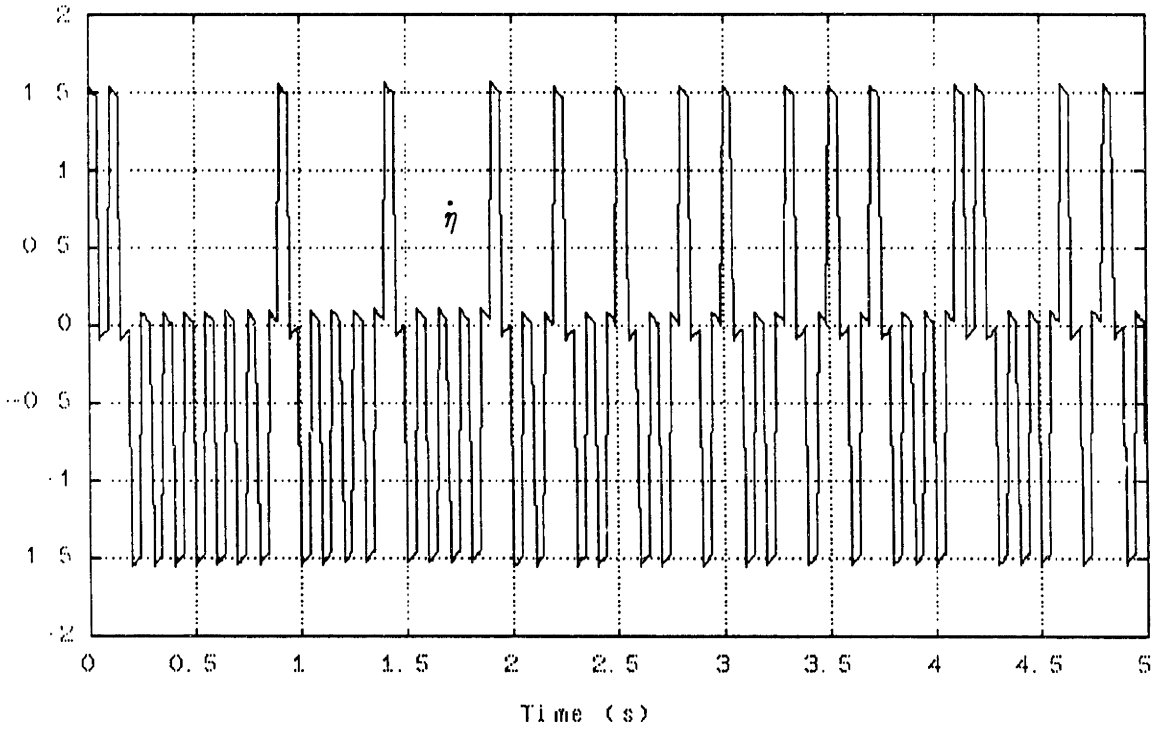

Figure 6.6.1h. Turntable angular velocity response. (rad/s)

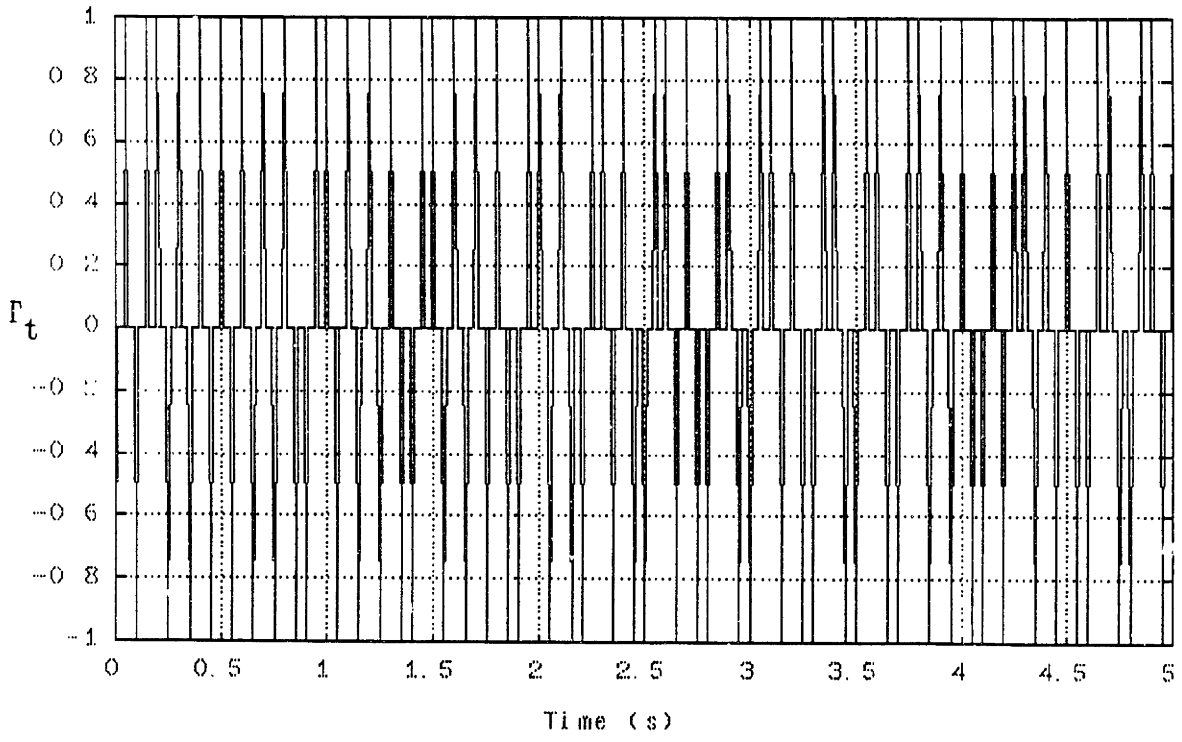

Figure 6.6.1i. Actuator activity (Nm). The fixed amplitude (1 Nm) pulsewidth modulated control is apparent here.

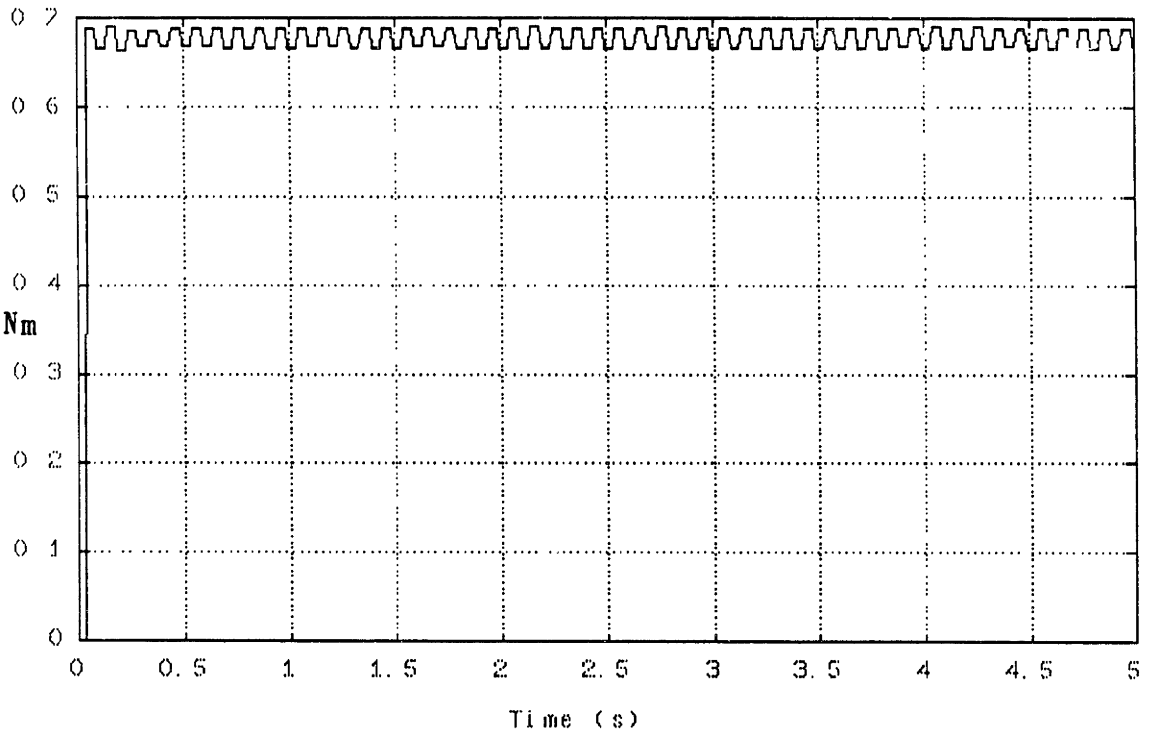

Figure 6.6.1j. Friction estimate. This estimate is obtained during periods of zero turntable torque actuation, when the unicycle yawing motion occurs in an unforced fashion. The stepping effect is due to the estimate lumping all effects other than linear frictionless response into a friction estimate, so that the viscous friction also is contained in this estimate. Since the yaw rate varies between approximately 0.1 rad/s and 0.9 rad/s at each alternate pulse, the viscous friction contribution alternates between pulses.

7.0 DISCUSSION AND CONCLUSION

The derivation of the equations of motion in appendix 1 demonstrates the ease of using Kane's approach for multibody systems. Also, the method lends itself well to extension of the linearized equations to incorporate nonlinear (smooth) effects as is illustrated by the inclusion of large yaw rates, $\dot{\psi}$ as not being a perturbation quantity. The method is well defined and yields a formal approach to deriving equations of motion, which places minimal emphasis on intuitive insight into the complex motions involved.

This study has yielded controllers of order equal to the plant. The possibility of these eventually being implemented with extra filtering of the outer loops, resulting in controllers of higher order than the plant is also suggested. As the main objective is to stabilize the unicycle, the fact that a controller of higher order than the model might be used is completely justifiable in the light of the difficulty experienced by human beings in riding the unicycle even though the 'order' of the human controller is certainly of much higher degree than the unicycle, although this is difficult to quantify in the nonlinear terms of the human controller. The dynamics of the unicycle are certainly within the bandwidth of the human capability in terms of response times, and the sensor and actuator data are much cleaner than could be hoped for in the 'robot', so this cannot be used as an excuse for failing to

maintain balance, although this is a nontrivial task and is often met with failure by the inexperienced cyclist. What is being suggested here, is that it is conceivable that in order to control 'difficult' plants it may be necessary to use controllers of order greater than the plant and that the structure must be well defined.

The unicycle is certainly one of the more challenging control design problems and this study serves well to highlight the limitations of plant inversion design approaches for non minimum-phase, unstable systems. These design approaches yield poor designs even before any nonlinear effects are considered. Much improved designs were achieved using variations on the LQG design approach combined with classical control evaluation techniques, such as gain and phase margins and loop transfer function shaping in the frequency domain.

A further significant point illustrated is the importance of good understanding of nonlinear issues dominant in the particular system. In the case of the unicycle, the greatest difficulty is the problem of compensating for friction effects in yawing motion. The linear lateral control system designed was completely inadequate in this regard and substantial thought and innovation was called upon to suggest solutions. It is of value to point out that linear friction in the form of viscous friction, is easily dealt with by including this in the linear model. This is the only form of friction dealt with in

the Stanford project [14].

The discontinuous, nonlinear Coulomb friction, which models both stiction and kinematic friction, was best dealt with in simulation by implementation of the linear lateral controller in a bang-bang framework, using simple ad hoc estimation to determine continuous estimates of friction between the wheel and the surface in yaw motion. This is only one suggestion and there are probably many methods, the problem is of course to identify a suitable method and the only true criteria for judgment is practical evaluation of these designs.

It has become clear through this study that a good approach to control design is to understand the dynamics of the system to be controlled as well as possible. Identification of parameters contributing to coupling of system dynamics yields insight into means of addressing control issues of subsystems of the dynamic model individually. Also of significance is time scale separation of the dynamics in the classical sense and manipulation of the structure to using these to advantage, apart from the nonlinear issues as discussed above.

Issues not addressed in this study include the station keeping problem. It is felt that a major achievement would be stabilizing the unicycle and as such the station keeping issue is regarded as an extension of this study. It is quite probable that at least for the lateral controller, a significantly

different strategy is necessary. The human unicyclist generates a for-aft sinusoidal motion when in this mode of operation and further study of this control strategy could yield invaluable insight into this problem.

APPENDIX 1 EQUATIONS OF MOTION USING KANE'S METHOD

Introduction

The rigid body equations of motion are derived here using the methodology known as "Kane's Equations" [2, 11]. The linearization reference condition is the unicycle in a vertical standing statically unstable equilibrium at constant forward speed. The equations of motion derived are nonlinear in yaw rate $\dot{\psi}$, which is allowed to become large in order to capture the interaction between roll angle and pitch angle errors when maneuvering through large yaw rates.

Since a controller is to be designed to maintain small ($< 5^{\circ}$) deviations from vertical in both pitch and roll and assuming that this is attained, these equations completely model the controlled rigid body dynamics of the unicycle and are used for validation simulations of the controller designs.

The complete linearized equations of motion are also presented as a specialization of the nonlinear in $\dot{\psi}$ equations, for linear controller design purposes.

A.1 Reference Frames

Define the following reference frames as illustrated in figure a.1:

1) Earth fixed Newtonian reference F_a.

2) Wheel axle fixed reference F_w.

3) Unicycle frame fixed reference F_f.

4) Turntable shaft fixed reference F_t.

The frames F_w, F_f and F_t are centered at the respective centres of mass of the elements referred to.

A.2 Notation

Define the following vector notation used throughout:

$^{a}v^{b}$ ≡ linear velocity of b in reference frame F_a

$^{f}\omega^{i}$ ≡ angular velocity of i in reference frame F_f

f_1 ≡ basis vector in frame F_f

A.3 Velocities (nonlinear)

Define the following angular velocities:

Turntable referance angular velocity	$\dot{\eta}_o t_3$
Turntable perturbation angular velocity	$\dot{\eta} t_3$
Wheel referance angular velocity	$\Omega_o w_2$
Wheel perturbation angular velocity	Ωw_2

Angular velocities of wheel, frame and turntable:

$$^{a}\omega^{F} = \dot{\psi} b_3 + \dot{\varphi} w_1 + \dot{\theta} w_2$$

$$^{a}\omega^{T} = \dot{\psi} b_3 + \dot{\varphi} w_1 + \dot{\theta} w_2 + (\dot{\eta} + \dot{\eta}_o) f_3$$

$$^{a}\omega^{W} = \dot{\varphi}w_1 + (\Omega + \Omega_o)w_2 + \dot{\psi}b_3$$

Linear velocities of mass centres:

$$^{a}v^{W} = {}^{a}\omega^{W} \times r_w w_3$$
$$= r_w(\Omega + \Omega_o)w_1 + r_w\dot{\psi}\sin(\varphi)w_1 - r_w\dot{\varphi}w_2$$

$$^{a}v^{F} = {}^{a}v^{W} + {}^{a}\omega^{f} \times r_f f_3$$
$$= (r_f\dot{\theta}\cos(\theta) + r_f\dot{\psi}\sin(\varphi)\cos(\theta) + r_w(\Omega + \Omega_o))w_1$$
$$+ r_w\dot{\psi}\sin(\varphi)w_1 + (r_f\dot{\psi}\cos(\varphi)\sin(\theta) - (r_w + r_f\cos(\theta))\dot{\varphi}w_2$$
$$- (r_f\dot{\theta}\sin(\theta) + r_f\dot{\psi}\sin(\varphi)\sin(\theta))w_3$$

$$^{a}v^{T} = {}^{a}v^{W} + {}^{a}\omega^{f} \times l_t f_3$$
$$= (l_t\dot{\theta}\cos(\theta) + l_t\dot{\psi}\sin(\varphi)\cos(\theta) + r_w(\Omega + \Omega_o))w_1$$
$$+ r_w\dot{\psi}\sin(\varphi)w_1 + (l_t\dot{\psi}\cos(\varphi)\sin(\theta) - (r_w + l_t\cos(\theta))\dot{\varphi}w_2$$
$$- l_t\dot{\theta}\sin(\theta)w_3 - l_t\dot{\psi}\sin(\varphi)\sin(\theta)w_3$$

A.4 Partial Velocities

$\frac{\partial}{\partial\Omega}(.)$:
$\frac{\partial}{\partial\Omega}(^{a}v^{W}) = r_w w_1$ $\quad$ $\frac{\partial}{\partial\Omega}(^{a}v^{F}) = r_w w_1$ $\quad$ $\frac{\partial}{\partial\Omega}(^{a}\omega^{T}) = 0$
$\frac{\partial}{\partial\Omega}(^{a}v^{T}) = r_w w_1$ $\quad$ $\frac{\partial}{\partial\Omega}(^{a}\omega^{W}) = w_2$ $\quad$ $\frac{\partial}{\partial\Omega}(^{a}\omega^{F}) = 0$

$\frac{\partial}{\partial\dot{\varphi}}(.)$:
$\frac{\partial}{\partial\dot{\varphi}}(^{a}v^{W}) = -r_w w_2$ $\quad$ $\frac{\partial}{\partial\dot{\varphi}}(^{a}v^{F}) = -(r_w + r_f)w_2$
$\frac{\partial}{\partial\dot{\varphi}}(^{a}v^{T}) = -(r_w + l_t)w_2$ $\quad$ $\frac{\partial}{\partial\dot{\varphi}}(^{a}\omega^{W}) = w_1$
$\frac{\partial}{\partial\dot{\varphi}}(^{a}\omega^{F}) = w_1$ $\quad$ $\frac{\partial}{\partial\dot{\varphi}}(^{a}\omega^{T}) = w_1$

$$\frac{\partial}{\partial\dot{\psi}}(.): \quad \frac{\partial}{\partial\dot{\psi}}({}^{a}_{v}W) = r_w\varphi w_1 \qquad \frac{\partial}{\partial\dot{\psi}}({}^{a}_{v}F) = (r_w + r_f)\varphi w_1 + r_f\theta w_2$$

$$\frac{\partial}{\partial\dot{\psi}}({}^{a}_{v}T) = (r_w + l_t)\varphi w_1 + l_t\theta w_2 \qquad \frac{\partial}{\partial\dot{\psi}}({}^{a}_{\omega}W) = \varphi w_2 + w_3$$

$$\frac{\partial}{\partial\dot{\psi}}({}^{a}_{\omega}F) = \varphi w_2 + w_3 \qquad \frac{\partial}{\partial\dot{\psi}}({}^{a}_{\omega}T) = \varphi w_2 + w_3$$

$$\frac{\partial}{\partial\dot{\theta}}(.): \quad \frac{\partial}{\partial\dot{\theta}}({}^{a}_{v}W) = 0 \qquad \frac{\partial}{\partial\dot{\theta}}({}^{a}_{v}F) = r_f w_1 - r_f\theta w_3$$

$$\frac{\partial}{\partial\dot{\theta}}({}^{a}_{v}T) = l_t w_1 - l_t\theta w_3 \qquad \frac{\partial}{\partial\dot{\theta}}({}^{a}_{\omega}W) = 0 \qquad \frac{\partial}{\partial\dot{\theta}}({}^{a}_{\omega}F) = w_2$$

$$\frac{\partial}{\partial\dot{\theta}}({}^{a}_{\omega}T) = w_2$$

$$\frac{\partial}{\partial\dot{\eta}}(.): \quad \frac{\partial}{\partial\dot{\eta}}({}^{a}_{v}W) = 0 \qquad \frac{\partial}{\partial\dot{\eta}}({}^{a}_{v}F) = 0 \qquad \frac{\partial}{\partial\dot{\eta}}({}^{a}_{v}T) = 0$$

$$\frac{\partial}{\partial\dot{\eta}}({}^{a}_{\omega}W) = 0 \qquad \frac{\partial}{\partial\dot{\eta}}({}^{a}_{\omega}F) = 0 \qquad \frac{\partial}{\partial\dot{\eta}}({}^{a}_{\omega}T) = \theta w_1 + w_3$$

A.5 Velocities (nonlinear in $\dot{\psi}$)

The velocities are linearized here, allowing for $\dot{\psi}$ being large and thus not considered a linearizing ("small") quantity.

$$\begin{aligned}
{}^{a}_{\omega}W &= \dot{\varphi}w_1 + (\Omega + \Omega_o + \dot{\psi}\varphi)w_2 + \dot{\psi}w_3 \\
{}^{a}_{\omega}F &= \dot{\varphi}w_1 + (\dot{\theta} + \dot{\psi}\varphi)w_2 + \dot{\psi}w_3 \\
{}^{a}_{\omega}T &= (\dot{\varphi} + \dot{\eta}_o\theta)w_1 + (\dot{\theta} + \dot{\psi}\varphi)w_2 + (\dot{\eta} + \dot{\eta}_o + \dot{\psi})w_3 \\
{}^{a}_{v}W &= r_w(\Omega + \Omega_o + \dot{\psi}\varphi)w_1 - r_w\dot{\varphi}w_2 \\
{}^{a}_{v}F &= (r_f\dot{\theta} + r_f\dot{\psi}\varphi + r_w(\Omega + \Omega_o + \dot{\psi}\varphi))w_1 + r_f\dot{\psi}\theta w_2 \\
&\quad - (r_w + r_f)\dot{\varphi}w_2 \\
{}^{a}_{v}T &= (l_t\dot{\theta} + r_w(\Omega + \Omega_o + \dot{\psi}\varphi) + l_t\dot{\psi}\varphi)w_1 + l_t\dot{\psi}\theta w_2 \\
&\quad - (r_w + l_t)\dot{\varphi}w_2
\end{aligned}$$

A.6 Rectilinear Accelerations (nonlinear in $\dot{\psi}$)

In this section we use extensively the angular velocity of frame F_w in inertial space, denoted by ${}^{a}\omega^{W} = \dot{\varphi}w_1 + \dot{\psi}\varphi w_2 + \ddot{\psi}w_3$.

$$
\begin{aligned}
{}^{a}a^{W} &= \frac{{}^{W}d}{dt}({}^{a}v^{W}) + {}^{a}\omega^{W} \times {}^{a}v^{W} \\
&= r_w(\Omega + \ddot{\psi}\varphi + 2\dot{\psi}\dot{\varphi})w_1 + r_w(\Omega_o\dot{\psi} + \Omega\dot{\psi} + \dot{\psi}\dot{\psi}\varphi - \ddot{\varphi})w_2 \\
&\quad - r_w\Omega_o\dot{\psi}\varphi w_3
\end{aligned}
$$

$$
\begin{aligned}
{}^{a}a^{F} &= \frac{{}^{W}d}{dt}({}^{a}v^{F}) + {}^{a}\omega^{W} \times {}^{a}v^{F} \\
&= (r_f\ddot{\theta} + (r_w + r_f)\ddot{\psi}\varphi + 2(r_w + r_f)\dot{\psi}\dot{\varphi} + r_w\Omega)w_1 \\
&\quad - \dot{\psi}\dot{\psi}\theta r_f w_1 + (r_w(\Omega_o + \Omega)\dot{\psi} + (r_w + r_f)(\dot{\psi}\dot{\psi}\varphi - \ddot{\varphi}))w_2 \\
&\quad + (r_f\ddot{\psi}\theta + 2r_f\dot{\psi}\dot{\theta})w_2 - r_w\Omega_o\dot{\psi}\varphi w_3
\end{aligned}
$$

$$
\begin{aligned}
{}^{a}a^{T} &= \frac{{}^{W}d}{dt}({}^{a}v^{T}) + {}^{a}\omega^{W} \times {}^{a}v^{T} \\
&= (l_t\ddot{\theta} + (r_w + l_t)(\ddot{\psi}\varphi + 2\dot{\psi}\dot{\varphi}) + r_w\Omega - l_t\dot{\psi}\dot{\psi}\theta)w_1 \\
&\quad + (l_t\ddot{\psi}\theta + (r_w + l_t)(\dot{\psi}\dot{\psi}\varphi - \ddot{\varphi}) + 2l_t\dot{\psi}\dot{\theta})w_2 \\
&\quad + r_w\dot{\psi}(\Omega + \Omega_o)w_2 - r_w\Omega_o\dot{\psi}\varphi w_3
\end{aligned}
$$

A.7 Inertia Forces

$$
\begin{aligned}
F^{W*} &= - m_w\, {}^{a}a^{W} \\
F^{F*} &= - m_f\, {}^{a}a^{F} \\
F^{T*} &= - m_t\, {}^{a}a^{T}
\end{aligned}
$$

A.8 Inertia Torques

First define the principle inertia dyadics for the wheel, frame and turntable:

$$\text{Turntable} \qquad I^T = I_1^T f_1 f_1 + I_2^T f_2 f_2 + I_3^T f_3 f_3$$
$$\text{Frame} \qquad I^F = I_1^F f_1 f_1 + I_2^F f_2 f_2 + I_3^F f_3 f_3$$
$$\text{Wheel} \qquad I^W = I_1^W w_1 w_1 + I_2^W w_2 w_2 + I_3^W w_3 w_3$$

Angular momentum about the mass centre of each element

$$H^W = I^W . {}^a\omega^A = I_1^W \dot{\varphi} w_1 + I_2^W (\Omega + \Omega_o + \dot{\psi}\varphi) w_2 + I_3^W \dot{\psi} w_3$$
$$H^F = I^F . {}^a\omega^F = I_1^F (\dot{\varphi} - \dot{\psi}\theta) f_1 + I_2^F (\dot{\theta} + \dot{\psi}\varphi) f_2 + I_3^F \dot{\psi} f_3$$
$$H^T = I^T . {}^a\omega^T = I_1^T (\dot{\varphi} - \dot{\psi}\theta) f_1 + I_2^T (\dot{\theta} + \dot{\psi}\varphi) f_2 + I_3^T (\dot{\eta}_o + \dot{\eta} + \dot{\psi}) f_3$$

Inertia torques are then given by: $-\frac{{}^a d}{dt}(H)$, where the superscript "a" refers to the time derivative taken in reference frame F_a.

$$T^{W*} = -\left(I_1^W \ddot{\varphi} + I_3^W \dot{\psi}\dot{\varphi} - I_2^W (\Omega_o + \Omega + \dot{\psi}\varphi)\dot{\psi}\right) w_1 - I_2^W (\Omega + \ddot{\psi}\varphi) w_2 - I_2^W \dot{\psi}\dot{\varphi} w_2 - \left(I_3^W \ddot{\psi} + I_2^W \Omega_o \dot{\varphi}\right) w_3$$

$$T^{F*} = -\left(I_1^F (\ddot{\varphi} - \ddot{\psi}\theta - \dot{\psi}\dot{\theta}) + (I_3^F - I_2^F)(\dot{\psi}\dot{\theta} + \dot{\psi}\dot{\varphi}) + I_3^F \ddot{\psi}\theta\right) w_1 - \left(I_2^F (\ddot{\theta} + \ddot{\psi}\varphi + \dot{\psi}\dot{\varphi}) + (I_1^F - I_3^F)(\dot{\psi}\dot{\varphi} - \dot{\psi}\dot{\psi}\theta)\right) w_2 - I_3^F \ddot{\psi} w_3$$

$$T^{T*} = -(I_1^T(\ddot{\varphi} - \ddot{\psi}\theta - \dot{\psi}\dot{\theta}) + (I_3^T - I_2^T)(\dot{\psi}\dot{\theta} + \dot{\psi}\dot{\psi}\varphi) + I_3^T\ddot{\psi}\theta)w_1$$
$$- I_3^T(\dot{\theta} + \dot{\psi}\varphi)\dot{\eta}_o w_1 - (I_1^T - I_3^T)(\dot{\psi}\dot{\varphi} - \dot{\psi}\dot{\psi}\theta)w_2$$
$$- I_2^T(\ddot{\theta} + \ddot{\psi}\varphi + \dot{\psi}\dot{\varphi})w_2 - I_3^T(\ddot{\eta} + \ddot{\psi})w_3$$

A.9 Generalized Inertia Forces

These are evaluated as the inner product of the specific partial velocity and inertia force. So, for example, the generalized force in the direction of the generalized speed Ω_o, is given by the sum of the inner products of the partial velocities with respect to Ω_o of each element and the inertia force of the element.

Generalized speed Ω direction:

$$F_\Omega^* = -m_w r_w^2(\dot{\Omega} + \ddot{\psi}\varphi + 2\dot{\psi}\dot{\varphi}) - m_f r_w(\ddot{\theta} r_f + \ddot{\psi}(r_w + r_f)\varphi + \Omega r_w)$$
$$- m_f r_w(2(r_w + r_f)\dot{\psi}\dot{\varphi} - r_f\dot{\psi}\dot{\psi}\theta) - m_t r_w(l_t\ddot{\theta} - l_t\dot{\psi}\dot{\psi}\theta)$$
$$- m_t r_w((r_w + l_t)\ddot{\psi}\varphi + 2(r_w + l_t)\dot{\psi}\dot{\varphi}) - I_2^W(\dot{\Omega} + \ddot{\psi}\varphi + \dot{\psi}\dot{\varphi})$$

Generalized speed $\dot{\varphi}$ direction:

$$
\begin{aligned}
F^{*}_{\dot{\varphi}} = &- m_w r_w^2((\Omega_o + \Omega)\dot{\psi} + \dot{\psi}\dot{\psi}\varphi - \ddot{\varphi}) + m_f(r_w + r_f)(r_f\ddot{\psi}\theta) \\
&+ m_f(r_w + r_f)(2r_f\dot{\psi}\dot{\theta} - (r_w + r_f)\ddot{\varphi} + (r_w + r_f)\dot{\psi}\dot{\psi}\varphi) \\
&+ m_f(r_w + r_f)r_w(\Omega_o + \Omega)\dot{\psi} + m_t(r_w + l_t)(l_t\ddot{\psi}\theta + 2l_t\dot{\psi}\dot{\theta}) \\
&+ m_t(r_w + l_t)((r_w + l_t)(\dot{\psi}\dot{\psi}\varphi - \ddot{\varphi}) + r_w(\Omega_o + \Omega)\dot{\psi}) - \\
I_1^W\ddot{\varphi} & \\
&- I_3^W\dot{\psi}\dot{\psi}\varphi + I_2^W(\Omega_o + \Omega + \dot{\psi}\varphi) - I_1^F(\ddot{\varphi} - \ddot{\psi}\theta - \dot{\psi}\dot{\theta}) - I_3^F\ddot{\psi}\theta \\
&- (I_3^F - I_2^F)(\dot{\psi}\dot{\theta} + \dot{\psi}\dot{\psi}\varphi) - I_1^T(\ddot{\varphi} - \ddot{\psi}\theta - 2\dot{\psi}\dot{\theta} - \dot{\psi}\dot{\psi}\varphi) \\
&- I_3^T(\theta\dot{\eta}_o + \dot{\psi}\dot{\theta} + \dot{\psi}\dot{\eta}_o\varphi + \dot{\psi}\dot{\psi}\varphi + \ddot{\psi}\theta)
\end{aligned}
$$

Generalized speed $\dot{\psi}$ direction:

$$
F^{*}_{\dot{\psi}} = - (I_3^W + I_3^F + I_3^T)\ddot{\psi} - I_3^T\ddot{\eta} - I_2^W\Omega_o\dot{\varphi}
$$

Generalized speed $\dot{\theta}$ direction:

$$
\begin{aligned}
F^{*}_{\dot{\theta}} = &- m_f r_f(r_w\Omega + r_f\ddot{\theta} + (r_w + r_f)(\ddot{\psi}\varphi + 2\dot{\psi}\dot{\varphi}) - r_f\dot{\psi}\dot{\psi}\theta) \\
&- m_t l_t(l_t\ddot{\theta} + (r_w + l_t)(\ddot{\psi}\varphi + 2\dot{\psi}\dot{\varphi}) + r_w\Omega - l_t\dot{\psi}\dot{\psi}\theta) \\
&- I_2^F(\ddot{\theta} + \ddot{\psi}\varphi + \dot{\psi}\dot{\varphi}) - (I_1^F - I_3^F)(\dot{\psi}\dot{\varphi} - \dot{\psi}\dot{\psi}\theta) - I_2^T(\ddot{\theta} + \ddot{\psi}\varphi) \\
&- I_2^T(2\dot{\psi}\dot{\varphi} - \dot{\psi}\dot{\psi}\theta) + I_3^T(\dot{\psi}\dot{\varphi} - \dot{\psi}\dot{\psi}\theta + \dot{\varphi}\dot{\eta}_o - \dot{\psi}\dot{\eta}_o\theta)
\end{aligned}
$$

Generalized speed $\dot{\eta}$ direction:

$$
F^{*}_{\dot{\eta}} = - I_3^T(\ddot{\eta} + \ddot{\psi})
$$

A.10 Active Forces

These are the moments acting externally due to gravity, wheel torque Γ_w, turntable torque Γ_t and friction effects. F representing Coulomb friction effects and $f_{\dot{\psi}}\dot{\psi}$ viscous friction effects. Both friction effects modelled are at the contact point between the wheel and surface. The gear ratios are represented by n_w for the wheel and n_t for the turntable, both referred to the unicycle frame.

$$T_a^W = m_w r_w g\varphi w_1 + n_w \Gamma_w w_2 + F w_3 - f_{\dot{\psi}}\dot{\psi} w_3$$

$$T_a^F = m_f(r_w + r_f)g\varphi w_1 + (m_f r_f g\theta - n_w \Gamma_w)w_2 + n_t \Gamma_t f_3$$
$$= (m_f(r_w + r_f)g\varphi + n_t \Gamma_t \theta)w_1 + (m_f r_f g\theta - n_w \Gamma_w)w_2 + n_t \Gamma_t w_3$$

$$T_a^T = m_t(r_w + l_t)g\varphi w_1 + m_t l_t g\theta w_2 - n_t \Gamma_t f_3$$
$$= (m_t(r_w + l_t)g\varphi - n_t \Gamma_t \theta)w_1 + m_t l_t g\theta w_2 - n_t \Gamma_t w_3$$

A.11 Generalized Active Forces

As for the generalized inertia forces, these are evaluated as the inner product of partial velocities and active forces.

Generalized speed Ω direction:

$$F_\Omega = n_w \Gamma_w$$

Generalized speed $\dot{\varphi}$ direction:

$$F_{\dot{\varphi}} = (m_w r_w + m_f(r_w + r_f) + m_t(r_w + l_t))g\varphi$$

Generalized speed $\dot{\psi}$ direction:

$$F_{\dot{\psi}} = F - f_{\dot{\psi}}\dot{\psi}$$

Generalized speed $\dot{\theta}$ direction:

$$F_{\dot{\theta}} = - n_w\Gamma_w + (m_f r_f + m_t l_t)g\theta$$

Generalized speed $\dot{\eta}$ direction:

$$F_{\dot{\eta}} = - n_t\Gamma_t$$

A.12 Equations of Motion

The equations of motion are now determined as the sum of generalized active and generalized inertia forces:

Generalized speed Ω direction:

$$\begin{aligned} & n_w\Gamma_w - m_f r_w(2(r_w + r_f)\dot{\psi}\dot{\varphi} - r_f\dot{\psi}\dot{\psi}\theta) - m_t r_w(l_t\ddot{\theta} - l_t\dot{\psi}\dot{\psi}\theta) \\ & - m_w r_w^2(\Omega + \ddot{\psi}\varphi + 2\dot{\psi}\dot{\varphi}) - m_f r_w(\ddot{\theta} r_f + \ddot{\psi}(r_w + r_f)\varphi + \Omega r_w) \\ & - m_t r_w((r_w + l_t)\ddot{\psi}\varphi + 2(r_w + l_t)\dot{\psi}\dot{\varphi}) - I_2^W(\Omega + \ddot{\psi}\varphi + \dot{\psi}\dot{\varphi}) \\ & = 0 \end{aligned}$$

Generalized speed $\dot{\varphi}$ direction:

$$
\begin{aligned}
&(m_w r_w + m_f(r_w + r_f) + m_t(r_w + l_t))g\varphi \\
&- m_w r_w^2((\Omega_o + \Omega)\dot{\psi} + \dot{\psi}\dot{\psi}\varphi - \ddot{\varphi}) + m_f(r_w + r_f)(r_f\ddot{\psi}\theta) \\
&+ m_f(r_w + r_f)(2r_f\dot{\psi}\dot{\theta} - (r_w + r_f)\ddot{\varphi} + (r_w + r_f)\dot{\psi}\dot{\psi}\varphi) \\
&+ m_f(r_w + r_f)r_w(\Omega_o + \Omega)\dot{\psi} + m_t(r_w + l_t)(l_t\ddot{\psi}\theta + 2l_t\dot{\psi}\dot{\theta}) \\
&+ m_t(r_w + l_t)((r_w + l_t)(\dot{\psi}\dot{\psi}\varphi - \ddot{\varphi}) + r_w(\Omega_o + \Omega)\dot{\psi}) - I_1^W\ddot{\varphi} \\
&- I_3^W\dot{\psi}\dot{\psi}\varphi + I_2^W(\Omega_o + \Omega + \dot{\psi}\varphi) - I_1^F(\ddot{\varphi} - \ddot{\psi}\theta - \dot{\psi}\dot{\theta}) - I_3^F\ddot{\psi}\theta \\
&- (I_3^F - I_2^F)(\dot{\psi}\dot{\theta} + \dot{\psi}\dot{\psi}\varphi) - I_1^T(\ddot{\varphi} - \ddot{\psi}\theta - 2\dot{\psi}\dot{\theta} - \dot{\psi}\dot{\psi}\varphi) \\
&- I_3^T(\dot{\theta}\dot{\eta}_o + \dot{\psi}\dot{\theta} + \dot{\psi}\dot{\eta}_o\varphi + \dot{\psi}\dot{\psi}\varphi + \ddot{\psi}\theta) = 0
\end{aligned}
$$

Generalized speed $\dot{\psi}$ direction:

$$
F - f_{\dot{\psi}}\dot{\psi} - (I_3^W + I_3^F + I_3^T)\ddot{\psi} - I_3^T\ddot{\eta} - I_2^W\Omega_o\dot{\varphi} = 0
$$

Generalized speed $\dot{\theta}$ direction:

$$
\begin{aligned}
&- n_w\Gamma_w + (m_f r_f + m_t l_t)g\theta \\
&- m_f r_f(r_w\Omega + r_f\ddot{\theta} + (r_w + r_f)(\ddot{\psi}\varphi + 2\dot{\psi}\dot{\varphi}) - r_f\dot{\psi}\dot{\psi}\theta) \\
&- m_t l_t(l_t\ddot{\theta} + (r_w + l_t)(\ddot{\psi}\varphi + 2\dot{\psi}\dot{\varphi}) + r_w\Omega - l_t\dot{\psi}\dot{\psi}\theta) \\
&- I_2^F(\ddot{\theta} + \ddot{\psi}\varphi + \dot{\psi}\dot{\varphi}) - (I_1^F - I_3^F)(\dot{\psi}\dot{\varphi} - \dot{\psi}\dot{\psi}\theta) - I_2^T(\ddot{\theta} + \ddot{\psi}\varphi) \\
&- I_2^T(2\dot{\psi}\dot{\varphi} - \dot{\psi}\dot{\psi}\theta) + I_3^T(\dot{\psi}\dot{\varphi} - \dot{\psi}\dot{\psi}\theta + \dot{\varphi}\dot{\eta}_o - \dot{\psi}\dot{\eta}_o\theta) = 0
\end{aligned}
$$

Generalized speed $\dot{\eta}$ direction:

$$
n_t\Gamma_t + I_3^T(\ddot{\eta} + \ddot{\psi}) = 0
$$

A.13 Linearized Equations of Motion

The linearized equations of motion are determind by eliminating all products of generalized speeds and/or coordinates as follows:

Generalized speed Ω direction:

$$- (m_w r_w^2 + m_f r_w^2 + m_t r_w^2 + I_2^W)\dot{\Omega} - r_w(m_f r_f + m_t l_t)\ddot{\theta} + n_w \Gamma_w = 0$$

Generalized speed $\dot{\varphi}$ direction:

$$\begin{aligned} &- (m_w r_w^2 + m_f(r_w + r_f)^2 + m_t(r_w + l_t)^2 + I_1^W + I_1^F + I_1^T)\ddot{\varphi} \\ &- I_3^W \dot{\eta}_o \dot{\theta} + (m_w r_w^2 + m_f r_w(r_w + r_f) + m_t r_w(r_w + l_t) + I_2^W)\Omega_o \dot{\psi} \\ &+ (m_w r_w + m_f(r_w + r_f) + m_t(r_w + l_t))g\varphi = 0 \end{aligned}$$

Generalized speed $\dot{\psi}$ direction:

$$- (I_3^W + I_3^F + I_3^T)\ddot{\psi} - I_3^T \ddot{\eta} - I_2^W \Omega_o \dot{\varphi} + F - f_{\dot{\psi}} \dot{\psi} = 0$$

Generalized speed $\dot{\theta}$ direction:

$$\begin{aligned} &- r_w(m_f r_f + m_t l_t)\dot{\Omega} - (m_f r_f^2 + m_t l_t^2 + I_2^F + I_2^T)\ddot{\theta} + I_3^T \dot{\eta}_o \dot{\varphi} \\ &+ (m_f r_f + m_t l_t)g\theta - n_w \Gamma_w = 0 \end{aligned}$$

Generalized speed $\dot{\eta}$ direction:

$$- I_3^T(\ddot{\eta} + \ddot{\psi}) - n_t\Gamma_t = 0$$

A.14 State Space Description of Linearized Equations.

The state space structure is given here for use with linear control design techniques. This is the standard form:

State vector $x^T(t) = [\Omega \quad \dot{\theta} \quad \theta \quad \dot{\varphi} \quad \varphi \quad \dot{\psi} \quad \dot{\eta}]$

Input vector $u^T(t) = [\Gamma_w \; \Gamma_t \; F]$

$$\dot{x}(t) = A\,x(t) + B\,u(t)$$
$$y(t) = C\,x(t)$$

For the equations as derived above we first write the form:

$$M\,\dot{x}(t) + K\,x(t) + B\,u(t) = 0$$

then

$$\dot{x}(t) = -M^{-1}K\,x(t) - M^{-1}B\,u(t)$$

Where the mass matrix M and stiffness matrix K are

$$M = \begin{bmatrix} M_{11} & M_{12} \\ M_{21} & M_{22} \end{bmatrix} \qquad K = \begin{bmatrix} K_{11} & K_{12} \\ K_{21} & K_{22} \end{bmatrix}$$

The partitions defined as follows

$$M_{11} = \begin{bmatrix} -((m_w + m_f + m_t)r_w^2 + I_2^W) & -(m_f r_f + m_t l_t)r_w & 0 \\ -(m_f r_f + m_t l_t)r_w & -(m_f r_f^2 + m_t l_t^2 + I_2^T + I_2^F) & 0 \\ 0 & 0 & 1 \end{bmatrix}$$

$$M_{12} = M_{21}^T = \begin{bmatrix} 0 & 0 & 0 & 0 \\ 0 & 0 & 0 & 0 \\ 0 & 0 & 0 & 0 \end{bmatrix}$$

$$M_{22} = \begin{bmatrix} \begin{bmatrix} -(m_w r_w^2 + m_f(r_w + r_f)^2 + I_1^W) \\ -(m_t(r_w + l_t)^2 + I_1^F + I_1^T) \end{bmatrix} & 0 & 0 & 0 \\ 0 & -1 & 0 & 0 \\ 0 & 0 & -(I_3^W + I_3^F + I_3^T) & -I_3^T \\ 0 & 0 & -I_3^T & -I_3^T \end{bmatrix}$$

$$K_{11} = \begin{bmatrix} 0 & 0 & 0 \\ 0 & 0 & (m_f r_f + m_t l_t)g \\ 0 & -1 & 0 \end{bmatrix}$$

$$K_{12} = \begin{bmatrix} 0 & 0 & 0 & 0 \\ I_3^T\dot{\eta}_o & 0 & 0 & 0 \\ 0 & 0 & 0 & 0 \end{bmatrix}$$

$$K_{21} = \begin{bmatrix} 0 & -I_3^T\dot{\eta}_o & 0 \\ 0 & 0 & 0 \\ 0 & 0 & 0 \\ 0 & 0 & 0 \end{bmatrix}$$

$$K_{22} = \begin{bmatrix} 0 & \begin{bmatrix} (m_w r_w + m_f r_f)g \\ +(m_f r_w + m_t(r_w + l_t))g \end{bmatrix} & \begin{bmatrix} r_w(m_w r_w + m_f(r_w + r_f))\Omega_o \\ +(r_w m_t(r_w + l_t) + I_2^W)\Omega_o \end{bmatrix} & 0 \\ 1 & 0 & 0 & 0 \\ -I_2^W\Omega_o & 0 & -f_{\dot{\psi}} & 0 \\ 0 & 0 & 0 & 0 \end{bmatrix}$$

The control distribution matrix B is

$$B = \begin{bmatrix} n_w & 0 & 0 \\ -n_w & 0 & 0 \\ 0 & 0 & 0 \\ 0 & 0 & 0 \\ 0 & 0 & 0 \\ 0 & 0 & 1 \\ 0 & -n_t & 0 \end{bmatrix}$$

Since we measure all states, the measurement matrix is the identity matrix

$$C = I_{7\times 7}$$

A.15 Discussion of Equations

As indicated in the introduction to this appendix, the nonlinear in $\dot{\psi}$ equations are derived here for use in validating the controller designed. The controller is designed for regulation of pitch and roll errors in both rates and angles and command following in heading and speed of the unicycle. Bearing this in mind we make the following assumption for the linear controller design strategy.

A.15.1 Decoupling of Lateral and Longitudinal Dynamics

Setting the turntable referance angular velocity, η_o to zero eliminates the coupling terms $I_3^T\dot{\eta}_o$ from partitions K_{12} and K_{21} in the stiffness matrix K thus decoupling the lateral and longitudinal dynamics for the purposes of linear controller design. These terms are included in the simulations for controller evaluation.

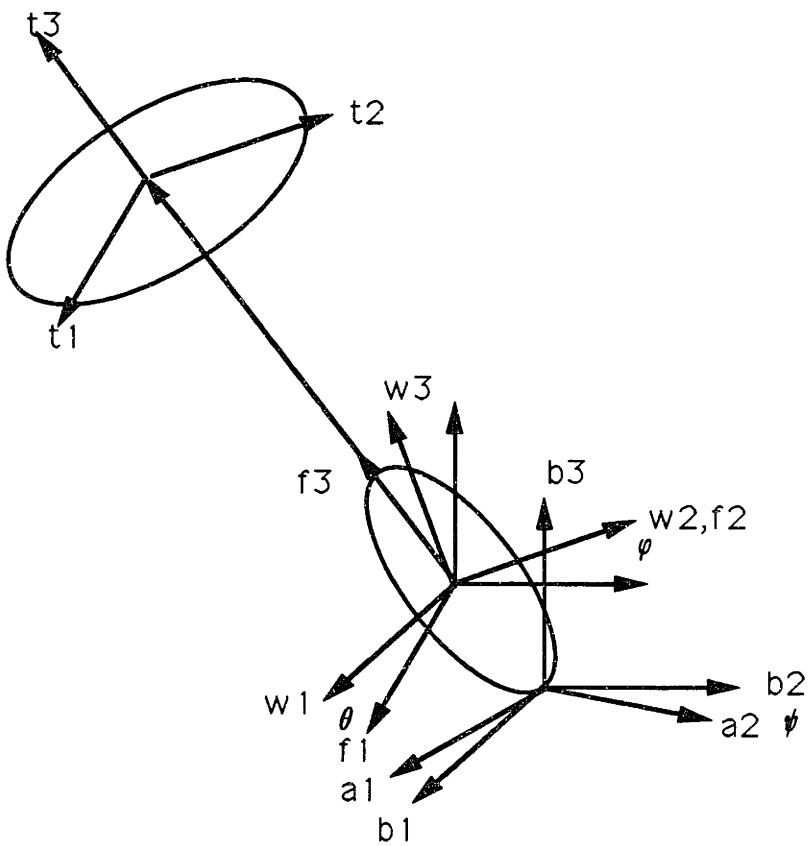

Figure a.1. Reference Frames Schematic

APPENDIX 2 VARIATION OF LQG DESIGN METHODOLOGY

Introduction

This appendix derives the result used in both the lateral and longitudinal linear controller designs. The derivation considers the lateral control problem of the unicycle. This result gives the designer freedom to select the Kalman Filter dynamics as pleased and always be guaranteed that these will not affect the desired regulator closed loop transfer function when viewed in the sense specified here.

A2.1 Variation of LQG Structure

The closed inner loop structure is shown in figure A2.1.1. The subscrpt 'lr' denotes lateral reduced order model, to distinguish from the full order model of section 4.1.

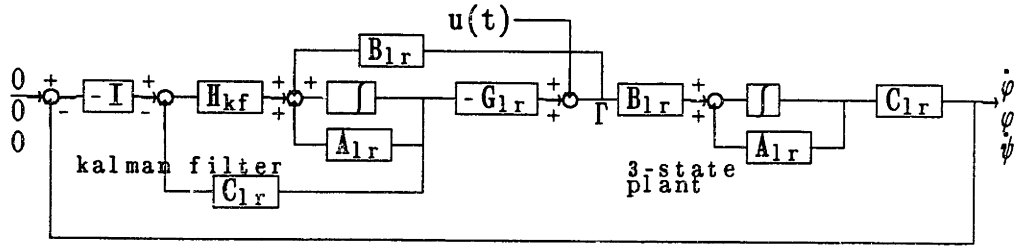

Figure A2.1.1 Inner LQG regulator loop

In the inner loop we wish to regulate the roll rate, roll angle and yaw rate and these are the states of the reduced order

lateral model. The input to the plant, $\Gamma(t)$ is the turntable torque and by the nature of the model, this is the natural place to break the regulator loop when appending the outer loop dynamics i.e. the integration of yaw rate to yield heading angle. This is so since the heading command generates a commanded torque to the turntable and this influences the status of the inner loop in the sense of input disturbances to the plant. The interesting result is that the filter dynamics do not show up in the outer loop transfer function relating the 'external' (outer loop) input $u(t)$ and the output $y(t) = [\dot{\varphi}\ \varphi\ \dot{\psi}]^T$.

We can easily show this result for the single input single output (SISO) case as follows. Consider the block diagram of figure A2.1.1 for an equivalent SISO system

The plant dynamics propogate by

$$\dot{x}(t) = A_{lr}x(t) + B_{lr}\Gamma(t)$$

or, in Laplace transform form

$$x(t) = \frac{B_{lr}\Gamma(s)}{(s - A_{lr})} \qquad \text{A2.1.1}$$

and for the filter

$$s\,\hat{x}(s) = \hat{A}_{lr}\hat{x}(s) + \hat{B}_{lr}\Gamma(s) - H_{kf}\hat{C}_{lr}\hat{x}(s) + H_{kf}C_{lr}x(s)$$

or

$$\hat{x}(s) = \frac{\hat{B}_{lr}\Gamma(s) + H_{kf}C_{lr}x(s)}{(s - \hat{A}_{lr} + H_{kf}\hat{C}_{lr})} \qquad \text{A2.1.2}$$

Substituting A2.1.1 in A2.1.2

$$\hat{x}(s) = \frac{1}{(s - \hat{A}_{lr} + H_{kf}\hat{C}_{lr})}(\hat{B}_{lr} + \frac{H_{kf}C_{lr}B_{lr}}{(s - A_{lr})})\Gamma(s) \qquad \text{A2.1.3}$$

The turntable motor torque can be written

$$\Gamma(s) = u(s) - G_{lr}\hat{x}(s)$$

including equation A2.1.3 yields

$$\Gamma(s) = u(s) - \frac{G_{lr}}{(S - \hat{A}_{lr} + H_{kf}\hat{C}_{lr})}(\hat{B}_{lr} + \frac{H_{kf}C_{lr}B_{lr}}{(s - A_{lr})})\Gamma(s)$$

rearranging

$$\Gamma(s) = \frac{u(s)(s - \hat{A}_{lr} + H_{kf}\hat{C}_{lr})}{(s - \hat{A}_{lr} + H_{kf}\hat{C}_{lr} + G_{lr}\hat{B}_{lr} + \frac{G_{lr}H_{kf}C_{lr}B_{lr}}{(s - A_{lr})})} \qquad \text{A2.1.4}$$

The output is given by

$$y(s) = C_{lr}x(s)$$

recalling A2.1.1 and A2.1.4 yields

$$y(s) = \frac{C_{lr}B_{lr}(s - \hat{A}_{lr} + H_{kf}\hat{C}_{lr})u(s)}{(s - A_{lr})(s - \hat{A}_{lr} + H_{kf}\hat{C}_{lr} + G_{lr}\hat{B}_{lr} + \frac{G_{lr}H_{kf}C_{lr}B_{lr}}{(s - A_{lr})})}$$

The denominator can be rewritten as, noting that since the filter is model based, $\hat{A}_{lr}=A_{lr}$, $\hat{B}_{lr}=B_{lr}$ and $\hat{C}_{lr}=C_{lr}$

$$s^2 - 2A_{lr}s + A_{lr}^2 + (B_{lr}G_{lr} + H_{kf}C_{lr})(s - A_{lr}) + H_{kf}C_{lr}B_{lr}G_{lr}$$

Now, since the filter is model based, by the separation principle this factors into the following

$$(s - A_{lr} + B_{lr}G_{lr})(s - \hat{A}_{lr} + H_{kf}\hat{C}_{lr})$$

so that the final form of the transfer function relating u(s) and the output y(s) is

$$y(s) = \frac{C_{lr}B_{lr}(s - \hat{A}_{lr} + H_{kf}\hat{C}_{lr})u(s)}{(s - \hat{A}_{lr} + H_{kf}\hat{C}_{lr})(s - A_{lr} + B_{lr}G_{lr})}$$

$$= \frac{C_{lr}B_{lr}u(s)}{(s - A_{lr} + B_{lr}G_{lr})}$$

where the final form shows pole-zero cancellation which can be shown to imply that the error ($\tilde{x}(t)=x(t) - \hat{x}(t)$) dynamics are uncontrollable from the input u(t). This becomes apparent when writing the error dynamics expression out as follows

Consider the MIMO augmented state space description for a structure as given by figure A2.1.1

$$\begin{bmatrix} \dot{x}(t) \\ \dot{\hat{x}}(t) \end{bmatrix} = \begin{bmatrix} A_{lr} & -B_{lr}G_{lr} \\ H_{kf}C_{lr} & \hat{A}_{lr} - H_{kf}\hat{C}_{lr} - \hat{B}_{lr}G_{lr} \end{bmatrix} \begin{bmatrix} x(t) \\ \hat{x}(t) \end{bmatrix}$$

$$+ \begin{bmatrix} B_{lr} \\ \hat{B}_{lr} \end{bmatrix} u(t)$$

Defining the state error as

$$\tilde{x}(t) = x(t) - \hat{x}(t)$$

we rewrite the state space model including the error state, thus

$$\begin{bmatrix} \dot{x}(t) \\ \dot{\tilde{x}}(t) \end{bmatrix} = \begin{bmatrix} A_{lr} - B_{lr}G_{lr} & B_{lr}G_{lr} \\ 0 & \hat{A}_{lr} - H_{kf}\hat{C}_{lr} \end{bmatrix} \begin{bmatrix} x(t) \\ \tilde{x}(t) \end{bmatrix}$$

$$+ \begin{bmatrix} B_{lr} \\ 0 \end{bmatrix} u(t)$$

Clearly the error dynamics are uncontrollable from the input u(t), implying pole-zero cancellation in the MIMO (multi input multi output) sense must occur here, which leads to the conclusion that the above result is valid in MIMO systems as well as SISO systems.

A third means of viewing this issue is that by definition in the Kalman filter derivation, the state error is orthogonal with the true state in order that the estimate be unbiased [8, 1].

$$E\{x(t)\tilde{x}^T(t)\} = 0$$

Hence the error state space cannot be reached from the true state space.

This property of the structure opens a very useful synthesis path in that the regulator loop may be designed independently by the separation principle and however the filter is defined, with the only condition being that it be model based in order for the seperation principle to be valid, will not affect the outer loop transfer function. Thus it is possible to design a regulator having all the desired characteristics and yielding a 'nice' closed loop transfer function and then shape the outer loop as desired around the regulator loop with full guarantee of retaining this loop transfer function when the inner loop filter is designed.

The real advantage in this approach being that the optimal filter for the existing process and plant noises of the inner loop, in order to obtain optimal estimates of the states, need not have high bandwidth as required in methods such as Loop Transfer Recovery, and thus all the inherently bad properties of the 'cheap' control solution such as very high gains and associated high frequency dynamics, attempted plant inversion and particularly the poor recovery associated with non minimum-phase systems, are avoided.

APPENDIX 3 MODEL PARAMETERS USED IN STUDY

The model parameters used are representative of the unicycle robot and are as defined in the Stanford study [14].

Unicycle Wheel:

mass	$m_w = 2.1$ kg
radius	$r_w = 0.2$ m
inertia	$I_1^W = I_3^W = 0.02$ kgm^2
	$I_2^W = 0.04$ kgm^2

Unicycle frame

mass	$m_f = 23.2$ kg
centre of mass	$r_f = 0.45$ m
inertia	$I_f^1 = 1.35$ kgm^2
	$I_f^2 = 1.51$ kgm^2
	$I_f^3 = 0.36$ kgm^2

Turntable

mass	$m_t = 24$ kg
centre of mass	$l_t = 0.8$ m
inertia	$I_t^1 = 0.3$ kgm^2
	$I_t^2 = 0.3$ kgm^2
	$I_t^3 = 0.6$ kgm^2

Friction coefficients in yaw between wheel and surface

$f_{\psi} = 0.0245$ Nms/rad

Gear ratios

wheel	$n_w = 12$
Turntable	$n_t = 36$

REFERENCES

1) Brown, R.G., Introduction to Random Signal Analysis and Kalman Filtering, John Wiley & Sons, Inc, 1983.

2) Course Notes, Applied Analytical Dynamics, Department of Aeronautics and Astronautics, MIT, Spring 1988.

3) Course Notes, Computer Control of Dynamic Systems, Department of Aeronautics and Astronautics, MIT, Fall 1987.

4) Course Notes, Multivariable Control Systems, Department of Aeronautics and Astronautics, MIT, Fall 1987, Spring 1988.

5) Franklin, G.F. and Powell, J.D., Digital Control of Dynamic Systems, Addison-Wesley Publishing Company, Reading, Massachusetts, 1980.

6) Freudenberg, J.S. and Looze, D.P., Right Half Plane Poles and Zeros and Design Tradeoffs in Feedback Systems, IEEE Transactions on Automatic Control, Volume AC-30, No. 6, June 1985.

7) Galil Motion Control, 1054 Elwell Ct, Palo Alto, CA 94303.

8) Gelb, A., editor, Applied Optimal Estimation, The M.I.T. Press, Cambridge, 1974.

9) Infranor Inc, Mavilor Motor Catalog, Box 1307, Naugatuck, Connecticut 06770.

10) Kailath, T, editor, Linear Systems, Prentice-Hall, Inc Englewood Cliffs, New Jersey, 1980.

11) Kane, T.R. and Levinson, D.A., Dynamics: Theory and Applications, McGraw-Hill, New York, 1985.

12) Kwakernaak, H. and Sivan, R., Linear Optimal Control Systems, Wiley Interscience, New York, 1972.

13) Marks, L.S., Baumeister, T., Standard Handbook for Mechanical Engineers, 7th ed, Mc Graw-Hill, New York, 1967.

14) Schoonwinkel, A., Design and Test of a Computer Stabilized Unicycle, PhD Thesis, Stanford University, Palo Alto, 1987.

15) Watson Industries Inc, Angular Rate Sensor Manual, 3041 Melby Road, Eau Claire, WI 54703.